BOLT BERANEK AND NEWMAN INC

CONSULTING · DEVELOPMENT · RESEARCH

4773 - 129115

Report 2091
Job 11366

SHOCK TRANSMISSION IN COUPLED BEAMS AND RIB STIFFENED STRUCTURES
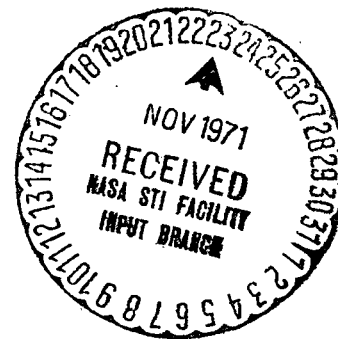
Larry D. Pope

Jerome E. Manning

Terry D. Scharton

Contract No. NAS8-21386

Final Report

CASE FILE COPY

NOV 1971
RECEIVED
NASA STI FACILITY
INPUT BRANCH

2 November 1971

Prepared for:

George C. Marshall Space Flight Center
Marshall Space Flight Center, Alabama 35812

CAMBRIDGE   NEW YORK   WASHINGTON   CHICAGO   LOS ANGELES   SAN FRANCISCO

SHOCK TRANSMISSION IN COUPLED BEAMS AND RIB STIFFENED STRUCTURES

Larry D. Pope

Jerome E. Manning

Terry D. Scharton

Contract No. NAS8-21386

Final Report

2 November 1971

Prepared for:

George C. Marshall Space Flight Center
Marshall Space Flight Center, Alabama 35812

ABSTRACT

Shock transmission in a simple coupled beam structure
and in a ring-stringer stiffened cylinder is investigated
experimentally and analytically using wave transmission
and statistical energy analysis concepts. The use of
the response spectrum to characterize the excitation
provided to a simple beam by a force pulse is studied.
Analysis of the transmission of a dilatation wave in a
periodically stiffened plate indicates that the stiffeners
are fairly transparent to the wave, but some of the dila-
tational energy is scattered into bending at each support.

TABLE OF CONTENTS

LIST OF FIGURES

I. INTRODUCTION

The high frequency vibration environments generated
by pyrotechnic shocks are an important aspect of space
vehicle dynamics. Pyrotechnic sources used for separating
vehicle stages or sections typically generate short duration,
high level forces which may excite bending, dilatational,
and shear waves in the structure.

When the waves traveling out from the source region
reach a discontinuity in the structure, such as a stiffening
ring or longitudinal, they are partially reflected and
partially transmitted. The discontinuities are usually
quite transparent to compressional waves and shear waves
which therefore transmit quickly away from the source
and decay slowly with distance from the source. The
decay arises from internal structural damping and from
small scattering into bending waves at the discontinuities.
On the other hand the discontinuities can be strong
reflectors of bending waves, so that multiple reflections
result in reverberant build-up and subsequent slow temporal
decay of the bending vibrational energy in a panel bay
defined by the circumferential and longitudinal stiffeners.
Because the bending wave transmission and reflection
characteristics of the stiffeners are quite selective
in frequency, the bending vibration response of a panel
bay may be quite narrow band in nature even though the
pyrotechnic shock spectrum is broadband. A representative
bending vibration response measured some distance from
the pyrotechnic shock excitation point is shown in Fig. 1.

The generation and transmission of pyrotechnic shock
induced vibration in space vehicles is a quite complicated
process, and a complete analytical description of the

process is not available. In this report some analytical and experimental results for a simple coupled beam structure and a model ring-stringer stiffened cylinder are presented with the hope that these results will provide some insight and guidance for formulating scaling laws or semi-empirical methods for treating full scale complex structures.

Part II of the report discusses the use of response measurements on distributed structures to define the energy spectrum of a pulse-like shock input. Part III presents a study of shock induced bending wave transmission in a simple coupled beam system. Part IV deals with the model ring-stringer stiffened cylinder and contains: (a) a statistical energy analysis of bending energy transmission, (b) measurements of bending energy transmission, (c) comparisons of transient and steady state transmission, and (d) an analysis and measurements of dilatational wave transmission and scattering into bending waves.

II. DETERMINATION OF THE SHOCK PULSE ENERGY SPECTRUM FROM MEASUREMENT OF THE RESPONSE OF A CONTINUOUS SYSTEM

Analytical methods for predicting the shock response of aerospace structures to pyrotechnic devices are essentially nonexistent. One of the reasons is that the exciting forces are seldom known. Generally, the forcing mechanisms are so complex that they are bypassed and we look directly at the structural response [1]. For instance, an almost constantly used device in shock analysis is the response shock spectrum [2]. It yields information concerning the frequency content of the response, but its applicability to subsequent prediction of the response of any equipment which might be attached to the structure is not straight-forward. It also seems useless for predicting the response of different structures to similar pyrotechnic devices. The problem, of course, is that it has no physical interpretation related to the actual shocked structure.

Recently, a rational procedure called "Statistical Energy Analysis" (SEA) [3], [4], [5] has been adapted to shock transmission problems [6]. Rather than attempting to describe the response of a structure on a mode by mode basis, this theory is concerned with quantities such as time average energies of various distinct groups of modal oscillators and with time average power flow between them on a band-limited basis. Originally developed for steady state calculations, the adaptation has been made to shock by considering so-called "short-time averages," this being possible because it has been

observed that the shocks can generally be described as quasi-steady vibrations of the resonant-ringing type with slowly varying envelope [7].

In very basic terms the complex shock transmission might, for instance, be described in the following manner. Consider two finite beams, connected, with some mismatch in impedance at the junction, one of the beams being excited by a complex point input force pulse, and both responding flexurally. Observed in each pass band will be a wave packet carrying energy away from the source. When the packet strikes the juncture, a direct wave will be observed in the second beam. If the impedance mismatch is large enough the level of the direct wave in the second beam will be small, almost all of the energy in the packet being reflected, establishing a reverberant vibration field in the first beam. The direct wave transmitted to the second beam also induces reverberation, but at a much lower energy level. Energy leaks out of the first beam into the second at the rate predicted by energy analysis. The dispersive nature of flexural waves assures that the flexural energy density moves in time toward spatial uniformity in each beam, and that the short-time average intensity of waves incident at the juncture eventually levels out, decaying slowly (we invoke the requirement that the response truly be resonant, the coupling and dissipative loss factors both being small).

From this discussion, it should be apparent that it is impractical to attempt to describe the direct waves in either

beam without knowing the exact forcing function. Prediction of the reverberant response of the second should be possible if the short-time space averaged response of the first is known. In this section, it is shown that the maximum short-time space averaged square of the response acceleration of the first beam is related to the band-limited energy spectrum of the forcing function.

A. The Energy Spectrum

Consider a complex mechanical system, a ribbed, multi-bayed shell, or a frame work consisting of beam elements. At sufficiently high frequencies, the panel bays or the beams will more or less respond as separate modal subsystems. If the ribs of the shell (or the junctures of the beams) represent sufficiently high impedances (say to flexural motion) and if the structural damping is light, energy injected by a device into one of the bays will be "trapped" by the ribs, giving rise to a resonant structural response. If the boundary impedances were infinite, and if there was absolutely no structural damping present, the panel (or beam) would store information concerning the Fourier amplitude spectrum of the pulse.

The response of a single mode, s, of the quasi-isolated system is obtained from

$$\frac{d^2\xi_s}{dt^2} + \frac{\omega_s}{Q_s}\frac{d\xi_s}{dt} + \omega_s^2\xi_s = \frac{1}{M_s}\int p(\underset{\sim}{x},t)\psi^s(\underset{\sim}{x})d\sigma \quad , \quad (II-1)$$

where M_s is the modal mass, $\psi^s(\underset{\sim}{x})$ the modal function, ω_s the

resonance frequency, and Q_s the modal dynamic magnification factor. The Fourier transform of the modal coordinate, $\xi_s(t)$, is

$$\Xi_s(\omega) = \frac{\int P(\underset{\sim}{x},\omega)\psi^S(\underset{\sim}{x})d\sigma}{M_s Y_s(\omega)} \quad , \tag{II-2}$$

where

$$Y_s(\omega) = \omega_s^2[1 - (\omega/\omega_s)^2 + i\eta_s] \quad .$$

We consider a point input at $\underset{\sim}{x}'$

$$p(\underset{\sim}{x},t) = \delta(\underset{\sim}{x} - \underset{\sim}{x}')f(t) \quad .$$

Then

$$\Xi_s(\omega) = \frac{\psi^S(\underset{\sim}{x}')F(\omega)}{M_s Y_s(\omega)} \quad . \tag{II-3}$$

According to Parseval's theorem [8], the temporal and frequency response amplitudes are related by

$$\int_{-\infty}^{\infty} \left|\xi_s(t)\right|^2 dt = \frac{1}{2\pi} \int_{-\infty}^{\infty} \left|\Xi_s(\omega)\right|^2 d\omega \quad . \tag{II-4}$$

Assuming that excitation begins at t = 0, and ceases at t = T, then

$$\int_T^{\infty} \left|\xi_s(t)\right|^2 dt = \frac{1}{2\pi} \int_{-\infty}^{\infty} \left|\Xi_s(\omega)\right|^2 d\omega - \int_o^T \left|\xi_s(t)\right|^2 dt \quad . \tag{II-5}$$

-6-

The integration indicated on the left-hand side is over the so-called residual vibration period. The concern here is to predict the maximum residual vibration amplitude (or energy). For sufficiently short pulses it is easy to show that the maximum residual response exceeds all maxima occurring during the forcing era (ultimately, a delta function input has all residual response).

If at $t = T$, $\xi_s = \delta_s$ and $\dot{\xi}_s = \dot{\delta}_s$, a solution for $t > T$ can be obtained from Eq. (II-1),

$$\xi_s(t) = \exp\left[-\frac{\eta_s \omega_s}{2}(t - T)\right]\hat{\xi}_s \cos(\omega_{sD}(t - T) - \phi_s) \qquad \text{(II-6)}$$

where

$$\hat{\xi}_s = \{[\dot{\delta}_s^2 + \eta_s \omega_s \dot{\delta}_s \delta_s + \omega_s^2 \delta_s^2]^{1/2}/\omega_{sD}\} \quad , \qquad \text{(II-7)}$$

$$\phi_s = \tan^{-1}\{[\frac{\eta_s \omega_s}{2}\delta_s + \dot{\delta}_s]/\omega_{sD}\delta_s\} \quad , \qquad \text{(II-8)}$$

and

$$\omega_{sD} = \omega_s(1 - \eta_s^2/4)^{1/2} \quad .$$

For light damping, this is a damped sinusoid at frequency $\omega_{sD} \simeq \omega_s$, with a maximum residual amplitude approximately given by $\hat{\xi}_s$.

The substitution of Eq.II-6 into the left-hand side of Eq.II-5 yields

$$\int_T^\infty \left| \xi_s(t) \right|^2 dt = \hat{\xi}_s^2 \left[\frac{\omega_{sD}^2}{2\eta_s \omega_s^3} + \frac{\eta_s \omega_{sD}^2}{4\omega_s^3} \cos^2 \phi_s + \frac{\omega_{sD}}{2\omega_s^2} \cos \phi_s \sin \phi_s \right] \quad . \quad (II\text{-}9)$$

For light damping, the first term dominates:

$$\int_T^\infty \left| \xi_s(t) \right|^2 dt \simeq \frac{\hat{\xi}_s^2}{2\eta_s \omega_s} \quad . \qquad (II\text{-}10)$$

With Eqs. II-3 and II-10, Eq. II-5 becomes

$$\hat{\xi}_s^2 \simeq \frac{\eta_s \omega_s}{\pi} \frac{\psi^{s^2}(x')}{M_s^2} \int_{-\infty}^\infty \frac{\left| F(\omega) \right|^2 d\omega}{\left| Y_s(\omega) \right|^2} - 2\eta_s \omega_s \int_0^T \left| \xi_s(t) \right|^2 dt \quad . \qquad (II\text{-}11)$$

If the force is sufficiently short, $\left| F(\omega) \right|$ will be relatively flat around ω_s. Since the square of the magnitude of the mode admittance function is highly peaked at $\omega = \omega_s$, and since, by hypothesis, $\left| F(\omega) \right|$ is smooth over a band of frequencies exceeding the modal bandwidth, Eq.II-11 can be approximated by

$$\hat{\xi}_s^2 = \frac{\eta_s \omega_s}{\pi} \frac{\psi^{s^2}(x') \left| F(\omega_s) \right|^2}{M_s^2 \omega_s^4} \int_{-\infty}^\infty \frac{d\omega}{[1 - (\omega/\omega_s)^2]^2 + \eta_s^2}$$

$$-2\eta_s \omega_s \int_0^T \left| \xi_s(t) \right|^2 dt \quad , \qquad (II\text{-}12)$$

yielding

$$\hat{\xi}_s^2 \simeq \frac{\psi^{s^2}(\underset{\sim}{x}')|F(\omega_s)|^2}{2M_s^2\omega_s^2} - 2\eta_s\omega_s \int_0^T |\xi_s(t)|^2 dt \quad . \quad \text{(II-13)}$$

The first term on the right-hand side of Eq. II-13 is the best estimate of the maximum response which we can make without knowledge of the time history of the modal displacement during the forcing era. The second term we assume can be ignored. Its presence is due to the finite forcing era and the dissipative and coupling losses. If $\eta_s = 0$, the Fourier amplitude spectrum is sampled by the modes, and conserved. We note that we must restrict the estimate in II-13 to those frequencies below that for which the first zero of $|F(\omega)|$ occurs.

In frequency band $\Delta\omega$, if the density of modes is n, there are $n\Delta\omega$ modes. The maximum energy of each cannot exceed

$$E_s = \frac{1}{2}\int \rho(\omega_s\hat{\xi}_s\psi^s(\underset{\sim}{x}))^2 d\sigma \quad , \quad \text{(II-14)}$$

where ρ is the areal or lineal material density. From Eq. II-13, it follows that our estimate is

$$E_s = \frac{\psi^{s^2}(\underset{\sim}{x}')|F(\omega_s)|^2}{4M_s} \quad . \quad \text{(II-15)}$$

The maximum energy contained by all of the modes in band $\Delta\omega$ at the conclusion of the force pulse cannot exceed

$$E_{\Delta\omega}^{max} = \sum_{s,\Delta\omega} \frac{\psi^{s^2}(\underset{\sim}{x}')|F(\omega_s)|^2}{4M_s} \quad . \qquad (II-16)$$

For the higher order modes of a two-dimensional structure, $M_s \simeq M_p/4$, where M_p is the total panel mass. If $|F(\omega_s)|$ is slowly varying over $\Delta\omega$,

$$E_{\Delta\omega}^{max} = \frac{|F(\omega)|^2}{M_p} \sum_{s,\Delta\omega} \psi^{s^2}(\underset{\sim}{x}') \quad . \qquad (II-17)$$

The expected value of the maximum energy in band $\Delta\omega$ is then*

$$\langle E_{\Delta\omega}^{max} \rangle = \frac{n|F(\omega)|^2 \Delta\omega}{4M_p} \quad . \qquad (II-18)$$

This energy is related to the filtered, maximum short time-space averaged square of the physically measurable acceleration of the panel. The panel energy at any instant after the pulse has concluded is approximately constant (except for the slow decay owing to the presence of some losses, it would be constant). We can write the instantaneous panel kinetic energy

---

*We can interpret this as the expected value for all possible source input positions, or, provided there are a sufficient number of modes in $\Delta\omega$, as an average over all modes having a wavenumber near the mean wavenumber for the band.

as

$$KE(t) = \sum_{s,\Delta\omega} \frac{1}{2}\int \rho\omega_s^2 \psi^{s^2}(\underset{\sim}{x})\hat{\xi}_s^2 \exp[-\eta_s\omega_s(t-T)]\cos^2(\omega_s(t-T)-\phi_s)d\sigma \; .$$

$$(II-19)$$

A short-time average, which must be performed over at least a
moderate number of half-periods, yields

$$<KE(t)>_t = \sum_{s,\Delta\omega} M_s\omega_s^2 \frac{\hat{\xi}_s^2}{4} \exp[-\eta_s\omega_s(t-T)] \qquad . \quad (II-20)$$

If all modes are equally energetic, the total short-time average
energy is

$$<E(t)>_t = \frac{nM_p}{8}\omega^2 \hat{\xi}^2 \exp[-\eta\omega(t-T)]\Delta\omega \qquad , \qquad (II-21)$$

where η is the average loss factor, ω is the band center
frequency, and $\hat{\xi}$ is the average maximum modal displace-
ment amplitude. The maximum short-time average energy is

$$<E_{\Delta\omega}^{max}> \simeq \frac{nM_p}{8\omega^2} \overset{\wedge}{\ddot{\xi}}{}^2 \Delta\omega \qquad . \qquad (II-22)$$

Here $\overset{\wedge}{\ddot{\xi}}$ is the maximum modal acceleration amplitude. This
quantity is related to the maximum short time-space averaged
square of the physically measurable acceleration. The actual
physically measurable acceleration at any point is

$$a(\underset{\sim}{x},t) = \sum_s \ddot{\xi}_s(t)\psi^s(\underset{\sim}{x}) \qquad . \qquad (II-23)$$

Assuming uniform areal mass, a space average of the squared acceleration gives

$$\langle a^2(t) \rangle_s = \frac{1}{4} \sum_{s, \Delta\omega} \ddot{\xi}_s^2(t) \quad .$$ (II-24)

The maximum short-time average is

$$\langle a^2 \rangle_{s,t}^{max} = \frac{1}{4} \sum_{s, \Delta\omega} \frac{\hat{\ddot{\xi}}_s^2}{2} \simeq \frac{n}{8} \hat{\ddot{\xi}}^2 \Delta\omega \quad .$$ (II-25)

Thus

$$\langle E_{\Delta\omega}^{max} \rangle = \frac{M_p \langle a^2 \rangle_{s,t}^{max}}{\omega^2} \quad ,$$ (II-26)

or

$$|F(\omega)|^2 \Delta\omega = \frac{4 M_p^2 \langle a^2 \rangle_{s,t}^{max}}{n \omega^2} \quad .$$ (II-27)

It can be shown that this result holds also for a one-dimensional structure if the total panel mass is replaced by the total beam mass. The quantity on the left in Eq. II-27 is an approximation for the band-limited energy spectrum of the forcing function, I, given by the relation

$$I \equiv \int_{\Delta\omega} |F(\omega)|^2 d\omega \quad .$$ (II-28)

For a two-dimensional structure, with mass density, ρ, area, A_p, thickness, h, and longitudinal wave speed c_ℓ,

$$I = \frac{2\rho^2 c_\ell h^3 A_p <a^2>_{s,t}^{max}}{\sqrt{3}\ \pi f^2} \quad , \qquad \text{(II-29)}$$

or alternately

$$I = \frac{2\pi M_p <a^2>_{s,t}^{max}}{\omega^2 G_\infty} \quad , \qquad \text{(II-30)}$$

where G_∞ is the frequency averaged point input conductance of the plate (or equivalently, the infinite plate point input admittance) [5].

For a one-dimensional structure (beam), with lineal density, ρ_ℓ, longitudinal wave speed, c_ℓ, length, ℓ, and radius of gyration, κ,

$$I = \frac{8\pi \kappa^{1/2} c_\ell^{1/2} \rho_\ell^2 \ell}{\omega^{3/2}} <a^2>_{s,t}^{max} \quad . \qquad \text{(II-31)}$$

B. Experimental Investigation

In order to check the reasonableness of these estimates, a simple set of experiments was performed. Basically the procedure consisted of:

(a) excitation of a simple system with a known force pulse,

(b) computation of the Fourier amplitude spectrum of the pulse, and then, for a fixed bandpass, $\Delta\omega$, the energy spectrum, I, and,

(c) comparison of I obtained directly from the force pulse with that computed from the system response by either Eq. II-29 or II-31.

The mechanical system tested consisted of a cross, constructed from four 1 x 1/8-inch x 5-ft long rectangular aluminum bars, welded along the one-inch dimension. The coupling (juncture) and structural loss factors were both less than 10^{-2}. The estimate for I, based on the response acceleration of the segment upon which the input was located, is given by Eq. II-31 which becomes

$$I \simeq 1.26 <g^2>_{s,t}^{max}/f^{3/2} \qquad , \qquad (II-32)$$

where $<g^2>_{s,t}^{max}$ is the maximum short time-space average square of the response acceleration in gravitational units.

The experimental configuration is shown in Fig. 2. A
Wilcoxon Model Z-602 impedance head was mounted close to
the free end of one beam segment. Since it was fairly
massive, the beam was essentially terminated at the impedance
head. By locating it near the end of the beam, its effect
on the beam response could be minimized. A mechanical
impacting device was used to strike the impedance head. The
resulting force pulse, transmitted to the beam, was measured
and is shown in Fig. 3. It is essentially a symmetrical
triangle with a duration of approximately 0.25 msec.

Shown in Figs. 4(a) - 4(f) are the filtered, squared, and
averaged response (for different time constants of the low
pass filter network) of an accelerometer mounted 39 inches
from the impedance head. The maximum space averaged mean
square acceleration can be estimated from these curves. This
is possible because of the dispersion occurring. It, in effect,
causes all points to become typical (if we can wait long enough,
that is; the energy loss must not be so fast that dispersion
cannot effectively spread the energy spatially). Consider, for
example, Fig. 4(e). When the beam is struck, an energy packet
travels down it at the group velocity. At 4000 Hz, the group
velocity is approximately 2300 ft/sec. The first peak (for the
1 msec averaging time constant) occurs approximately 1.3 msec
after the first peak occurs at the accelerometer located very
near the input (it incidentally does not occur simultaneously
with the force). In another 0.6 msec, this packet strikes the
right end of the beam and is reflected. About 3 msec after the
first response at the accelerometer is noted, the mean square
acceleration levels outs, then decays slowly. The maximum space

averaged mean square acceleration is given by the maximum value
of this slowly decaying signal. It is indicated on the curves
by the dashed line labeled "LEVEL". That this is a good estimate
of the space average level can be seen directly from Fig. 4(e)
by comparing the solid curve (for the accelerometer at 39 inches)
with the broken curve, the response of the accelerometer at
25 inches. The responses at both points, at any instant after
the leveling out has occurred, are essentially the same. The
estimates for the maximum space averaged mean square accelerations,
based on the levels found in Figs. 4(a)-4(f) are given in Table I.
The estimates for the octave band energy spectrum, I, computed
from the response is also given. The "true" energy spectrum was
computed directly from the force pulse using the relation

$$I = \frac{F_o^2 \, T^2}{4} \, \frac{\sin^4(\frac{\omega T}{4})}{(\frac{\omega T}{4})^4} \Delta\omega \, . \qquad (24)$$

The results are compared in Fig. 5. Of course,
what has been used here in the prediction is the measured maximum
short time-space average of the squared acceleration resulting
from a source shock at only one input position. It is unlikely
that either the effects of beam damping or the change in the
beam dynamics due to the attached impedance head are dominant
in causing the 2 to 8 dB error which exists (the pulse length
is sufficiently short that the role which damping plays during
the forcing era must be negligible, the effect of damping is
probably greater during the time in which we wait for dispersion
to spread the energy uniformly along the beam so that measure-
ment at only one position will suffice). A more complete
experiment would have involved comparisons for a large number
of source locations.

Table I. Reverberant response of the impacted beam segment
of the cross to the symmetrical triangular pulse.

Octave Band Center Frequency	$\langle g^2 \rangle_{s,t}^{max}$	$I(lb^2-sec)$
250	0.025	7.9×10^{-6}
500	0.50	4.0×10^{-5}
1000	0.50	2.0×10^{-5}
2000	2.50	3.52×10^{-5}
4000	1.00	4.98×10^{-6}
8000	0.17	2.99×10^{-7}

III. SHOCK INDUCED WAVE TRANSMISSION IN A SIMPLE COUPLED BEAM SYSTEM

Theoretical and experimental studies to estimate the shock transmission between connected beams were performed with the beam-beam junction described in the preceding section. Excitation was provided by a point input off the center line of one beam segment.

A. Power Balance Equations

The structure is considered to consist of four discrete sets of modal oscillators. A power balance for any one of the four reverberant beam segments yields

$$\frac{dE_i}{dt} = \pi_i^{in} - \sum_{j \neq i} \pi_{ij}^{trans} - \pi_i^{diss} , \qquad (III-1)$$

where E_i is the short time average total energy of segment, I,

π_i^{in} is the time average input power for segment, i,

π_{ij}^{trans} is the time average power being transmitted,

and π_i^{diss} is the time average power dissipated in segment, i.

The power being dissipated is given by

$$\pi_i^{diss} = \eta_i \omega_i E_i \ , \qquad\qquad (\text{III-2})$$

and that being transmitted by

$$\pi_{ij}^{trans} = \omega \eta_{ij} n_i [\frac{E_i}{n_i} - \frac{E_j}{n_j}] \ , \qquad (\text{III-3})$$

where ω is the band center frequency, η_{ij} and η_i are the coupling and dissipative loss factors, and n_i is the beam modal density.

Here only the residual or free vibration period is considered. Thus, we take $\pi_i^{in} = 0$ and assume that at $t = 0$, the energy is diffused spatially in beam 1 and has a level, $E_1(0)$, and that the other beams are at rest.

For beam segment 1, Eq. III-1 becomes

$$\frac{d\theta_1}{dt} + \omega(\eta_1 + \eta_{12} + \eta_{13} + \eta_{14})\theta_1 - \omega\eta_{12}\theta_2$$

$$- \omega\eta_{13}\theta_3 - \omega\eta_{14}\theta_4 = 0 \ , \qquad\qquad (\text{III-4})$$

where $\theta_1 = E_1/n_1$.

Since the beams are identical, we have

$$n_i = n_j \, ,$$

$$n_{ij} = n_{ik} \; ; \; n_{ji} = n_{ki} \, , \qquad\qquad (III\text{-}5)$$

$$E_i = E_j \; ; \; i,j \neq 1 \, , \qquad\qquad (III\text{-}6)$$

$$n_i = n_j \, . \qquad\qquad (III\text{-}7)$$

Further, according to the consistency relations

$$n_i n_{ij} = n_j n_{ji} \, , \qquad\qquad (III\text{-}8)$$

and since $n_i = n_j$, it also follows that

$$\qquad\qquad\qquad\qquad (III\text{-}9)$$
$$n_{ij} = n_{ji} \, .$$

Thus the response of the cross is given by the two equations

$$[\frac{d}{dt} + \omega(n_1 + 3n_{12})]\theta_1 - 3\omega n_{12}\theta_2 = 0 \qquad\qquad (III\text{-}10)$$

$$- \omega n_{12}\theta_1 + [\frac{d}{dt} + \omega(n_1 + n_{12})]\theta_2 = 0 \, . \qquad\qquad (III\text{-}11)$$

The solution of these equations can be most conveniently obtained using Laplace transforms. The solutions are

$$\frac{E_1(t)}{E_1(0)} = \frac{e^{-\omega\eta_1 t}}{4} (3e^{-4\omega\eta_{12}t} + 1) , \qquad \text{(III-12)}$$

$$\frac{E_2(t)}{E_1(0)} = \frac{e^{-\omega\eta_1 t}}{4} (1 - e^{-4\omega\eta_{12}t}) . \qquad \text{(III-13)}$$

These relations hold for each of the various frequency bands.

B. Calculation and Measurement of Loss Factors

The value of the coupling loss factor depends upon the distribution of energy over the various mode forms of each segment. Assuming the input shock spectrum is relatively flat over a band of frequencies, $\Delta\omega$ (typically an octave or third-octave), the input energy is shared equally by all modes. If E is the total resonant energy in a beam then the energy in flexural modes E^f is

$$E^f = \left[\frac{n^f}{n^f + n^T + n^S + n^\ell}\right] E . \qquad \text{(III-14)}$$

where n^f, n^T, n^S and n^ℓ represent the modal densities of flexural, torsional, shear, and longitudinal modes respectively.

The modal densities are given by the following relations:[9]

Flexural modes (two planes)

$$n^f = \frac{\ell}{(2\pi\kappa c_\ell f^{1/2})}\left(1 + \sqrt{\frac{h}{w}}\right) \, , \qquad \text{(III-15)}$$

where h is the smaller of the beam dimensions (1/8-inch)

  ℓ is the length (5 ft)

  κ is the flexural radius of gyration (based on h)

and c_ℓ is the longitudinal wave speed (17,000 ft/sec)

Torsional modes

$$n^T = \sqrt{3}\ell w/c_\ell h \, . \qquad \text{(III-16)}$$

Shear modes

$$n^S = 2\sqrt{3}\ell/c_\ell \, . \qquad \text{(III-17)}$$

Longitudinal modes

$$n^\ell = 2\ell/c_\ell \, . \qquad \text{(III-18)}$$

With the assumed equipartition of modal energies, the distribution of energy over the various mode forms is shown in Fig. 6. This figure shows that the low-frequency behavior is dominated by flexural modes, and by torsional modes above about 8500 Hz. The energy in longitudinal and shear modes contribute, but insignificantly. Although these results cannot be considered universal, for the assumed flat spectrum as input, and for the slender beam, they are quite reasonable. On the basis

of these results, the longitudinal and shear modal energies are neglected. The coupling loss factor between the $i\underline{th}$ and $j\underline{th}$ beam segments is then given by

$$\eta_{ij} = \frac{\Pi_{ij}^{trans}}{\omega E_i} , \qquad (III-19)$$

where Π_{ij}^{trans} is power flowing from the $i\underline{th}$ segment into segment j which has been appropriately terminated (i.e., as if infinite as viewed from the junction), and

$$\eta_{ij} \equiv \frac{n_i^T \eta_{ij}^T + n_i^f \eta_{ij}^f}{n_i^T + n_i^f} ; \qquad (III-20)$$

where η_{ij}^T is the torsional coupling loss factor and η_{ij}^f is the flexural coupling loss factor.

Because of the cross configuration, we assume that Π_{ij}^{trans} is due to flexure only at the cross ($\eta_{ij}^T = 0$). The total energy is equiparted among the flexural and torsional modes after passing through the junction.

1. Computation of the coupling loss factor η_{ij}

The moment impedance of a semi-infinite beam is given by [10]

$$Z_j = (1 + i)\rho_{\ell j}\kappa_j^2 c_{\ell j}^2 c_{fj}^{-1} , \qquad (III-21)$$

where ρ_ℓ is lineal density

c_f is the flexural wave speed.

For the cross configuration (4 semi-infinite beams)

$$Z_T = 4(1 + i)\rho_{\ell j}\kappa_j^2 c_j^2 c_{fj}^{-1} .$$

If the $i\underline{th}$ segment is reverberant, the field in that segment is composed of a large number of standing waves, centered at frequency ω. If $X/2$ is the complex amplitude of a flexural wave incident upon the junction, the space-time mean-square displacement of the beam is

$$<x^2>_{s,t} = \frac{|X|^2}{4} \quad .$$ (III-22)

The complex incident angular velocity amplitude at the junction due to the incoming wave is related to the complex displacement amplitude by

$$\left| \dot{\theta}_i^{inc} \right|^2 = k_{fi}^2 \omega^2 \frac{|X|^2}{4}$$ (III-23a)

$$= k_{fi}^2 \omega^2 <x^2>_{s,t} \quad .$$ (III-23b)

This can be related to the total time average beam energy

$$E_{flex}^i = M_{beam} \omega^2 <x^2>_{s,t} \quad ,$$ (III-24)

or

$$E_{flex}^i = \frac{M \left| \dot{\theta}_i^{inc} \right|^2}{k_{fi}^2} \quad .$$ (III-25)

The power transmitted from i to j is given by

$$\Pi_{ij}^{trans} = Re[Z_j]<\dot{\theta}_j^2>_t \quad .$$ (III-26)

A moment, τ, applied to the cross by beam segment i induces an angular velocity of the cross

$$\dot{\theta}_{cross} = \dot{\theta}_i = \frac{\tau}{\sum\limits_{j \neq i} Z_j} = \dot{\theta}_j \quad .$$ (III-27)

The moment, $-\tau$, that the cross exerts on the beam yields a beam angular velocity $-\tau/Z_i$. Continuity at the junction requires

$$\dot{\theta}_i = \dot{\theta}_i^f - \tau/Z_i \quad , \tag{III-28}$$

where $\dot{\theta}_i^f$ = angular velocity at the end of segment i, if disconnected from the junction, and is given by

$$\dot{\theta}_i^f = 2\dot{\theta}_i^{inc} \quad . \tag{III-29}$$

From Eqs. III-27, 28

$$\dot{\theta}_i = \dot{\theta}_i^f - \left(\sum_{j \neq i} Z_j / Z_i \right) \dot{\theta}_i$$

or

$$\dot{\theta}_i = \frac{Z_i}{Z_T} \dot{\theta}_i^f = 2\dot{\theta}_i^{inc} \frac{Z_i}{Z_T} \quad . \tag{III-30}$$

Now

$$\Pi_{ij}^{trans} = Re[Z_j] \langle \dot{\theta}_j^2 \rangle_t$$

$$= Re[Z_j] \langle \dot{\theta}_i^2 \rangle_t$$

$$= 2Re[Z_j] \left| \frac{Z_i}{Z_T} \right| \left| \dot{\theta}_i^{inc} \right|^2 \quad . \tag{III-31}$$

From Eq. III-19, it follows that

$$\eta_{ij}^f = \frac{2k_{fi}^2}{\omega M_i} \left| \frac{Z_i}{Z_T} \right|^2 Re[Z_j] \quad . \tag{III-32}$$

Finally

$$\eta_{ij} = \frac{n_i^T \eta_{ij}^T + n_i^f \eta_{ij}^f}{n_i^T + n_i^f} = \frac{n_i^f}{n_i^T + n_i^f} \eta_{ij}^f \quad .$$

So that

$$\eta_{ij} \begin{pmatrix} \text{avg. torsional} \\ \text{and flexural} \\ \text{modes} \end{pmatrix} = \frac{n_i^f}{n_i^T + n_i^f} \frac{2k_{fi}^2}{\omega M_i} \left| \frac{Z_i}{Z_T} \right|^2 \text{Re}[Z_i] . \qquad \text{(III-33)}$$

2. Measurement of Coupling and Internal Loss Factors

The coupling loss factor, η_{ij}, was measured by terminating three of the beam segments. The decay of the energy in the ith segment from the steady state level, E_o is then given by

$$\frac{E_i}{E_o} = e^{-\omega \eta_i t} \cdot e^{-\sum_{j \neq i} \omega \eta_{ij} t}$$

$$= e^{-\omega(\eta_i + 3\eta_{ij})t} \qquad \text{(III-34)}$$

since all segments j are terminated. The internal loss factor for the ith segment was also measured for an identical (disconnected) segment and is shown in Fig. 7.

A comparison of the theoretical coupling loss factor and that experimentally measured is also shown in Fig. 7. The measured values were found to be bounded by Eqs. III-32, 33.

C. Calculated and Measured Energy Transmission Results

The analytical predictions of the energy as a function of time in the driven and undriven beams given by Eqs. III-12, 13 are plotted in Figs. 8 and 9 respectively using the measured values of the coupling and dissipation loss factors shown in Fig. 7.

The short time average energies of the driven and undriven beams were measured using the experimental configuration shown in Fig. 2. The response of the undriven beam for the octaves centered at 2, 4, and 8 kHz is shown in Fig. 10.

The calibration is 2 volts/g^2 as in Part III. The curves shown are for a typical point on beam 2, and represent the space averaged, mean square response. The curves are labeled according to the time constant of the low pass filter network.

The theoretical predictions given in Fig. 9 can be mapped on to Fig. 10. We have

$$\frac{E_2(t)}{E_1(0)} = \frac{M_2 \langle a_2^2 \rangle_{s,t}/\omega^2}{M_1 \langle a_1^2 \rangle_{s,t}^{max}/\omega^2} \qquad . \qquad (III-35)$$

Since $M_1 = M_2$

$$\frac{E_2(t)}{E_1(0)} = \frac{\langle g_2^2 \rangle_{s,t}}{\langle g_1^2 \rangle_{s,t}^{max}} \qquad . \qquad (III-36)$$

The maximum short time-space averaged square of the response acceleration of beam 1 is given in Table I of Part II. The mapping is

$$[E_2(t)/E_1(0)] \times \langle g_1^2 \rangle_{s,t}^{max} \times 2 \text{ volts/}g^2 \Big/ \begin{array}{l} \text{Voltage scale of} \\ \text{Figs. 4(d)-4(f)} \end{array} \qquad .$$

$$(III-37)$$

The results are shown in Figs. 10(a) - 10(c). In each
case, the shape of the curve is predicted very well, as
is its duration. The levels are reasonably accurate.
The 2000 Hz case is almost perfectly predicted. The
levels of the prediction for the other two cases are
lower than experimentally observed, by factors of two
to four. Since these are ratios of energies, this re-
presents a 3 to 6 dB error.

IV. SHOCK TRANSMISSION IN A MODEL RING-STRINGER STIFFENED CYLINDER

A. Statistical Energy Analysis (SEA) of Pyrotechnic Shock Bending Energy Transmission

This problem is amenable to SEA because the high-frequency energy content of a pyrotechnic shock excites a large number of vibration modes. However, in using SEA we must be careful to distinguish between the direct shock pulse and the reverberant vibration buildup and decay.

The direct pulse is that part of the pyrotechnic shock which propagates along the structure without reflection. At each discontinuity in the structure part of the energy of the direct pulse is reflected and forms the reverberant vibration field. SEA can be used to study the reverberant vibration field. However, classical wave propagation techniques must be used to study the direct pulse. The direct pulse may consist of both bending and dilatational energy, but the bending energy in the direct pulse is attenuated rapidly by discontinuities and therefore is generally unimportant. In this section, we investigate the reverberant bending energy field, and in Section D we return to the direct dilatational wave and its scattering into bending waves.

The use of SEA results in a more simplified formulation of the shock transmission problem than would use of a more classical approach. However, the SEA formulation for shock transmission in a cylindrical shell with many ribs and stringers is still quite complex because of the large number of structural sub-elements required in the formulation. Because of this complexity we will study, first, a number of simplified problems involving ribbed plates. Solution of these problems will give us some basic

insight into shock transmission in a cylindrical shell with many ribs and stringers. Then, we will use this insight to gain an understanding of the more complex problem.

The steps involved in SEA are:

1. Divide the complete structural assembly being studied into groups of modes;
2. Determine the paths of energy exchange;
3. Write the power balance equations for each group of modes;
4. Compute the required input powers, coupling loss factors, damping loss factors and modal densities;
5. Solve the power balance equations for the modal energies in each mode group;
6. Relate the modal energies to the response variable of interest.

Each of these steps will be discussed in turn for the particular problems under consideration.

The first problem which we will consider is shock transmission in a plate across a number of beams which divide the plate into subelements as shown in Fig. 11. The beams shown have rectangular cross-sections. However, our analysis will be equally valid for "T", "I", "U", "L" or other cross-sections.

The first step of SEA is to divide the structure into groups of modes. This step is accomplished in two parts. First, the complete structural assembly is divided into structural subelements. Then, the modes of the subelements are futher divided into groups of similar modes--similar to the extent that they have

resonance frequencies in the same band of frequencies, are similarly coupled to modes in other groups, have nearly equal damping loss factors and are similarly excited by external sources of vibration.

The division of the complete assembly into structural subelements is quite obvious for the problem at hand, as it is for most problems. The subelements of the ribbed plate consist of each subpanel and beam.

Although the division into subelements is usually obvious, the choice of boundary conditions for each subelement is not. The boundary conditions must be selected so that the motion of the complete assembly in a given frequency band can be accurately described by the collective motion of all substructure modes which have resonance frequencies in the band. A technique which insures the correct choice of boundary conditions for each substructure will be used in computing the coupling loss factors.

The division of the substructure modes into groups of similar modes requires much insight and some idea as to the power input, coupling and damping of each mode. This second division is particularly difficult for the problem under consideration because the coupling between modes of the beams and the modes of the subpanels can vary significantly for the different subpanel modes because of wave coincidence effects.

Ungar[11] and Heckl[10] have studied beam-plate structures like that shown in Fig. 11. Ungar obtained expressions for the vibration transmission across infinite beam-plate structures, Fig. 12a. These expressions show that the ratio of power transmitted, Π_{trans}, to the power incident, Π_{inc}, for steady state vibration

at a given frequency depends strongly on the angle of incidence
(a typical result is shown in Fig. 12b).In general,* two large
peaks occur at which $\Pi_{trans} = \Pi_{inc}$. These peaks occur at angles
where the trace wavelength of the incident wave equals the free
bending wavelength or the free torsional wavelength in the beam
(conditions of wave coincidence.) For waves with angles of
incidence less than these coincidence angles, the vibration
transmission is governed by the density per unit length and the
rotational moment of inertia of the beam. For waves with angles
of incidence above the coincidence angles, the vibration trans-
mission depends on the bending and torsional stiffness of the
beam. Angles of incidence between the two coincidence angles
represent a mixed condition.

Heckl [10] has found a similar result for beam-plate structures
infinite in one direction and simply supported along two lines
in the other direction, Fig. 13a.Two large peaks in the ratio of
power transmitted to power incident occur for a given mode
shape in the transverse (y) direction at the resonance frequen-
cies of the bending and torsional modes with the same mode shape
in the y direction (a condition of wave coincidence). A typical
result is shown in Fig. 13b.

We conclude, based on Ungar's and Heckl's results, that in a
given frequency band some of the resonant plate modes can be
well coupled to beam modes while other modes are not. Strictly
speaking, however, this result is limited to beam plate
configurations in which the beam mode shapes agree identically

---

*It is possible for only one peak to occur. This happens when the
bending wavespeed in the beam equals the torsional wavespeed.

with the y dependence of some of the plate modes. This
condition only occurs when the plate and beam boundary conditions
are simple supports. For other more realistic boundary
conditions the beam mode shapes will differ from the y de-
pendence of the plate mode shapes in the "edge correction
terms" (exponential terms, $e^{-\alpha}$ and $e^{-\alpha(L-x)}$, in the bending mode
shapes.) Because of the differences in these edge correction
terms, each mode in the plate will be coupled to some extent
with each mode of the beam. The extent of the coupling depends,
of course, on the exact mode shapes and resonance frequencies
of the beam and plate modes. The coupling between a beam mode
and various plate modes will be more uniform at low frequencies
where the wavelength of the beam vibration is comparable to the
length of the beam, since then the edge correction terms will
enter more significantly into the mode shape.

The difference in the edge correction terms for the beam and the
plate also tend to couple the modes of the plate (we mean here
the modes of the plate with three edges simply-supported and
the four edge clamped.)

We now come to a branching point in our analysis. We can solve
exactly an idealized model of the beam-plate structure following,
for example, Ungar's approach [12], or we can make some hypotheses
about the type of vibration field in the structure and follow the
SEA approach. In this report we follow the latter approach.
We hypothesize that each mode of the subpanels with a resonance
frequency in a given octave band has the same energy (equiparti-
tion of energy). We further hypothesize that each beam bending
mode with a resonance in a given octave band will be strongly
coupled to beam torsional modes and will have the same modal

energy. With these two hypotheses the division of the modes
into groups is straight-forward. Modes with resonance frequencies
in a given octave band should be divided into subpanel modes
and beam modes. We group beam bending modes and torsional modes
together since, by hypothesis, they have the same modal energy.
The division is shown in Fig. 14.

The second step of SEA is to determine the paths of energy
exchange. One path is obvious. This path is between the subpanel
modes and the beam modes. A second path is less obvious. The
modes of adjacent subpanels will be coupled through nonresonant
motion of beam bending and torsional modes with resonant fre-
quencies below the frequency band of interest. The paths of
energy exchange are shown in Fig. 14.

The third step of SEA is to write the power balance equations.
·For the i th plate we write

$$\Pi_{P_i}^{(in)} = \Pi_{P_i}^{(diss)} + \sum_{j=i,i-1} \Pi_{P_i, B_j}^{(trans)}$$

$$+ \sum_{j=i-1,i+1} \Pi_{P_i, P_j}^{(trans)} + \frac{d}{dt} E_{P_i}$$

(IV-1)

where $\Pi_{P_i}^{(in)}$ is the short time-average power input from external
sources in the octave band $\Delta\omega$, $\Pi_{P_i}^{(diss)}$ is the short time-
average power transmitted to other groups of modes and E_{P_i} is the

short time-average vibratory energy in plate i. By "short time-average" we mean an average over a few cycles of vibration at the band center frequency.

For the i th beam we write

$$\Pi_{B_i}^{(in)} = \Pi_{B_i}^{(diss)} + \sum_{j=i,i+1} \Pi_{B_i,P_j}^{(trans)}$$

$$+ \frac{d}{dt} E_{B_i} \quad , \tag{IV-2}$$

where the power and energy variables are short time-averages.

The power input in Eqs. IV-1,2 is the power input from two sources. First it includes the power input from the pyrotechnic device, if any, which acts on the i th element, and second, it includes the power to the reverberant field from the direct shock pulse. The remaining power and energy variables can be related to the modal energies through a loss factor and a modal density. The power dissipated is given by

$$\Pi_i^{(diss)} = \omega \eta_{i,diss} \, n_i \, \Delta\omega \, \theta_i \quad , \tag{IV-3}$$

where ω is the band center frequency, $\eta_{i,diss}$ is the dissipation loss factor, n_i is the modal density and θ_i is the modal energy. The power transmitted is given by

$$\Pi_{i,j}^{(trans)} = \omega \, \eta_{i,j} \, n_i \Delta\omega(\Theta_i - \Theta_j) \, , \qquad (IV-4)$$

where $\eta_{i,j}$ is a coupling loss factor. It follows from Eq. IV-4 that since $\Pi_{i,j}^{(trans)} = \Pi_{j,i}^{(trans)}$

$$\eta_{i,j} \, n_1 = \eta_{j,i} \, n_j \, . \qquad (IV-5)$$

This result is often useful in simplifying the power balance equations.

The total energy is written

$$E_i = n_i \, \Delta\omega \, \Theta_i \, . \qquad (IV-6)$$

With these results we can write Eqs. IV-1,2 as

$$\frac{d\Theta_{P_i}}{dt} + \eta_{P_i,diss} \Theta_{P_i} + \sum_{j=i,i-1} \eta_{P_i,B_j} (\Theta_{P_i} - \Theta_{B_j})$$

$$+ \sum_{j=i-1,i+1} \eta_{P_i,P_j} (\Theta_{P_i} - \Theta_{P_j}) \qquad (IV-7)$$

$$= \frac{1}{\omega n_{P_i} \Delta\omega} \Pi_{P_i}^{(in)} \, ,$$

and

$$\frac{d\theta_{B_i}}{dt} + \eta_{B_i,diss}\,\theta_{B_i} + \sum_{j=i,i+1} \eta_{B_i,P_j}(\theta_{B_i} - \theta_{P_j})$$

$$= \frac{1}{\omega n_{B_i} \Delta\omega}\,\Pi_{B_i}(in) \ . \qquad\qquad (IV-8)$$

Eqs. IV-7,8 are the basic SEA equations describing the beam-plate structure. To find a history of the short time-average modal energy we solve the coupled differential equations. However, we must first calculate the required loss factors, modal densities and input powers. The fourth step of SEA is to calculate these needed variables.

The modal density of a flat panel is found in Ref. 5 to be

$$n_{P_i}(\omega) = \frac{1}{4\Pi}\frac{A_{P_i}}{(\kappa c_\ell)_{P_i}} \ . \qquad\qquad (IV-9)$$

where A_{P_i} is the area of the subpanel, κ is its radius of gyration and c_ℓ is the longitudinal wavespeed in the panel. In terms of a bending moment of inertia we can write

$$\kappa c_\ell = \frac{EI}{\rho_s} \ , \qquad\qquad (IV-10)$$

where E is Young's modulus, I is the bending moment of inertia, and ρ_s is the density per unit area of the panel.

The modal density of the beams in our problem is taken to be the sum of the modal densities of bending and torsional modes,

$$n_{B_i}(\omega) = n_{BB}(\omega) + n_{BT}(\omega) \, , \qquad \text{(IV-11)}$$

where $n_{BB}(\omega)$ is the density of bending modes and $n_{BT}(\omega)$ is the density of torsional modes. These two modal densities are found in Ref. 5 to be

$$n_{BB}(\omega) = \frac{1}{2\pi} \frac{L}{(\omega \kappa c_1)^{1/2}} \, , \qquad \text{(IV-12)}$$

and

$$n_{BT}(\omega) = \frac{1}{\pi} \frac{L}{c_t} \, , \qquad \text{(IV-13)}$$

where L is the length of the beam and c_t is the torsional wave-speed in the beam.

The dissipation loss factors are impossible to calculate unless a special damping treatment has been applied to the structure.

Thus, we must rely either on measurements or on empirical
estimates of the damping loss factor. For this problem we will
take

$$\eta_{B_i, \text{diss}} = 0 , \qquad\qquad\qquad (IV-14)$$

and

$$\eta_{P_i, \text{diss}} = 10^{-2} . \qquad\qquad\qquad (IV-15)$$

The coupling loss factor between a beam and a subpanel used in
Eqs. IV-7,8 is a composite loss factor accounting for power
exchange between the plate modes and both bending and torsional
modes of the beam. Since we have assumed equipartition of energy
between the bending and torsional modes, we can write this
composite coupling loss factor as

$$\eta_{B_i, P_i} = \frac{\eta_{BB}}{\eta_{BB} + \eta_{BT}} \eta_{BB,P} + \frac{\eta_{BT}}{\eta_{BB} + \eta_{BT}} \eta_{BT,P} , \qquad (IV-16)$$

where $\eta_{BB,P}$ is the coupling loss factor between bending modes of
the beam and the subpanel modes, $\eta_{BT,P}$ is the coupling loss
factor between torsional modes of the beam and the subpanel modes

n_{BB} is the modal density of bending modes and n_{BT} is the modal density of torsional modes in the beam. The modal densities are given by Eqs. IV-12,13.

In calculating the coupling loss factors, $\eta_{BB,P}$ and $\eta_{BT,P}$, we can use either a mode by mode computational approach or a wave-impedance approach. Because of its simplicity we choose the wave-impedance approach. Using this approach to compute $\eta_{BB,P}$ we prescribe the motion of the beam as

$$v_B (x,t) = V_i \, \psi_i (x) \, e^{i\omega_i t} \quad , \qquad (IV-17)$$

where v_B is the velocity of the beam in a direction normal to the subpanels, V_i is a complex amplitude, $\psi_i(x)$ is the i th mode shape and ω_i is the i th mode resonance frequency. The force between the beam and the subpanels due to this prescribed motion can be written as

$$f_{BP} (x,t) = e^{i\omega_i t} \sum_j F_j \, \psi_j(x) \quad , \qquad (IV-18)$$

where F_j are complex amplitudes to be determined and $\psi_j(x)$ is the j th mode shape of the beam. Using a generalized impedance formulation we can write

$$F_j = Z_{ji} \, V_i \quad , \qquad (IV-19)$$

where Z_{ji} is the impedance (normally a function of frequency).
The time-average power radiated from the beam to one subpanel
can be written in terms of this impedance as

$$\Pi_{in} = \frac{1}{4} |V_i|^2 \, \text{Re} \, Z_{ii}(\omega_i) \int_0^{L_B} dx \psi_i^2(x) \, , \qquad (IV-20)$$

where L is the length of the beam. In deriving Eq. IV-20 we
have made use of the orthogonality of the mode shapes. By
proper normalization of the mode shapes we can write Eq. IV-20
as

$$\Pi_{in} = \frac{1}{4} |V_i|^2 \, L_B \, \text{Re} \, Z_{ii}(\omega_i) \, . \qquad (IV-21)$$

Equation IV-21 gives the time-average power input from the
ith bending mode of the beam to one subpanel. To find the
coupling loss factor we must average Eq. IV-21 over all bending
modes of the beam with resonant frequencies in the band $\Delta\omega$.
Then by analogy to the basic power flow relation, Eq. IV-4,
we can write

$$\eta_{BB,P} = \frac{1}{2m_B\omega} \, \text{Re} \, \overline{Z_{ii}(\omega_i)} \qquad (IV-22)$$

where $\overline{Z_{ii}(\omega_i)}$ is the impedance averaged over all bending modes of
the beam with resonant frequencies in the band $\Delta\omega$ and m_B is the
mass per unit length of the beam. If the spatial variations of

the mode shapes $\psi_i(x)$ have a scale which is long compared to the bending wavelength in the plate at ω_i, the impedance $Z_{ii}(\omega_i)$ will be approximately equal to the line impedance of the subpanel,

$$Z_{ii}(\omega_i) \approx Z_{line}(\omega_i) \; . \tag{IV-23}$$

If we assume that the resonance frequencies of the beam are random variables distributed in frequency as a Poisson process, we can replace the average over modes with an average over frequency. Then, if we futher assume that the bandwidth $\Delta\omega$ encompasses many resonances of the subpanel we can replace the frequency average value of the impedance with that of an infinite subpanel. With these steps Eq. IV-22 becomes

$$\eta_{BB,P} = \frac{1}{2m_B\omega} \; Re \; Z_{line,inf}(\omega) \; , \tag{IV-24}$$

where $Z_{line, inf}$ is the line impedance of an infinite panel and ω is the band center frequency. The line impedance of the infinite panel is well known yielding the result

$$\eta_{BB,P} = \frac{m_P}{m_B} \frac{1}{k_P} \; , \tag{IV-25}$$

where m_P is the mass per unit area of the panel and k_P is the free bending wavenumber in the panel.

Following an identical approach we find the coupling loss factor
between torsional modes in the beam and the subpanel modes to be

$$\eta_{BT,P} = \frac{m_P}{\rho_B I_B} \frac{1}{k_P^3} ,$$

(IV-26)

where ρ_B is the material density in the beam and I_B is the rota-
tional moment of inertia of the beam.

The coupling loss factors given by Eqs. IV-25,26 along with the
modal densities given by Eqs. IV-12,13 can be used in Eq. IV-16 to
calculate the composite coupling loss factor between a beam and
a subpanel.

Finally, we must calculate the coupling loss factor between modes
of adjacent subpanels through nonresonant motion of the beam.
Calculation of this coupling loss factor is made quite difficult
because of the coherance between nonresonant bending and tor-
sional motion of the beam. As for our previous calculations we
will use the wave-impedance approach in calculating this coupling
loss factor. Following this approach we replace the finite beam-
plate structure by the infinite structure shown in Fig. 15. Our
assumption, made previously, that every subpanel mode has the
same energy allows us to represent the subpanel vibration field
by a diffuse field in each semi-infinite subpanel. The diffuse
field consists of incoherent bending waves traveling in every
direction. Waves traveling in different directions have the same
amplitude so that the panel mean-square velocity at a point $\underline{x}$
can be written as

$$\langle v^2(\underline{x},t)\rangle_{t,\Delta\omega} = \langle v_0^2\rangle_{t,\Delta\omega} \int_0^{2\pi} d\theta \quad , \tag{IV-27}$$

where $\langle v_0^2\rangle_{t,\Delta\omega} d\theta$ is the mean-square velocity of waves with
frequencies in the band $\Delta\omega$ incident from the angles θ to $\theta + d\theta$.
We see from Eq.IV-27 that the mean-square velocity in the band $\Delta\omega$
does not depend on the value of $\underline{x}$. By assuming a diffuse field
we can compute the power transmitted from one subpanel to the
other using Ungar's results. The mean-square velocity of the
transmitted wave is related to the mean-square velocity of the
incident wave by a transmission coefficient, τ,

$$\langle v_{trans}^2(\theta)\rangle_{t,\Delta\omega} = \tau(\theta,\omega) \langle v_{inc}^2(\theta)\rangle_{t,\Delta\omega} . \tag{IV-28}$$

In general the transmission coefficient varies both as a func-
tion of θ and as a function of ω. We have assumed that $\Delta\omega$ is
small so that the value of $\tau(\theta,\omega)$ at the band-center-frequency
is used in Eq.IV-28. Ungar presents expressions for the trans-
mission coefficient. Typically, they appear as in Fig. 16
with large peaks occurring at angles corresponding to coincidence
between incident waves and bending waves in the beam and between
incident waves and torsional waves in the beam. The transmission
coefficient for angles above the coincidence angles, Region V in
Fig. 16, is governed by the bending and torsional stiffness of
the beam and is typically very small. The transmission coeffi-
cient in Regions II and IV is large because in these regions the

motion of the beam is resonant (either in bending or torsion). However, since we have already obtained coupling loss factors for resonant bending and torsional motion of the beam, we will ignore these regions here. In Region I the transmission coefficient is governed by the mass density per unit length and the rotational moment of inertia of the beam. In Region III, the transmission coefficient is governed by the rotational stiffness and the mass density per unit length if the angle of coincidence for bending modes is greater than that for torsional modes; or by the bending stiffness and the rotational moment of inertia if the angle of coincidence for bending modes is less than that for torsional modes.

To compute the transmission of energy via nonresonant motion of the beam, we will neglect transmission from waves with angles of incidence in Region V. Furthermore we will approximate the value of the transmission coefficient for angles below the largest coincidence angles by its value at $\theta = 0$, normal incidence to the beam. The approximation is shown in Fig. 16. With this approximation the average power transmitted across length L_B of the beam is given by

$$\Pi_{trans} = m_P \langle v_0^2 \rangle_{t,\Delta\omega} \; c_{b,P}(\omega) \; \sin\theta_{lim} \; \tau(o,\omega) \; L_B \,, \quad (IV\text{-}29)$$

where θ_{lim} is the largest coincidence angle and $c_b(\omega)$ is the bending wavespeed in the subpanel. From Ref.10 we find

$$\tau(0,\omega) = \left[1 + \left(\frac{\alpha_n - \beta_n - 2}{\alpha_n\beta_n - \beta_n + \alpha_n} \right)^2 \right]^{-1} \,, \quad (IV\text{-}30)$$

where

$$\alpha_n = 4 \frac{m_P}{m_B} \frac{1}{k_P} \quad, \tag{IV-31}$$

and

$$\beta_n = 4 \frac{m_P}{\rho_B I_B} \frac{1}{k_P^3} \quad. \tag{IV-32}$$

We can write the time-average energy in an area A_p of the panel as

$$E_P = m_P A_P \ 2\pi \ \langle v_0^2 \rangle_{t,\Delta\omega} \quad. \tag{IV-33}$$

It follows then, from Eqs. IV-29,33 and from the definition of the coupling loss factor, that

$$\eta_{P_i,P_{i+1}} = \frac{L_B \ \sin \Theta_{lim} \ \tau(0,\omega)}{2\pi \ k_P \ A_P} \quad. \tag{IV-34}$$

We have now completed step 4 of SEA.

The next step, step 5, is to solve the power balance equations,
Eqs. IV-7,8 : These equations take the form

$$\frac{d\Theta_i}{dt} - \sum_j \eta_{ij} \Theta_j = \frac{\Pi_i}{\omega n_i \Delta\omega} \quad , \tag{IV-35}$$

where, by convention,

$$\eta_{ii} = -\eta_{i,diss} - \sum_j \eta_{ij} \quad , \tag{IV-36}$$

and Θ_i represents the short-time-average modal energy in group i,
η_{ij} is a coupling loss factor between group i and group j,
n_i is the modal density of group i, ω is the band center fre-
quency, $\Delta\omega$ is the bandwidth and Π_i is the short-time-average
power input to group i.

Since all modal energies can be set to zero at t=0, a Laplace
transform solution is quite simple, at least conceptually. By
taking the Laplace transform of Eq. IV-35 we obtain a set of
linear algebraic equations which can be solved for the Laplace
transform of each modal energy. Inverse transformation into the
time domain can be difficult if there are many mode groups.
However, in most cases sufficient simplifications can be made
that the inverse transformation can be accomplished.

The sixth and last step of SEA is to relate the short-time-
average modal energies to the response variable of interest.

Since we have assumed the vibration of each group of modes to be resonant, the short-time-average kinetic energy equals the short-time-average potential energy in each structure. Thus, we can write

$$n_{P_i} \theta_{P_i} = m_{P_i} A_{P_i} \langle v_{P_i}^2(\underline{x},t) \rangle_{t,\Delta\omega,\underline{x}}$$

(IV-37)

$$= 3 E_{P_i} A_{P_i} \langle \varepsilon_{P_i}^2(\underline{x},t) \rangle_{t,\Delta\omega,\underline{x}} \quad ,$$

where $\langle v_{P_i}^2(\underline{x},t) \rangle_{t,\Delta\omega,\underline{x}}$ is the short-time-average space-average velocity squared in the band $\Delta\omega$ for plate P_i, E_{P_i} is Young's modulus and $\langle \varepsilon_{P_i}^2(\underline{x},t) \rangle_{t,\Delta\omega,\underline{x}}$ is the short-time-average space-average strain squared in the band $\Delta\omega$ on the surface of plate P_i. We can write similar expressions for each beam.

If the frequency bandwidth $\Delta\omega$ is an octave or less we can write

$$\langle a_{P_i}^2(\underline{x},t) \rangle_{t,\Delta\omega,\underline{x}} \simeq \omega^2 \langle v_{P_i}^2(\underline{x},t) \rangle_{t,\Delta\omega,\underline{x}} \quad ,$$

(IV-38)

and

$$\langle d_{P_i}^2(\underline{x},t) \rangle_{t,\Delta\omega,\underline{x}} \simeq \frac{1}{\omega^2} \langle v_{P_i}^2(\underline{x},t) \rangle_{t,\Delta\omega,\underline{x}} \quad .$$

(IV-39)

where a($\underline{x}$,t) is the acceleration, d($\underline{x}$,t) is the displacement, and ω is the band center frequency.

In many problems of practical interest, one needs more than spatial-average response estimates. For example, one may only be interested in the response at one point or in the response at a point where stress concentrations are known to occur. Lyon [13] has developed procedures to estimate spatial response concentrations based on the spatial-average estimates for steady-state vibrations. Whether his results can be used for the transient case or not is unclear at the present time.

B. Experimental Study of Shock Bending Energy Transmission

A number of experiments have been carried out to determine the transmission of bending wave energy across ribs and stringers on the model ring-stringer stiffened cylinder shown in Fig. 17. A point impulsive source was used to inject energy into one subpanel of the shell at t = 0. Acceleration time-histories were obtained at the center-point of each subpanel and at a number of points on the ribs and stringers using the test set-up shown in Fig. 18. A number of recorded acceleration time-histories are shown in Figs. 19-29. The measured attenuation of the bending-wave shock from subpanel to subpanel is compared with measured values for attenuation of *steady-state* bending-wave vibrations and with SEA predictions in Section IV-C of this report.

The set-up shown in Fig. 18 for the shock transmission experiments utilized a Tektronix pulse generator to generate an electronic pulse 50 μsec in duration. This pulse was then fed into a MacIntosh 40 watt ac power amplifier. Output from the power

amplifier was used to excite a point-drive mechanical shaker
connected to the center-point of one subpanel (panel 4-2)
shown in Fig. 17. The orientation of the applied force
was normal to the subpanel so that excitation of longitudinal
waves in the shell would be negligible. The frequency
response of the power amplifier and shaker is nominally flat,
±3 dB from 50 Hz to 10,000 Hz. Thus, the shape of the elec-
tronic impulse -- which has a Fourier amplitude spectrum
that is flat from 0 Hz to 20,000 Hz -- was somewhat altered
in being converted into an applied force on the cylindrical
shell. Since the frequency range in which we took measurements
was within the 50 Hz to 10,000 Hz limits, the loss of signal
energy outside of this range was not important. The phase
response of the power amplifier-shaker combination is not
known. However, by driving a simple mass with the shaker,
it was determined that the decay-rate of the impulse response
of the shaker is at least an order of magnitude faster than
the measured vibration decay-rate on the driven subpanel
for all frequencies in the 50-10,000 Hz range. Therefore,
we can consider the force applied to the subpanel to be
impulsive.

Acceleration measurements were taken using a B & K 2 gm.
accelerometer. The accelerometer output was conditioned
and amplified using a General Radio Sound Level Meter and
then filtered into octave bands using a General Radio Filter
Set. The filtered acceleration signal was attenuated by
a HP-variable attenuator and displayed on a Tektronix oscilloscope.
The attenuator was used to change the level of the displayed
signal in controlled 1 dB steps so that visual selection
of the peak acceleration envelop amplitude could be easily
made. The frequency response of the acceleration measurement

system is flat (±3 dB) over the range 50-20,000 Hz. The transient response is sufficiently accurate to measure the slowly varying envelopes of the observed acceleration signal. Mass loading of the subpanels by the 2 gm. accelerometer is not significant in the frequency range of interest.

The measurement procedure was to excite the shell with periodic impulses. The interval between pulses was made long enough that the vibration resulting from one pulse decayed almost to zero before the next pulse. The pulse input to the shaker was used to trigger the oscilloscope sweep so that the complete response time-history could be observed. Acceleration measurements were taken by mounting the accelerometer on the structure with Duc-Seal -- a special clay. This mounting technique is valid for lightweight accelerometers which are not to be excited to high g levels. Gain on the accelerometer output was adjusted using the GR Sound Level Meter and HP attenuator so that the peak of the acceleration envelope was 3 cm from zero on the oscilloscope display.

Acceleration measurements were taken at a number of points on the cylindrical shell. A code was used to number each subpanel, rib segment, and stringer segment as shown in Fig. 17. Using this code panel i-j is the ith circumferential subpanel and the jth longitudinal subpanel of the shell. For the test structure used there are 8 stringers so that i = 1 to 8 and 4 rings -- including each end ring -- so that j = 1 to 3. The excited subpanel is panel 4-2. Ring and stringer segments are identified by the subpanels they separate. Ring segment 4-2/4-1 is between panels 4-2 and 4-1. Stringer segment 4-2/5-2 is between panels 4-2 and 5-2.

All panel measurements, except those on the excited panel, were taken at the center point of the panel. Measurements at the center point of the excited panel, panel 4-2, could not be taken because of space limitations near the shaker attachment point. Thus, measurements at 3 points on panel 4-2 were taken. The location of these 3 points was selected randomly.

All ring and stringer measurements were taken at the mid-point of each ring or stringer segment. The orientation of the accelerometer was such as to measure acceleration in the radial direction -- normal to the surface of the shell. Measurements of the torsional motion of each segment were not taken.

Figures 19-29 show photographs of the oscilloscope traces with a smoothed-signal envelope superimposed. The envelope curves were drawn in after visual inspection of the time-histories. These curves do not follow the signal envelope exactly. They represent a best effort at smoothing out the fluctuations in signal amplitude. These seemingly random fluctuations result from complex interactions of the different frequency components of the shock. SEA does not take into account these complex interactions and, therefore, cannot predict the extent of the resulting fluctuations.

The photographs in Figs.19-29 show typical characteristics of pyrotechnic shock pulses. As the measurement point is moved away from the point of excitation -- the peak of the shock envelope is at a lower level of vibration and occurs later.

C. Comparison of Transient and Steady-State Bending Energy Decay from Substructure to Substructure

1. Simplified Solution to the Transient Power Balance Equations

The use of SEA for transient problems leads to a set of ordinary differential equations describing the dynamic behavior of a complex structure (see Section IV.A). This set of equations is much easier to solve than the partial differential equations of motion. However, solution of the SEA equations is still quite difficult and often requires use of analog or digital computational facilities.

SEA is often used in the design stage of a vehicle to obtain vibration estimates for the structure. In such a case, an exact solution to the SEA transient power balance equations is not needed. In this section a simplified solution to the SEA equations is found. This solution is based on approximations which in many cases of practical interest are valid. It will show that the decrease in peak vibration envelope levels from bay to bay of the ring-stringer stiffened cylinder for transient excitation equals the decrease in steady-state vibrations.

To show the above result we consider the case in which shock transmission takes place in a chain of coupled substructures. The first element of the chain is excited by an impulsive source. Thus, the transient power balance equation for the first element is

$$n_1 \frac{d\theta_1}{dt} + \omega n_1 n_1 \theta_1 + \omega n_{12} n_1 (\theta_1 - \theta_2) = E_o \delta(t) \quad , \qquad \text{(IV-40)}$$

where θ_1 is the modal energy in element 1, η_1 is the damping loss factor, η_{12} is the coupling loss factor between elements 1 and 2, n_1 is the modal density of element 1, E_o is the total energy injected into the element from external sources, and $\delta(t)$ is the impulsive Dirac-Delta function

$$\int_{-\varepsilon}^{\varepsilon} dt\ \delta(t) = 1 \quad , \qquad (\text{IV-41})$$

where ε is arbitrarily small.

The transient power balance equations for the second and all other elements except the last is

$$n_i \frac{d\theta_i}{dt} + \omega\eta_i n_i \theta_i + \omega\eta_{i,i+1}\ n_i(\theta_i - \theta_{i+1})$$

$$(\text{IV-42})$$

$$= \omega\eta_{i,i-1}\ n_i(\theta_{i-1} - \theta_i)$$

where i refers to a particular element in the chain, i-1 is the element closer to the source, and i+1 is the element further away from the source. For the last element in the chain the transient power balance equation is

$$n_N \frac{d\theta_N}{dt} + \omega\eta_N n_N \theta_N = \omega\eta_{N,N-1}\ n_N(\theta_{N-1} - \theta_N) \ , \qquad (\text{IV-43})$$

where N refers to the last element in the chain.

Equations IV-40-42 can be simplified if the ratio

$$\frac{n_{i,i-1}}{n_{i,t}} \ll 1 \quad , \qquad (\text{IV-44})$$

where

$$\eta_{i,t} = \eta_i + \eta_{i,i-1} + \eta_{i,i+1} \quad , \tag{IV-45}$$

for all values of i. When Eq. IV-44 holds a perturbation solution in the variables $\eta_{i,i-1}/\eta_{i,t}$ can be obtained which shows that the power flowing from element i to element i+1 is small compared to the power dissipation in element i. Then Eq. IV-40 can be simplified to

$$n_1 \frac{d\theta_1}{dt} + \omega \eta_1 n_1 \theta_1 = E_0 \delta(t), \text{ if } \frac{\eta_{12}}{\eta_1} \ll 1 \ . \tag{IV-46}$$

Equation IV-42 can be simplified to

$$n_i \frac{d\theta_i}{dt} + \omega \eta_i n_i \theta_i = \omega \eta_{i,i-1} n_i \theta_{i-1}, \text{ if } \frac{\eta_{i,i+1}}{\eta_i} \ll 1 \quad , \tag{IV-47}$$

and Eq. IV-43 can be simplified to be

$$n_N \frac{d\theta_N}{dt} + \omega \eta_N n_N \theta_N = \omega \eta_{N,N-1} n_N \theta_{N-1} \quad . \tag{IV-48}$$

If we further assume that all elements in the chain are equally damped,

$$\eta_i = \eta \text{ for all i} \quad , \tag{IV-49}$$

Eqs. IV-46 through IV-48 can be solved for the modal energies as a function of time. The solutions are

$$\theta_1(t) = \frac{E_0}{n_1} e^{-\omega \eta t} \quad , \qquad t > 0 \quad , \tag{IV-50}$$

$$\theta_2(t) = \frac{E_0}{n_1} \omega \eta_{21} t e^{-\omega \eta t} \quad , \qquad t > 0 \quad , \tag{IV-51}$$

and

$$\theta_i(t) = \frac{E_0}{n_1} \frac{1}{(i-1)!} \omega^{(i-1)} \prod_{j=1}^{i-1} \eta_{j+1,j} t^{(i-1)} e^{-\omega \eta t} \quad ,$$

$$t > 0 \quad , \tag{IV-52}$$

where

$$i! = i(i - 1)(i - 2)(i - 3) - - - (1) \quad , \tag{IV-53}$$

and

$$\prod_{j=1}^{i-1} \eta_{j+1,j} = \eta_{21}\eta_{32}\eta_{43} - - - \eta_{i,i-1} \quad . \tag{IV-54}$$

The solutions given by Eqs. IV-50 through IV-52 are in the general form

$$\theta_i(t) = \frac{E_o}{\eta_1} A_i \, t^{(i-1)} \, e^{-\omega\eta t} \quad , \tag{IV-55}$$

where A_i is an amplitude

$$A_i = \frac{1}{(i - 1)!} \, \omega^{(i-1)} \prod_{j=1}^{i-1} \eta_{j+1,j} \quad . \tag{IV-56}$$

A maximum in the modal energy occurs when

$$t_M = \frac{i - 1}{\omega\eta} \quad . \tag{IV-57}$$

The amplitude of the peak is

$$\theta_i^{MAX} = \theta_i(t_M) = \frac{E_o}{n} A_i \left(\frac{i - 1}{\omega\eta}\right)^{i-1} e^{(1 - i)} \cdot \tag{IV-58}$$

It is now interesting to compare the peak amplitude of the modal energy in element i with that in the next element i + 1. To do this we find the ratio of peak modal energies

$$\frac{\theta_{i+1}^{MAX}}{\theta_i^{MAX}} = \frac{\eta_{i+1,i}}{\eta} \, e^{-1} \left(\frac{i}{i - 1}\right)^{i-1} \quad . \tag{IV-59}$$

For large values of i we can write simply

$$\frac{\theta_{i+1}^{MAX}}{\theta_i^{MAX}} = \frac{\eta_{i+1,i}}{\eta} \quad , \qquad\qquad (IV\text{-}60)$$

where we have assumed

$$\eta_i = \eta \qquad\quad \text{all } i \quad , \qquad\qquad (IV\text{-}61)$$

$$\frac{\eta_{i,i+1}}{\eta_i} << 1 \qquad \text{all } i \quad , \quad \text{and} \qquad (IV\text{-}62)$$

$$i >> 1 \quad . \qquad\qquad (IV\text{-}63)$$

Using the conditions given by Eqs. IV-61, 62 in obtaining
solutions for the transmission of steady-state vibrations
we obtain a result identical to Eq. IV-60,

$$\frac{\theta_{i+1}^{SS}}{\theta_i^{SS}} = \frac{\eta_{i+1,i}}{\eta} \quad , \qquad\qquad (IV\text{-}64)$$

where θ_i^{SS} represents the steady-state modal energy of element i.

Our conclusion then is that THE DECREASE IN PEAK MODAL ENERGY
FROM ELEMENT TO ELEMENT DURING TRANSIENT EXCITATION IS EQUAL
TO THE DECREASE IN MODAL ENERGY DURING STEADY-STATE EXCITATION.
Sufficient conditions for this conclusion are given by Eqs. IV-61 to 63.
However, these conditions may not be necessary. We expect
that the conclusion above is of general use for all pyrotechnic
shock problems. Since steady-state data and/or calculations
are generally available, this is a very useful conclusion.

2. Experimental Data

The peak level of the bending wave shock signal was obtained for each measured time-history shown in Figs. 19-29. The decrease in these levels from subpanel to subpanel and from beam segment to beam segment is shown in Figs. 30-36. In these figures the ratios of the envelope peak acceleration of one subpanel or beam segment to the envelope peak acceleration of a subpanel or beam segment farther away from the excited subpanel are plotted in dB as a function of the octave-band center frequency. The dB scale is defined as

$$dB = 20 \log_{10} \frac{a_{i,pk}}{a_{j,pk}} , \qquad (IV-65)$$

where $a_{i,pk}$ is the envelope peak acceleration of substructure i and $a_{j,pk}$ is the envelope peak acceleration of substructure j, where substructure j is farther from the excited panel than substructure i. Positive dB values in Figs. 30-36 indicate a reduction in the amplitude as the distance between source and measurement point increases.

Also plotted in Figs. 30-36 are data from steady-state vibration measurements on the same cylindrical shell. In general the agreement between the decrease in steady-state vibration levels from substructure to substructure and the decrease in the peak shock envelope levels is good. The only trend which can be observed is a tendency for the reduction of shock levels to be greater than that for steady-state vibration levels. The data indicate that the steady-state vibration data can be used to form an approximate upper bound for the bending-wave shock envelope peak level. This result is in keeping with analytical results obtained in Section IV-C-1.

3. Comparison of Calculated and Measured Spatial Decay
   of Peak Bending Energy

In Section IV.C.1 an expression (Eq. IV-64) for the ratio
of maximum bending in subpanel i+1 to that in subpanel i
was derived. In this section that expression is evaluated
and compared with the model cylinder data.

The value of the coupling loss factor from subpanel i+1
to subpanel i is given by Eq. IV-34 for nonresonant transmission
and is related to the loss factor η_{B_i,P_i} given by Eq. IV-16
for resonant transmission.

In the steady-state case, the ratio of the subpanel modal
energies computed on the basis of resonant transmission is [9]

$$\frac{\theta_{P_{i+1}}}{\theta_{P_i}} = \frac{\eta_{PB}\eta_{BP}}{[(\eta_B + \eta_{BP}^2)(\eta_P + \eta_{PB}) - \eta_{BP}\eta_{PB}]} \quad , \qquad (\text{IV-66})$$

which with the assumptions,

$$\eta_B \ll \eta_{BP} \quad , \qquad (\text{IV-67a})$$

$$\eta_P \gg \eta_{PB}/2 \quad , \qquad (\text{IV-67b})$$

reduces to

$$\frac{\theta_{P_{i+1}}}{\theta_{P_i}} = \frac{\eta_{PB}/2}{\eta_P} \quad . \qquad (\text{IV-68})$$

Comparison of Eq. IV-68 with Eq. IV-64 and utilizing the modal
density and coupling loss factor relation in Eq. IV-5 indicates
that for resonant transmission

$$\eta_{P_{i+1}, P_i} = \frac{(\eta_{BB} + \eta_{BT})}{4\eta_P} \eta_{B_i, P_i} \quad , \qquad (\text{IV-69})$$

where η_{B_i, P_i} is given by Eq. IV-16.

Numerical evaluation of the resonant and nonresonant subpanel to subpanel coupling loss factors given by Eqs. IV-69 and IV-34 respectively for the model cylinder shown in Fig. 17 indicates that the resonant coupling dominates over the entire frequency range of interest.

The peak shock bending energy decay from subpanel to subpanel calculated from Eqs. IV-64 and IV-69 and an assumed internal loss factor of $\eta_i = 10^{-2}$ is shown in Fig. 37. Also shown on Fig. 37 are the peak shock transmission data taken from Fig. 30. The measured decay from the driven panel (4-2) to the adjacent panel (5-2) agrees well with the analytical prediction. The data show somewhat less decay from undriven panels to adjacent panels farther removed from the source than the theory predicts, particularly at high frequencies. This anomaly has been previously observed in periodically supported structures [14].

D. Dilatational Wave Transmission and Scattering into
    Bending Waves

The preceding extension of statistical energy analysis
to transient problems has been possible because complex
structures usually can be subdivided into lightly coupled
substructures (modal sets). In flexure, ribs on a panel
can be subdivided into individual beam elements extending
between junctures. This subdivision is possible because
flexural waves will be almost totally reflected at a
juncture, the flexural modes of one beam segment being
lightly coupled to the modes of the other segments forming
the juncture. Similarly, the flexural modes of one panel
bay will be lightly coupled to those of another bay,
flexural waves being almost totally reflected by the ribs.

Consider, however, the transmission of panel dilata-
tional waves through a rib. The rib will reflect poorly
except at very high frequencies (or at incidence angles well
removed from the normal). If the panel is broken into bays
by other ribs, dilatational reverberation cannot arbitrarily
be assumed to exist within the bays. An essentially blocked
or free termination is required to ensure sufficient re-
flection. For a finite panel, only the boundaries clearly
represent strong reflectors. This suggests that the dila-
tational modes of the entire panel are an appropriate modal
set.

If the dilatational modes are lightly coupled to the flexural modes of the individual bays, say through the ribs, statistical energy analysis can be used to determine the rate at which energy flows to flexure. This leads to the flexural response. While identification of lightly coupled modal groups does not in itself assure that statistical energy analysis will give the correct answers, if reverberation of the modal groups exists, reasonable estimates might be obtained. A factor which complicates the simple picture given here is that a rib represents a non-conservative coupling device, since power will be dumped to distortion as well as to flexure.

Reflections at boundaries and ribs will induce a con-tinuous energy exchange, from dilatation to distortion and vice versa. Without losses to flexure, and in the absence of structural damping, some proportioned time average energy could be related to each. With rib losses, this conversion process continues as the total energy level decreases. If the ribs losses were due solely to dilatation, ultimately all energy input to dilatation (or distortion for that matter) could be assigned to dilatation. A similar statement could be made for distortion. Since dilatation and distortion will induce panel flexure through physically similar rib interactions, it seems reasonable to assume that power flow from dilatation and distortion to flexure is proportioned as the energies. If equipartition of modal energies is

assumed, the power to flexure is proportioned as the modal densities. This assumption infers, from a flexural standpoint, that all energy can be assigned to either dilatation or distortion because the coupling loss factors would be equal. In this report, all energy is assumed to be in dilatation. Whenever the term "dilatational energy" is used, it implies the sum of the instantaneous dilatation and distortion energy.

This section is devoted to the development of analytical methods for predicting the short time-space average flexural response of a ribbed panel to an in-plane dilatational shock. Without *a priori* knowledge that ribs do not induce dilatational reverberation, the harmonic problem is first solved to show that this is the case and to show that dilatational modes are lightly coupled to flexural modes. With the information derived, the nonresonant dilatation to flexure coupling loss factor is computed and the solution formulated within the statistical energy analysis format.

1. Transmission of Harmonic Dilatational Waves Through Reinforcing Beams

In order to deal with a tractable problem, the analysis of an infinite plate to which a uniform straight beam is attached is considered, the line of attachment being narrow, extending from $x = 0^-$ to 0^+, as shown in Fig. 38. The shear center of the rib and its center of gravity are not

necessarily coincident, but lie on the same line normal
to the panel surface, the c.g. being a distance R away
from the panel and the shear center a distance ε away from
the c.g. (ε positive in the outward direction).

Specific Normal Impedance of the Rib

Let $f_o(y,t)$ be the load applied to the rib, acting along
the attachment. The flexural motions are governed by

$$\rho_r A_r \frac{\partial^2 x_o}{\partial t^2} + Y_o A_r \kappa_r^2 \frac{\partial^4 x_{sc}}{\partial y^4} = f_o(y,t) , \qquad \text{(IV-70)}$$

where x_o is the displacement of the c.g. and x_{sc} is the
displacement of the shear center.

Let x be the displacement along the line of attachment.
Then

$$x_o = x + R\theta_r , \qquad \text{(IV-71)}$$

and

$$x_{sc} = x + (R + \varepsilon)\theta_r . \qquad \text{(IV-72)}$$

Let f_o be of the form

$$f_o = \overline{F}_o \exp[i(k_t y - \omega t)] . \qquad \text{(IV-73)}$$

We take

$$x = \overline{X} \exp[i(k_t y - \omega t)] , \qquad \text{(IV-74)}$$

$$\theta_r = \overline{\theta}_r \exp[i(k_t y - \omega t)] . \qquad \text{(IV-75)}$$

Substitution of Eqs. IV-71 to 75 into IV-70 and use of $v = -i\omega x$, where v is the velocity of the line of attachment gives

$$(\overline{Y}_r)^{-1}\overline{V} - i\omega(\overline{Y}_r')^{-1}\overline{\theta}_r = \overline{F}_o , \qquad (\text{IV-76})$$

where

$$\overline{Y}_r = \{-i\omega\rho_r A_r[1 - (k_t/k_r)^4]\}^{-1} , \qquad (\text{IV-77})$$

and

$$\overline{Y}_r' = \{-i\omega\rho_r A_r[R - (R + \varepsilon)(k_t/k_r)^4]\}^{-1} . \qquad (\text{IV-78})$$

The torsion of the beam is governed by

$$J\frac{\partial^2\theta_r}{\partial t^2} = GK\frac{\partial^2\theta_r}{\partial y^2} + \overline{m}_o^r - (R + \varepsilon)\overline{f}_o . \qquad (\text{IV-79})$$

Here J is the polar moment of inertia per unit of length of the beam, G is the shear modulus, K is the torsional constant of the beam cross section [15], GK is the torsional stiffness, and $\overline{m}_o^r$ is the moment per unit length applied along the line of attachment. For harmonics, this becomes

$$(k_t^2 GK - \omega^2 J)\overline{\theta}_r = \overline{M}_o^r - (R + \varepsilon)\overline{F}_o . \qquad (\text{IV-80})$$

For applied moment M_o^p (per unit length) to the panel,

$$-i\omega\bar{\theta}_p = \frac{\bar{M}_o^p}{Z_m^p} , \qquad (IV-81)$$

where Z_m^p is the moment impedance per unit length of the panel given by [10]

$$Z_m^p = (2Y_o h\kappa^2 k_p/\omega)(1-i), \qquad (IV-82)$$

k_p being the panel bending wavenumber.

Continuity requires

$$M_o^r = -M_o^p \stackrel{\Delta}{=} M_o , \qquad (IV-83)$$

and

$$\bar{\theta}_r = \bar{\theta}_p = \bar{\theta} . \qquad (IV-84)$$

Substitution of Eqs. IV-81, 83 and 84 into IV-80 yields

$$(i\omega Z_m^p + \omega^2 J - k_t^2 GK)\bar{\theta} = (R + \varepsilon)\bar{F}_o. \qquad (IV-85)$$

Elimination of $\bar{\theta}$ from IV-85 and 76 gives the specific rib impedance:

$$Z_r = (\bar{Y}_r)^{-1} \left\{ 1 - \frac{i\omega(\bar{Y}_r')^{-1}(R + \varepsilon)}{\{i\omega[Z_m^p + (R + \varepsilon)(\bar{Y}_r')^{-1}]\} + [\omega^2 J - k_t^2 GK]} \right\} .$$

$$(IV-86)$$

The resistive part is due to a power loss to panel flexure. The imaginary part reveals a reduced reaction of the rib owing to its rotation.

Power Loss to Flexure

The time average power per unit length dumped to panel bending by the harmonic dilatational wave is

$$<\pi_\ell>_t^{flex} = \frac{|M_\ell|^2 Re\ [Z_m^p]}{2|Z_m^p|^2}$$

$$= \frac{\omega^2 (R + \epsilon)^2 |\overline{Y}_r^{-1}|^2 Re[Z_m^p]|\overline{V}|^2}{2|\{i\omega[Z_m^p + (R + \epsilon)(\overline{Y}_r^-)^{-1}]\} + [\omega^2 J - k_t^2 GK]|^2} \ . \qquad (IV-87)$$

Harmonic Transmission Coefficients

As previously noted, the incidence of a harmonic dilatational wave on a rib will result not only in reflected and transmitted dilatational waves, but in distortional waves as well. In this section we will develop the harmonic transmission coefficients.

In Fig. 39, the four possible reflected and transmitted in plane waves are shown, two dilatational waves and two distortional waves. The displacement normal to the wavefront for the incident longitudinal wave is

$$\phi_1 = A_1 \exp\left[-i(\omega t + \frac{\omega}{c_\ell}\cos\alpha_1 x + \frac{\omega}{c_\ell}\sin\alpha_1 y)\right] \quad . \qquad \text{(IV-88)}$$

The x and y displacements are

$$\xi_1 = \phi_1 \cos\alpha_1 \quad , \quad \eta_1 = \phi_1 \sin\alpha_1 . \qquad \text{(IV-89)}$$

For the reflected and transmitted waves, we have

$$\phi_2 = A_2 \exp\left[-i(\omega t - \frac{\omega}{c_\ell}\cos\alpha_2 x + \frac{\omega}{c_\ell}\sin\alpha_2 y + \delta_2)\right] \quad , \qquad \text{(IV-90)}$$

$$\xi_2 = -\phi_2 \cos\alpha_2 \quad ; \quad \eta_2 = \phi_2 \sin\alpha_2 \quad , \qquad \text{(IV-91)}$$

$$\phi_3 = A_3 \exp\left[-i(\omega t - \frac{\omega}{c_T}\cos\alpha_3 x + \frac{\omega}{c_T}\sin\alpha_3 y + \delta_3^T)\right] \quad , \qquad \text{(IV-92)}$$

$$\xi_3 = \phi_3 \sin\alpha_3 \quad ; \quad \eta_3 = \phi_3 \cos\alpha_3 \quad , \qquad \text{(IV-93)}$$

$$\phi_4 = A_4 \exp[-i(\omega t + \frac{\omega}{c_\ell} \cos\alpha_4 x + \frac{\omega}{c_\ell} \sin\alpha_4 y + \delta_4] \quad , \tag{IV-94}$$

$$\xi_4 = \phi_4 \cos\alpha_4 \quad ; \quad \eta_4 = \phi_4 \sin\alpha_4 \quad , \tag{IV-95}$$

$$\phi_5 = A_5 \exp[-i(\omega t + \frac{\omega}{c_T} \cos\alpha_5 x + \frac{\omega}{c_T} \sin\alpha_5 y + \delta_5^T)] \quad , \tag{IV-96}$$

$$\xi_5 = \phi_5 \sin\alpha_5 \quad ; \quad \eta_5 = -\phi_5 \cos\alpha_5 \quad , \tag{IV-97}$$

The stresses and strains are related through the Lamé constants, λ and μ, by [16]

$$\sigma_{xx} = 2\mu \delta_{xx} + \lambda(\delta_{xx} + \delta_{yy} + \delta_{zz}) \quad , \tag{IV-98}$$

$$\sigma_{yy} = 2\mu \delta_{yy} + \lambda(\delta_{xx} + \delta_{yy} + \delta_{zz}) \quad , \tag{IV-99}$$

$$\sigma_{xy} = 2\mu \delta_{xy} \quad , \tag{IV-100}$$

where σ_{xx}, σ_{yy}, σ_{xy} are the normal and shear stresses and the strains are given by

$$\delta_{xx} = \xi_x = \frac{\partial \xi}{\partial x} \quad ; \quad \delta_{yy} = \eta_y = \frac{\partial \eta}{\partial y} \quad , \tag{IV-101}$$

$$\delta_{xy} = \frac{1}{2}(\eta_x + \xi_y) \quad . \tag{IV-102}$$

-69-

Summing forces along a rib element yields

$$\frac{h}{EA_r} [\sigma_{xy}^{(1,2,3)} - \sigma_{xy}^{(4,5)}]_{x=0} + \frac{\partial^2 \eta}{\partial y^2} = \frac{1}{c_\ell^2} \frac{\partial^2 \eta}{\partial t^2} \qquad \text{(IV-103)}$$

Continuity of particle displacement along the rib gives

$$\eta_1 + \eta_2 + \eta_3)_{x=0} = \eta_4 + \eta_5)_{x=0} = \eta \qquad \text{(IV-104)}$$

Summing forces across a rib element, we obtain

$$h[\sigma_{xx}^{(1,2,3)} - \sigma_{xx}^{(4,5)}]_{x=0} = Z_r \frac{\partial}{\partial t} (\xi_1 + \xi_2 + \xi_3)_{x=0} = Z_r \overline{V} \quad ,$$

$$\text{(IV-105)}$$

where it is assumed that all shear at $x = 0$ is carried by the rib. Continuity of particle displacement requires

$$\xi_1 + \xi_2 + \xi_3)_{x=0} = \xi_4 + \xi_5)_{x=0} = \xi \quad .$$

$$\text{(IV-106)}$$

After some manipulation, the following results can be obtained:

Transmission Coefficient (the ratio of the transmitted power in the dilatational wave, ϕ_4, to that in the incident wave, ϕ_1)

$$\alpha_t = \left| \frac{A_4}{A_1} \right|^2 \qquad \text{(IV-107)}$$

<u>Reflection Coefficient</u> (the ratio of the reflected power in the dilatational wave, ϕ_2, to that in the incident wave, ϕ_1)

$$\alpha_r = \left|\frac{A_2}{A_1}\right|^2 \qquad (\text{IV-108})$$

<u>Flexural Loss Coefficient</u> (the ratio of the power flowing away from the rib due to panel flexure to that in the incident wave, ϕ_1)

$$\alpha_f = \frac{\omega^2(R + \epsilon)^2\left|\overline{Y}_r^{-1}\right|^2 \text{Re}[Z_m^p]\left|(\frac{A_2}{A_1} - 1)\cos\alpha_1 - \frac{A_3}{A_1}\frac{C_T}{C_\ell}\sin\alpha_1\right|^2}{h\rho c_\ell\cos\alpha_1\left|\{i\omega[Z_m^p + (R + \epsilon)(\overline{Y}_r')^{-1}]\} + [\omega^2 J - k_t^2 GK]\right|^2} \ , \qquad (\text{IV-109})$$

where the complex amplitude ratios are to be determined by solving the following set of equations:

$$\left|\begin{matrix} \beta_2 & \beta_3 & \beta_4 & \beta_5 \\ \beta_7 & \beta_8 & \beta_9 & \beta_{10} \\ \beta_{11} & 1 & -\beta_{11} & 1 \\ -1 & \beta_{12} & -1 & -\beta_{12} \end{matrix}\right| \left\{\begin{matrix} A_2/A_1 \\ A_3/A_1 \\ A_4/A_1 \\ A_5/A_1 \end{matrix}\right\} = \left\{\begin{matrix} -\beta_1 \\ -\beta_6 \\ -\beta_{11} \\ -1 \end{matrix}\right\} \ , \qquad (\text{IV-110})$$

with

$$\beta_1 = \frac{Z_r}{h}\cos\alpha_1 - \frac{\lambda + 2\mu\cos^2\alpha_1}{c_\ell} \qquad (\text{IV-111})$$

$$\beta_2 = -\frac{Z_r}{h} \cos \alpha_2 - \frac{\lambda + 2\mu \cos^2 \alpha_2}{c_\ell} \qquad \text{(IV-112)}$$

$$\beta_3 = \frac{Z_r}{h} \sin \alpha_3 + \frac{2\mu}{c_T} \cos \alpha_3 \sin \alpha_3 \qquad \text{(IV-113)}$$

$$\beta_4 = \frac{\lambda + 2\mu \cos^2 \alpha_4}{c_\ell} \qquad \text{(IV-114)}$$

$$\beta_5 = \frac{2\mu}{c_T} \cos \alpha_5 \sin \alpha_5 \qquad \text{(IV-115)}$$

$$\beta_6 = \frac{\omega^2}{c_\ell^2} (\sin \alpha_1 - \sin^3 \alpha_1) + i \frac{2h\mu}{EA_r} (\frac{\omega}{c_\ell} \sin \alpha_1 \cos \alpha_1) \qquad \text{(IV-116)}$$

$$\beta_7 = \frac{\omega^2}{c_\ell^2} (\sin \alpha_1 - \sin^3 \alpha_1) + i \frac{2h\mu}{EA_r} (\frac{\omega}{c_\ell} \sin \alpha_2 \cos \alpha_2) \qquad \text{(IV-117)}$$

$$\beta_8 = \frac{\omega^2}{c_\ell^2} \cos \alpha_3 - \frac{\omega^2}{c_T^2} \sin^2 \alpha_3 \cos \alpha_3 + \frac{ih\mu}{EA_r} \frac{\omega}{c_T} (\cos^2 \alpha_3 - \sin^2 \alpha_3) \qquad \text{(IV-118)}$$

$$\beta_9 = \frac{2i\mu h}{EA_r} \frac{\omega}{c_\ell} \cos \alpha_4 \sin \alpha_4 \qquad \text{(IV-119)}$$

$$\beta_{10} = \frac{i\mu h}{EA_r} \frac{\omega}{c_T} (\sin^2 \alpha_5 - \cos^2 \alpha_5) \qquad \text{(IV-120)}$$

$$\beta_{11} = \sin \alpha_1 / \cos \alpha_3 \qquad \text{(IV-121)}$$

$$\beta_{12} = \sin \alpha_3 / \cos \alpha_1 \qquad \text{(IV-122)}$$

$$\alpha_2 = \alpha_4 = \alpha_1 \tag{IV-123}$$

$$\alpha_3 = \alpha_5 = \text{arc sin} \; (\frac{c_T}{c_\ell} \sin \alpha_1) \tag{IV-124}$$

$$\delta_2 = \delta_4 = \delta_3^T = \delta_3^T = \delta_5^T = 0 \tag{IV-125}$$

$$k_t = \frac{\omega}{c_\ell} \sin \alpha_1 \tag{IV-126}$$

The Lamé constants can be computed from the material para-
meters Y_o (elastic modulus) and σ (Poisson's ratio):

$$\lambda = \frac{\sigma Y_o}{(1+\sigma)(1-2\sigma)} \quad , \tag{IV-127}$$

$$\mu = \frac{Y_o}{2(1+\sigma)} \quad , \tag{IV-128}$$

The relations between the wavespeeds and the Lamé constants
are

$$c_\ell = \sqrt{\frac{\lambda+2\mu}{\rho}} \quad , \tag{IV-129}$$

$$c_T = \sqrt{\frac{\mu}{\rho}} \quad , \tag{IV-130}$$

Estimates for the Harmonic Transmission Coefficients for
a Model Panel-Rib System

Shown in Fig. 40 is a ribbed cylinder model which is
similar to the cylinder used in the bending wave experiments
(Fig. 17) except for the stiffener cross-section dimensions.
It is of a configuration reasonably suited for application
of the theoretical relations. The transmission, reflection,
and flexural loss coefficients for a rib of the configuration
on the cylinder, and for the same skin thickness are shown
in Fig. 41. These indicate that reflection of harmonic
dilatational waves by a rib will not induce dilatational
reverberation within the bays except perhaps at very high
frequencies.

2. Determination of the Coupling Loss Factor

The time average power dumped to panel bending by a
harmonic dilatational wave originating from any direction
is given by Eq. (IV-87), where $|V|^2_i$ is the square of the mag-
nitude of the complex velocity along the rib line. In
terms of the time mean square velocity along the rib line,
we may rewrite (IV-87) using $<v^2>_t = |V|^2/2$. This can be
related to the incident incoming wave complex velocity
amplitude.

If ϕ_1 is the incoming wave displacement, then the incoming wave velocity is

$$v_1 = -i\omega\phi_1 \quad . \tag{IV-131}$$

The incoming wave complex displacement amplitude A_1 is related to the rib line complex velocity amplitude by

$$v = i\omega A_1 e^{-i\frac{\omega}{c_\ell}\sin\alpha_1 y}\left[\left(\frac{A_2}{A_1} - 1\right)\cos\alpha_1 - \frac{A_3}{A_1}\frac{c_T}{c_\ell}\sin\alpha_1\right] \tag{IV-132}$$

Thus the incoming wave complex velocity amplitude $V_1 \equiv -i\omega A_1$ is related to the rib line complex velocity amplitude. Assuming reverberation exists, then

$$|V|^2 \rightarrow \left|\left(\frac{A_2}{A_1} - 1\right)\cos\alpha_1 - \frac{A_3}{A_1}\frac{c_T}{c_\ell}\sin\alpha_1\right|^2 <v^2>_{s,t}\frac{d\alpha_1}{\pi} \tag{IV-133}$$

where $<v^2>_{s,t}$ is the band-limited space-time mean square in-plane particle velocity over the entire panel. The time average total energy of the panel is $E = M<v^2>_{s,t}$,* where M is the total panel mass, and the time average power

---

*We assume that the time average kinetic energy is equal to the sum of the time average potential energies of the dilatation and the distortion. Recall $<v^2>_{s,t}$ is the sum of the space-time mean square velocities for simultaneous diffuse (incoherent) dilatation and distortion fields.

flow from the in-plane modes to the flexural modes is

$$<\pi>_t = \omega\eta_{df} M<v^2>_{s,t} \quad , \qquad \text{(IV-134)}$$

where ω is the band center frequency and η_{df} is the dilatation to flexure coupling loss factor.

The time average power flow from the dilatational modes to the flexural modes is, from Eq. (IV-87), also given by

$$<\pi>_t = 2\ell <\pi_\ell>_t, \qquad \text{(IV-135)}$$

where ℓ is the total rib length, which is doubled to account for waves incident from both sides.

From (IV-134) and (IV-135), the coupling loss factor is obtained,

$$\eta_{df} = \frac{\ell\omega}{M} < \frac{(R+\epsilon)^2\left|\overline{Y}_r^{-1}\right|^2 Re[Z_m^p]\left|(\frac{A_2}{A_1}-1)\cos\alpha_1 - \frac{A_3}{A_1}\frac{c_T}{c_\ell}\sin\alpha_1\right|^2}{\left|\{i\omega[Z_m^p + (R+\epsilon)(\overline{Y}_r^\prime)^{-1}]\} + [\omega^2 J - k_t^2 GK]\right|^2} >_{\Delta\omega,\alpha_1}$$

$$\qquad \text{(IV-136)}$$

where $<>_{\Delta\omega,\alpha_1}$ indicates averages over the desired frequency band and the frontal incidence angles.

From Eq. IV-109, it is apparent that this becomes

$$\eta_{df} = \frac{\ell h \rho c_\ell \langle \alpha_f \cos \alpha_1 \rangle \Delta \omega, \alpha_1}{M \omega} \quad .$$ (IV-137)

Figure 43 shows that α_f for the model cylinder is approximately independent of α_1 and is reasonably flat in frequency. Frequency averaging is unnecessary if $\Delta \omega$ doesn't exceed an octave or so.

Since $M = A \rho h$, the nonresonant dilatation to flexure coupling loss factor is approximately

$$\eta_{df} = \frac{2 \ell c_\ell \alpha_f}{\pi^2 A f} \quad .$$ (IV-138)

To assure reverberation, the least dimension should be not less than a dilatational wavelength (preferably two wavelengths). For one wavelength,

$$W \geq \frac{17000}{f} \text{ ft} \quad .$$ (IV-139)

For the 6 ft long cylinder shown in Fig. 40, $f_{min} \simeq 2800$ Hz. The computed dilatation to flexure coupling loss factor for the cylinder is shown in Fig. 42. Also shown is the value measured with a Spencer-Kennedy Model 507 Decay Rate Meter.

Excitation was pulsed band-limited random noise provided by a shaker driving into the plane of the skin at one point on the end of the cylinder. The dilatational energy decay was observed by placing an accelerometer at the opposite end. The rate of decay was essentially the same for all circumferential positions of the accelerometer.

The agreement between theory and measurement is satisfactory in view of the structural complexity of the cylinder. No attempt has been made to account for rib interactions, rib stiffening of panels, or curvature. Obviously the theory may be quite erratic in the quality of its prediction from structure to structure. Without considerable additional experimental verification, the dilatation to flexure coupling loss factor should be viewed more qualitatively than quantitatively.

3. Shock Analysis

The ribbed panel is assumed to consist of two discrete sets of modal oscillators, dilatational panel modes {d}, and flexural panel modes {f}. A power balance for either set yields

$$\frac{dE_i}{dt} = \Pi_i^{in} - \Pi_{ij}^{trans} - \Pi_i^{diss} , \qquad (IV-140)$$

where E_i is the short time average total energy of set, i,

Π_i^{in} is the short time average input power for set, i,

Π_{ij}^{trans} is the short time average power being transmitted

and Π_i^{diss} is the short time average power dissipated in

set, i.

The power being dissipated is

$$\Pi_i^{diss} = n_i \omega_i E_i , \qquad (IV-141)$$

and that being transmitted is

$$\Pi_{ij}^{trans} = \omega n_{ij} n_i (\frac{E_i}{n_i} - \frac{E_j}{n_j}). \qquad (IV-142)$$

Here only the residual or free vibration period is considered. Let $\pi_d^{in} = 0$, and assume at $t = 0$, the dilatational energy is diffused spatially in the panel, and has a level, $E_d(0+)$, and that the flexural energy level is zero.

For dilatation, Eq. IV-140 becomes

$$\frac{d\theta_d}{dt} + \omega(\eta_d + \eta_{df})\theta_d - \omega\eta_{df}\theta_f = 0 , \qquad (IV-143)$$

and for flexure

$$\frac{d\theta_f}{dt} + \omega(\eta_f + \eta_{fd})\theta_f - \omega\eta_{fd}\theta_d = 0 . \qquad (IV-144)$$

It is assumed that the dilatational dissipation loss factor is much smaller than the coupling loss factor,

$$\eta_d << \eta_{df} . \qquad (IV-145)$$

Since the flexural modal density of the panels is much larger than the dilatational modal density,

$$n_f >> n_d , \qquad (IV-146)$$

Equations IV-143 and IV-144 become

$$\frac{dE_d}{dt} + \omega \eta_{df} E_d = 0 \; , \tag{IV-147}$$

and
$$\frac{dE_f}{dt} + \omega \eta_f E_f - \omega \eta_{df} E_d = 0 \; . \tag{IV-148}$$

The solution of Eq. IV-147 is

$$E_d = E_d(0+) e^{-\omega \eta_{df} t} \; . \tag{IV-149}$$

Equation IV-149, of course, has no sense except as the total energy in dilatation and distortion, which is assumed to be proportioned according to the modal densities.

Substitution of this result into Eq. IV-148 gives the total short time average energy of the flexural modes

$$E_f(t) = E_d(0+) \frac{\eta_{df}}{\eta_{df} - \eta_f} \left[e^{-\omega \eta_f t} - e^{-\omega \eta_{df} t} \right] \; . \tag{IV-150}$$

Note the restriction $\eta_{df} \neq \eta_f$. This result is shown in Fig. 43. The band-limited short-time space averaged mean square flexural acceleration of the panel is obtained from

$$\langle a_f^2 \rangle_{s,t} = \frac{\omega^2}{M} E_f(t) \; . \tag{IV-151}$$

REFERENCES

1. "Aerospace Systems Pyrotechnic Shock Data," Martin Marietta Corporation Report MCR-69-611, Vol. I-VI, March 1970.

2. C. T. Morrow, "The Shock Spectrum," *Electrical Manufacturing*, August 1959.

3. R. H. Lyon and G. Maidanik, "Statistical Methods in Vibration Analysis," AIAA Journal 2 (6), 1964.

4. R. H. Lyon, *Random Noise and Vibration in Space Vehicles*, Shock and Vibration Monograph SVM-1, Chapter 3, 1967.

5. P. W. Smith, Jr. and R. H. Lyon, "Sound and Structural Vibration," NASA Contractor Report 160, 1965.

6. J. E. Manning, "Study of Pyrotechnic Shock in the RVTO Phase 1A Reentry Vehicle," Bolt Beranek and Newman Report No. 1578, March 1968.

7. J. E. Manning and K. Lee, "Predicting Mechanical Shock Transmission," Shock and Vibration Bulletin, 37, (4), 1968.

8. H. P. Hsu, *Outline of Fourier Analysis*, Unitech Division, Educational Services Corporation, New York, 1967.

9. R. H. Lyon and T. D. Scharton, "Vibrational-Energy Transmission in a Three-Element Structure," *J. Acoust. Soc. Am.* 38 (2), 253-261 (1966).

10. Manfred A. Heckl, "Compendium of Impedance Formulas,"
    BBN Report No. 774, submitted to the Office of Naval
    Research under Contract Nonr 2322(00) Task No. NR 264-017,
    26 May 1961, Eq. VI-2.

11. E. E. Ungar, "Transmission of Plate Flexural Waves
    through Reinforcing Beams; Dynamic Stress Concentrations,"
    J. Acoust. Soc. Am. 33, p. 633 (1961).

12. E. E. Ungar, "Steady-State Responses of One-Dimensional
    Periodic Flexural Systems," *J. Acoust. Soc. Am.* 39,
    p. 887 (1966).

13. R. H. Lyon, "Spatial Response Concentrations in Extended
    Structures," *Trans. of the A.S.M.E., J. Engrg. Ind.*,
    pp. 754-758 (1967).

14. M. A. Heckl, "Investigations on the Vibrations of
    Grillages and Other Simple Beam Structures," *J. Acoust.
    Soc. Am.* 36, 7, pp. 1335-1343, July 1964.

15. C. T. Wang, *Applied Elasticity* (McGraw-Hill Book Company,
    Inc., New York, 1953).

16. H. Kolsky, *Stress Waves in Solids*, Oxford University
    Press, London (1953).
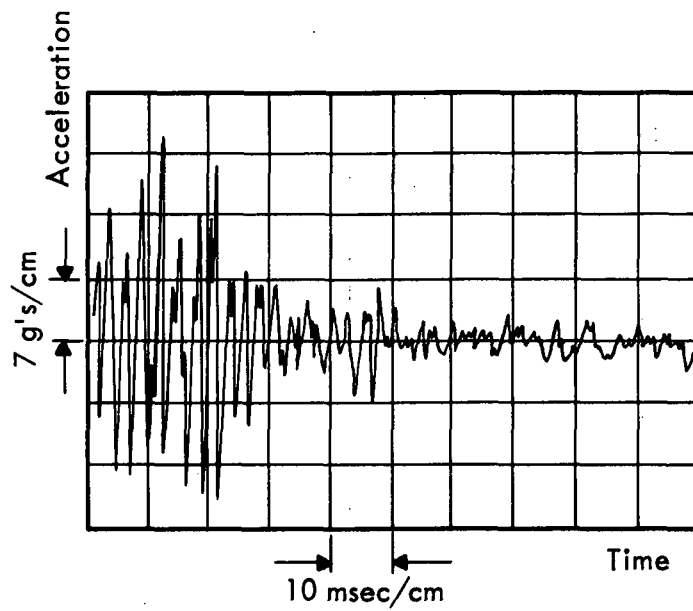
FIGURE 1. PYROTECHNIC SHOCK AT AN EQUIPMENT
POINT AFTER IGNITION OF A SEPARATION NUT
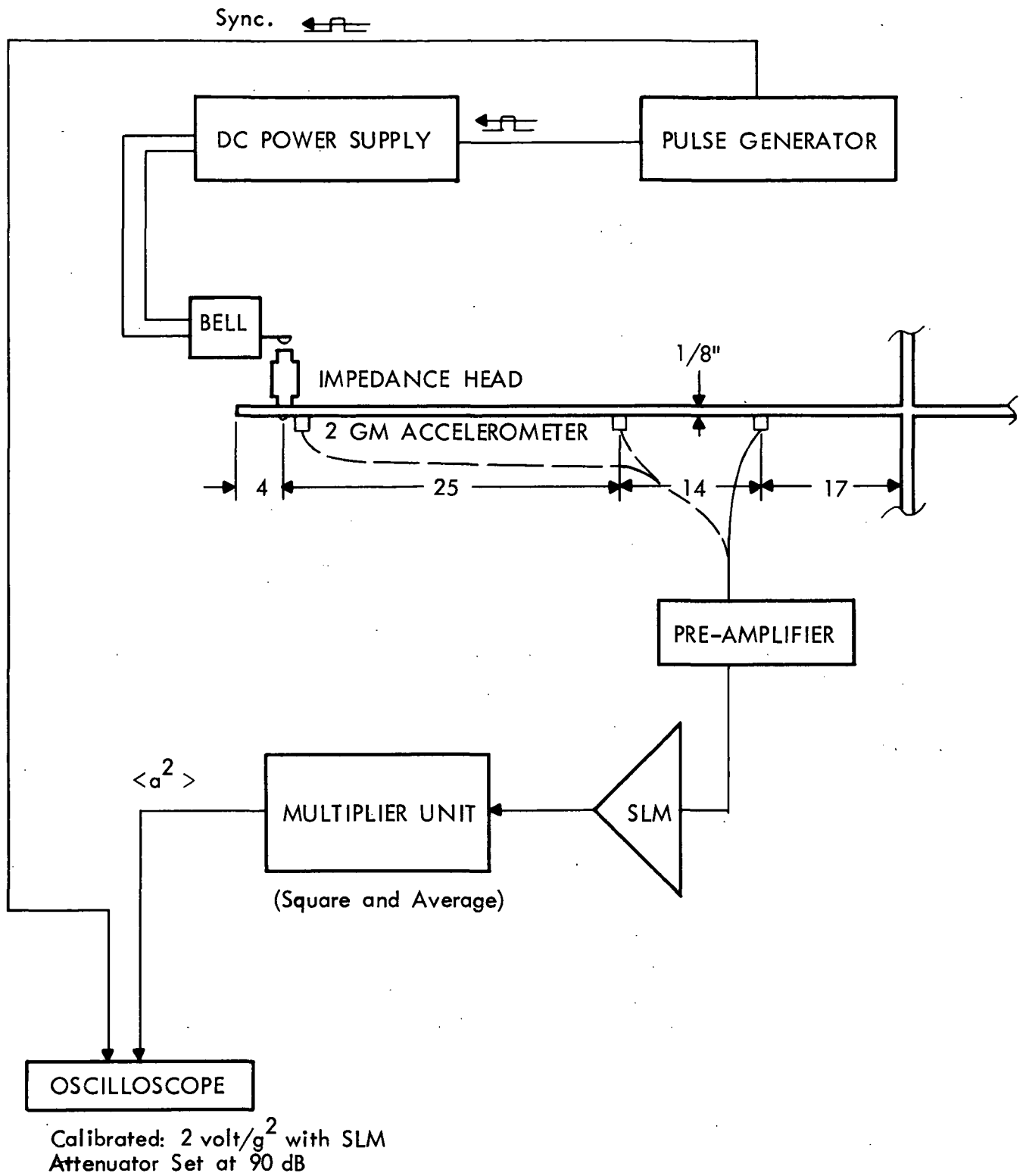
FIGURE 2. MEASUREMENT OF MEAN SQUARE ACCELERATION

F(t)

T

0.2 0.4

Time

$F_o = 0.83$ lb.
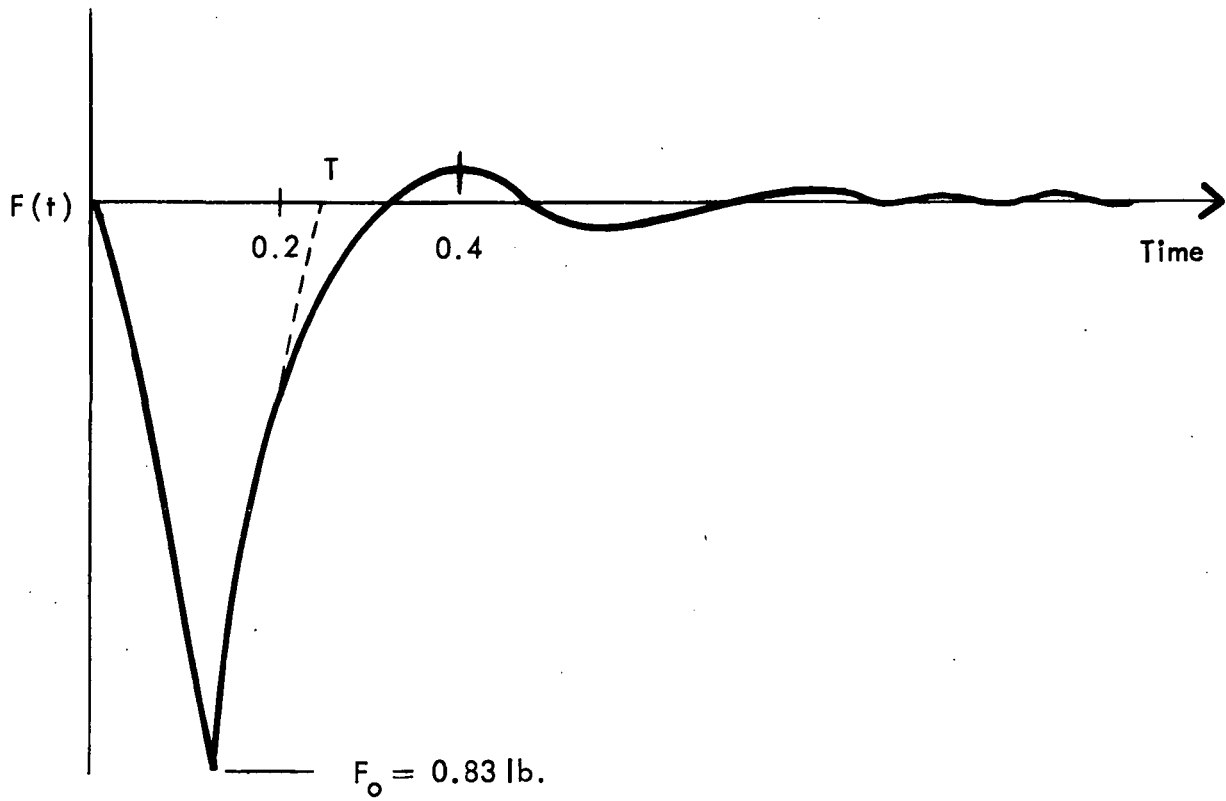
FIGURE 3.   SYMMETRICAL TRIANGULAR PULSE

250 Hz

10 msec/div
0.5 volt/div
SLM attn 80 dB

1 msec
5 msec
Level
10 msec

4a

500 Hz

10 msec/div
0. 1 volt/div
SLM attn 100 dB

3 msec
10 msec
Level

4b

1000 Hz

2 msec/div
0.1 volt/div
SLM attn 100 dB

1 msec
Level
3 msec
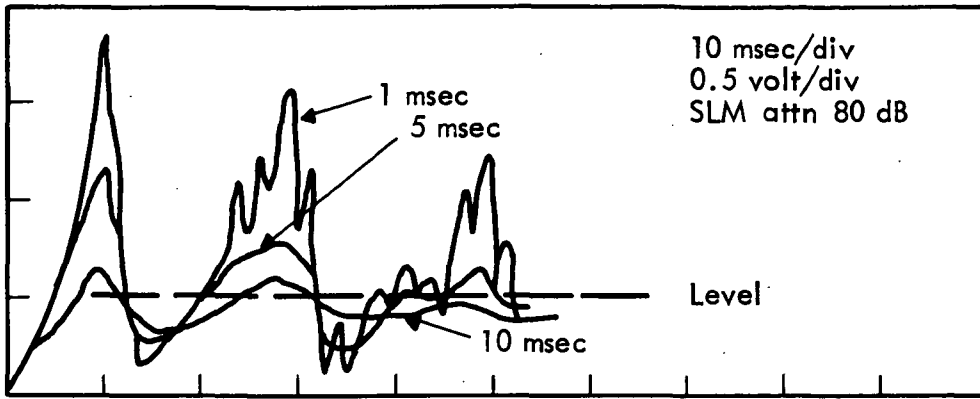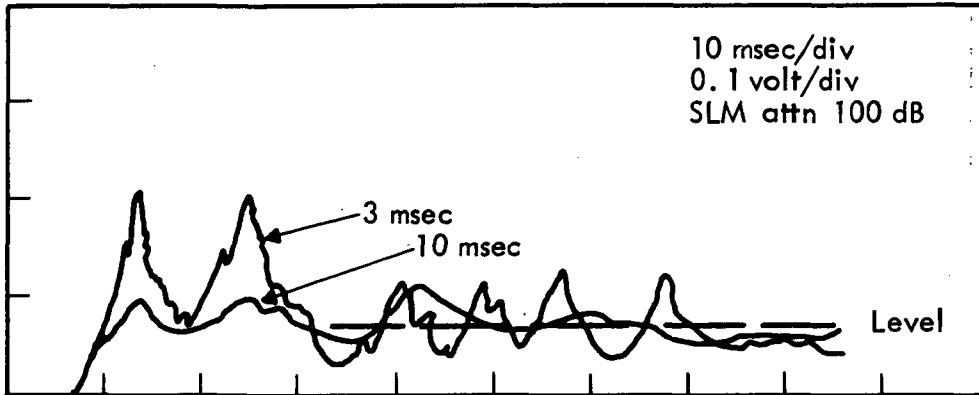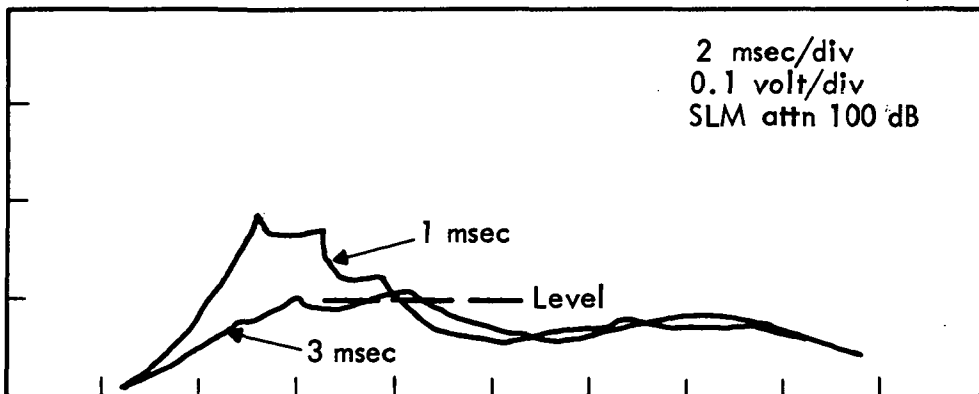
4c

FIGURE 4.   FILTERED, MEAN SQUARE ACCELERATION RESPONSE
OF BEAM

2000 Hz

2 msec/div
0.5 volt/div
SLM attn 100 dB

1 msec

Level

3 msec

4 d

4000 Hz

2 msec/div
2 volt/div
SLM attn 90 dB

1 msec (25")

1 msec (39")

Level

3 msec

4 e

8000 Hz

1 msec/div
0.5 volt/div
SLM attn 90 dB

1 msec

Level

3 msec
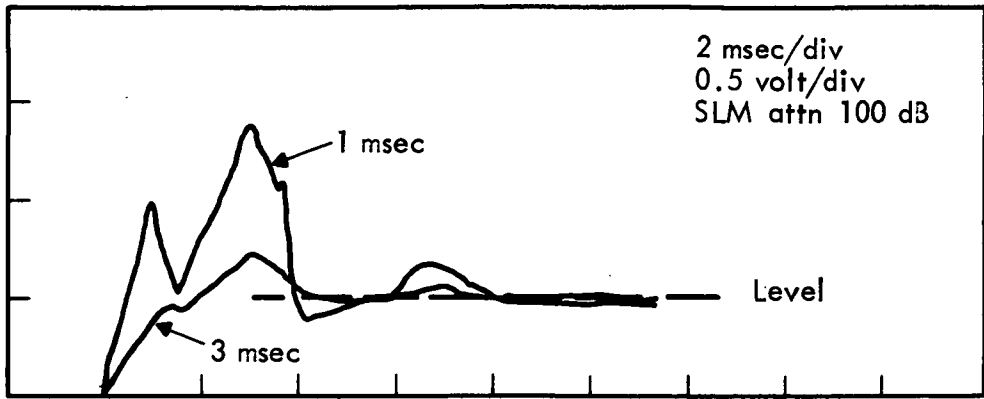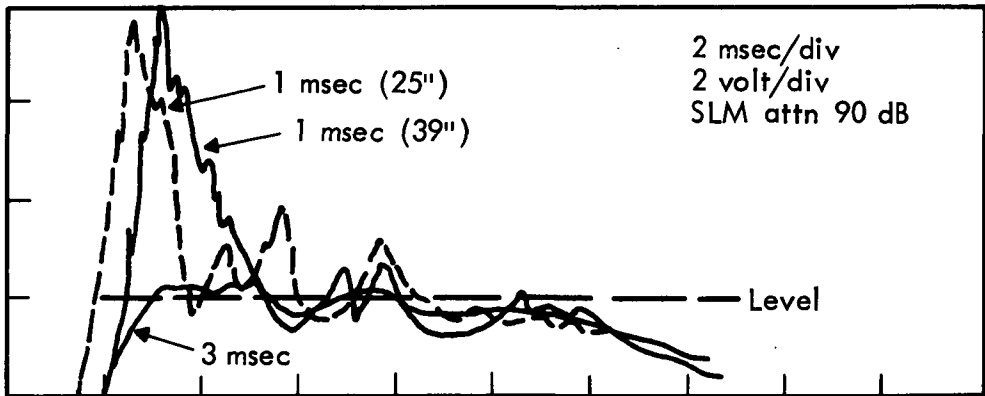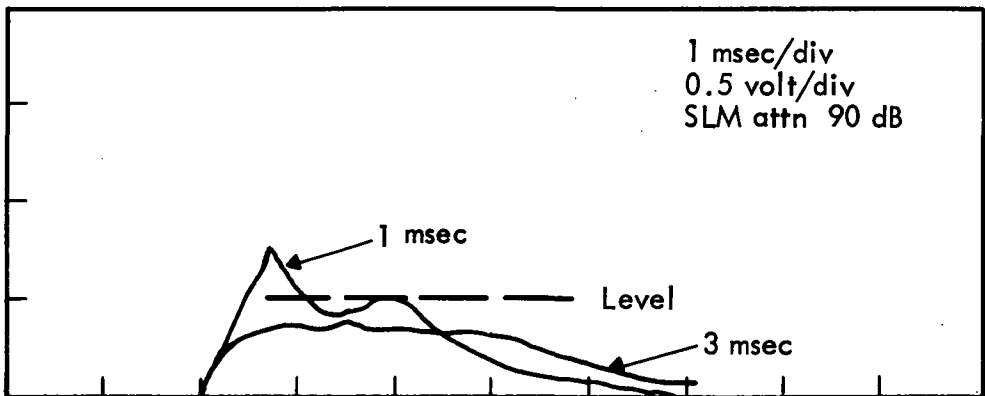
4 f

FIGURE 4.   CONTINUED
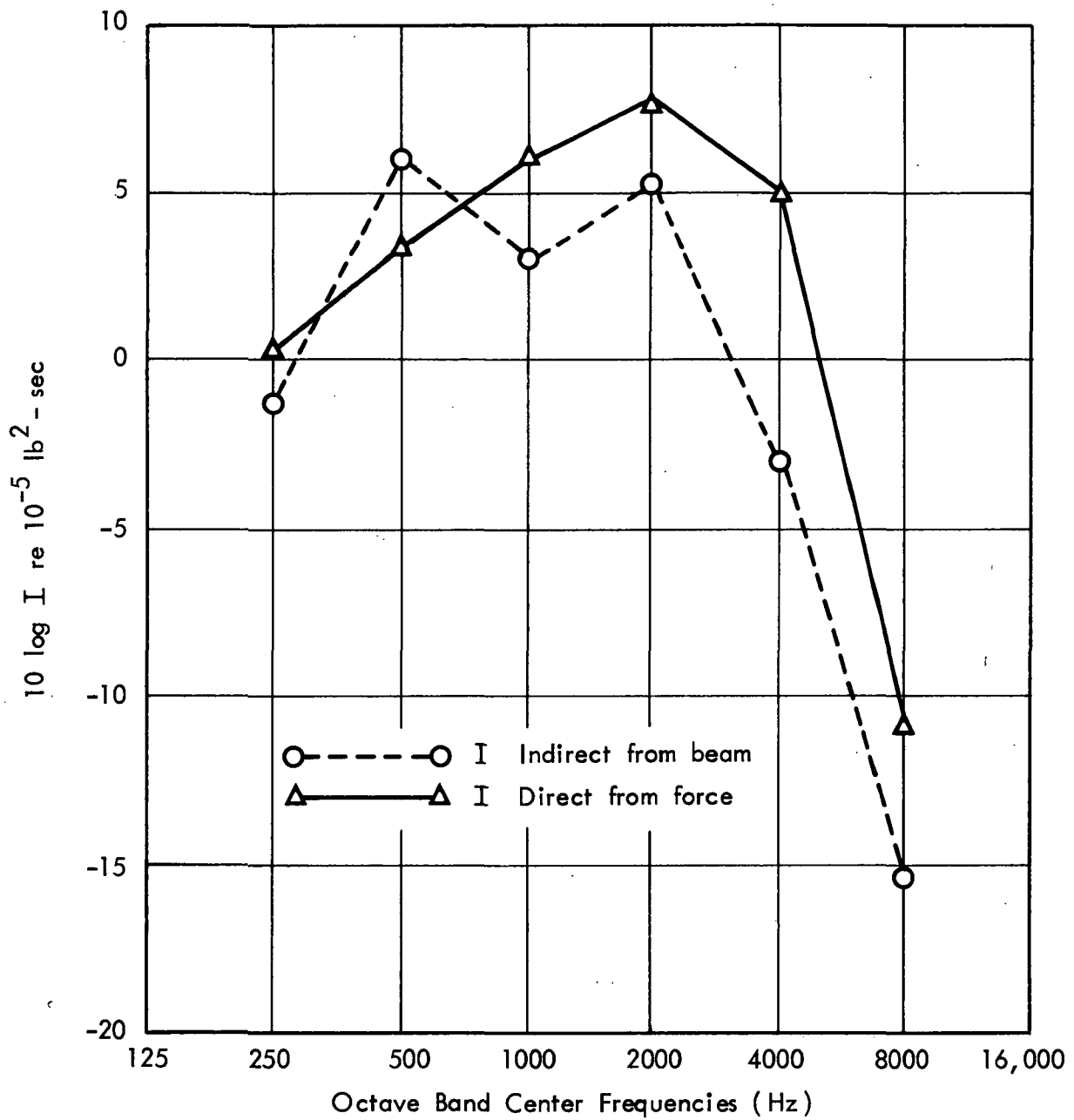
FIGURE 5.   A COMPARISON OF ESTIMATED (INDIRECT) AND "TRUE"
(DIRECT) OCTAVE BAND ENERGY SPECTRUMS
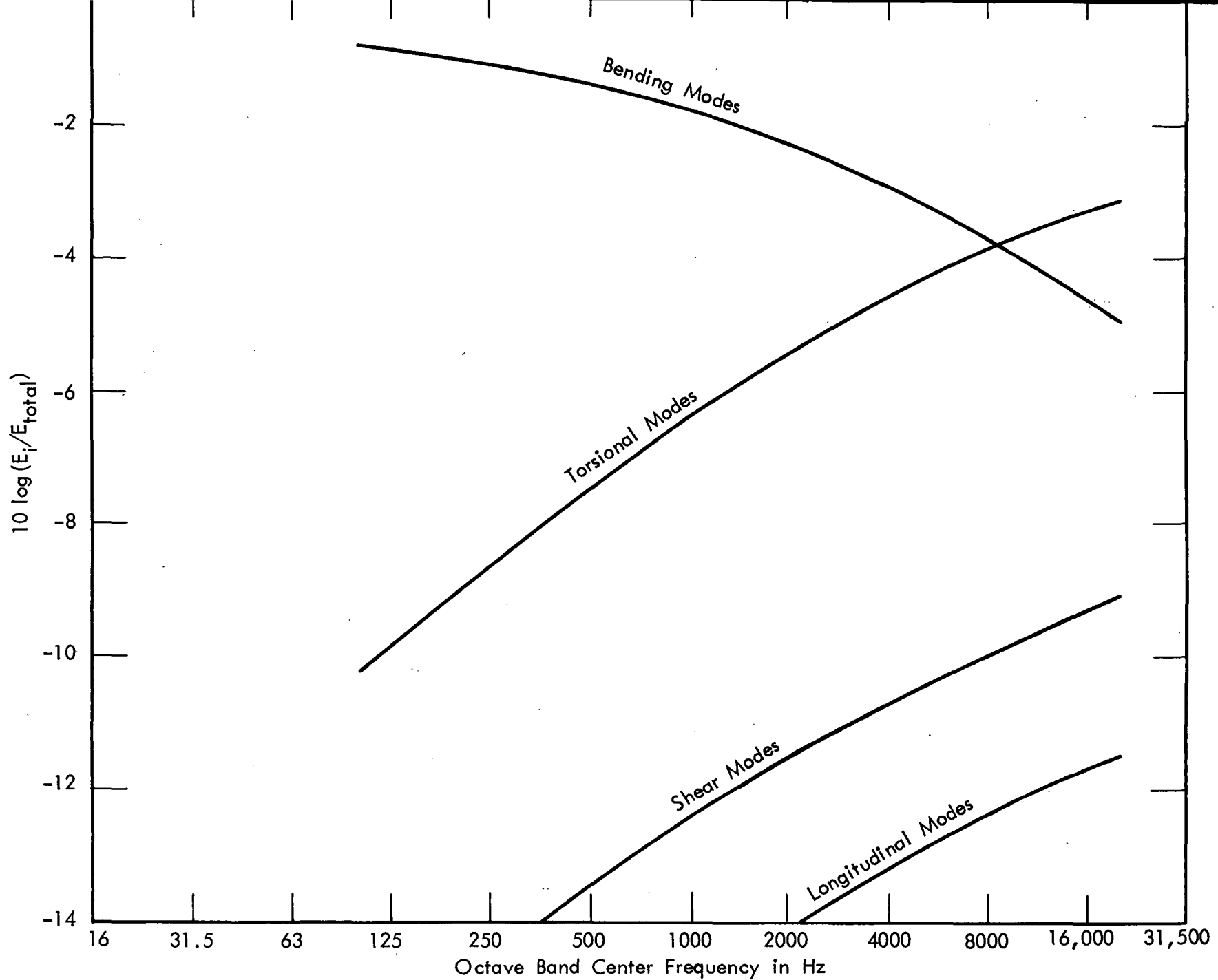
FIGURE 6. RATIO OF TOTAL MODAL ENERGIES TO TOTAL BEAM ENERGY
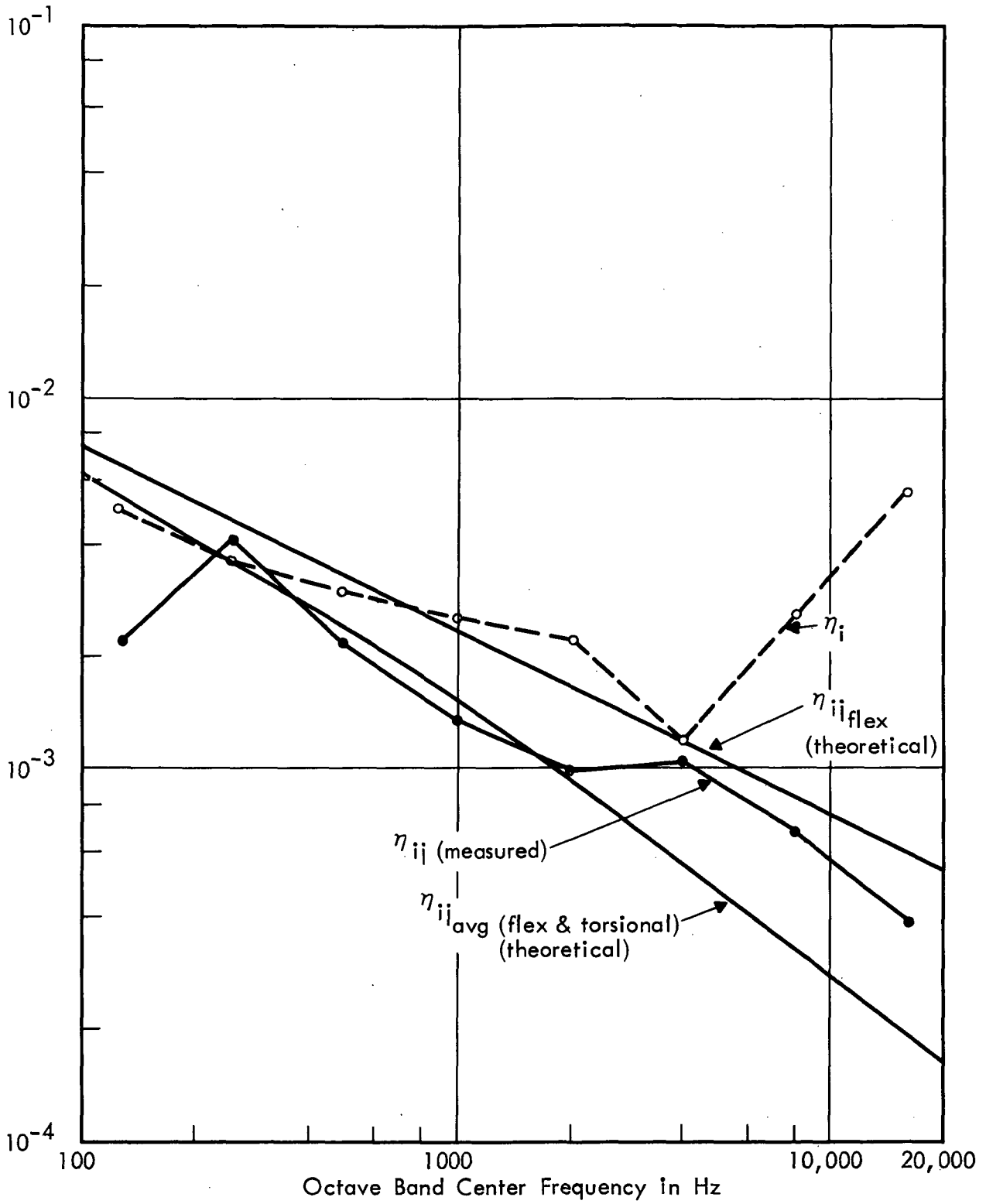
FIGURE 7.   COUPLING LOSS FACTOR, η_{ij} AND
INTERNAL LOSS FACTOR η_i
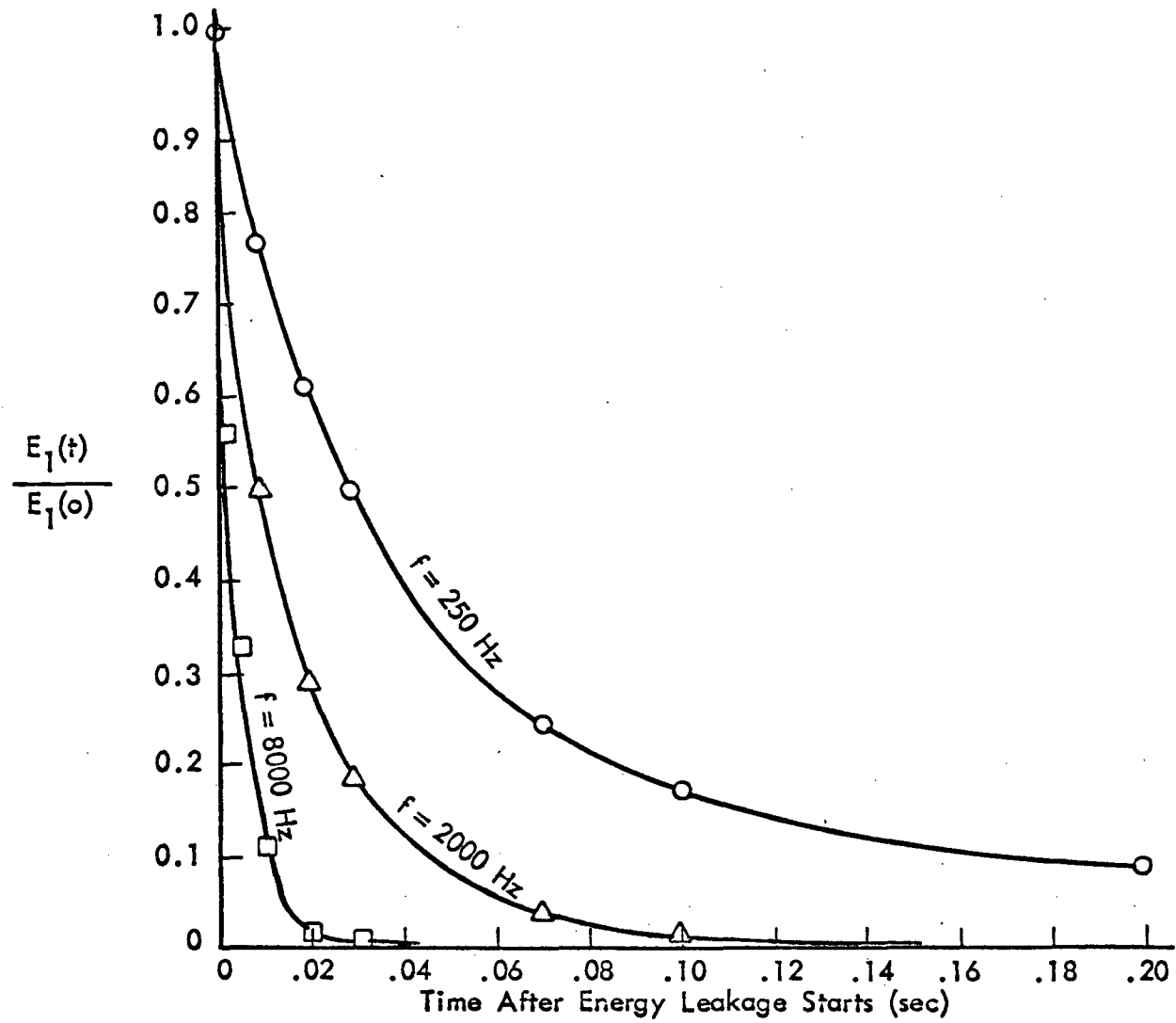
FIGURE 8.   DECAY OF THE ENERGY LEVEL OF BEAM 1
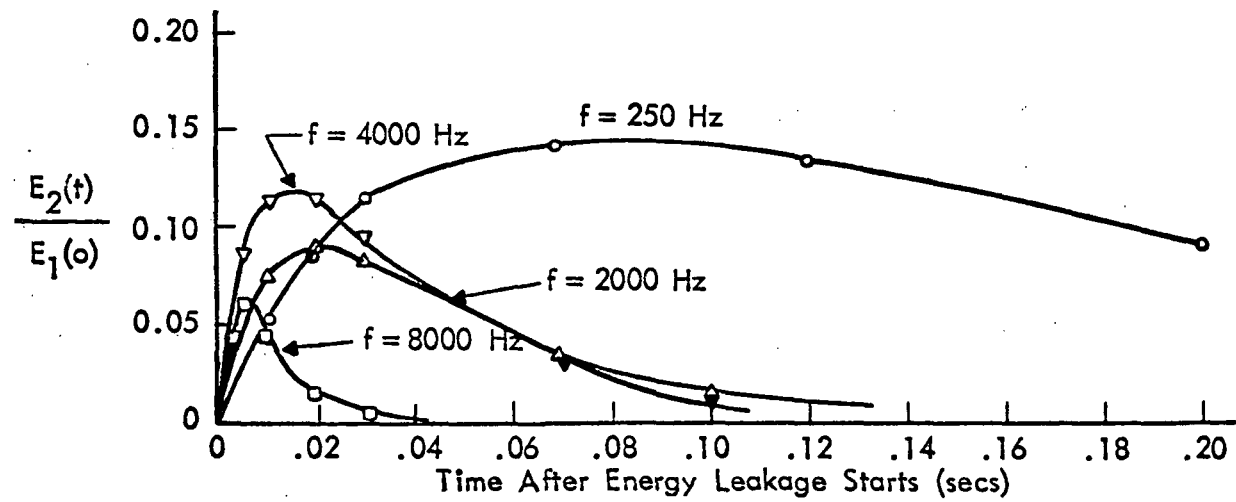
FIGURE 9. RATIO OF THE TOTAL SHORT-TIME AVERAGE
ENERGY OF BEAM 2 TO THE TOTAL ENERGY
INPUT IN BEAM 1 FOR THE VARIOUS
FREQUENCY BANDS

8000 Hz

0.05 volt/div
20 msec/div
SLM = 90 dB

——— Experimental
▲——▲ Theoretical

3 msec

(a)

4000 Hz

0.1 volt/div
20 msec/div
SLM = 90 dB

——— Experimental
▲——▲ Theoretical

10 msec

(b)

2000 Hz

0.2 volt/div
20 msec/div
SLM = 90 dB

——— Experimental
▲——▲ Theoretical

10 msec
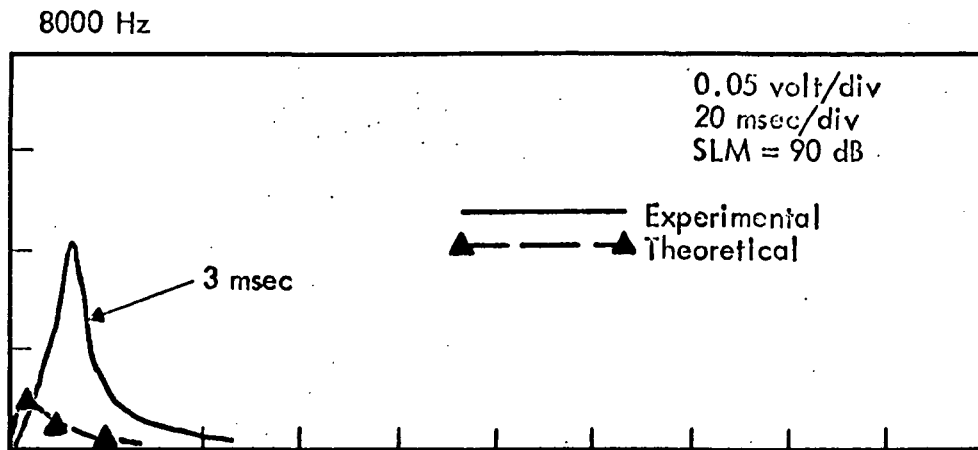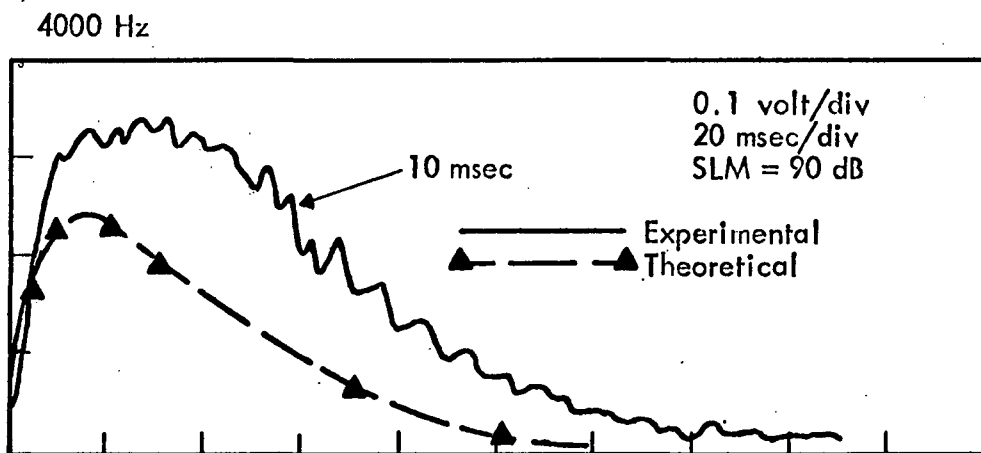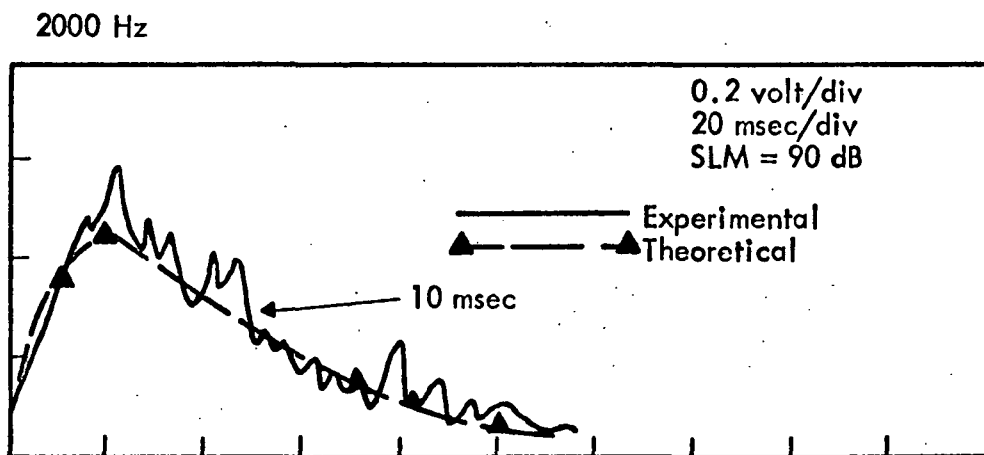
(c)

FIGURE 10.   COMPARISON OF EXPERIMENTAL AND THEORETICAL
             RESULTS
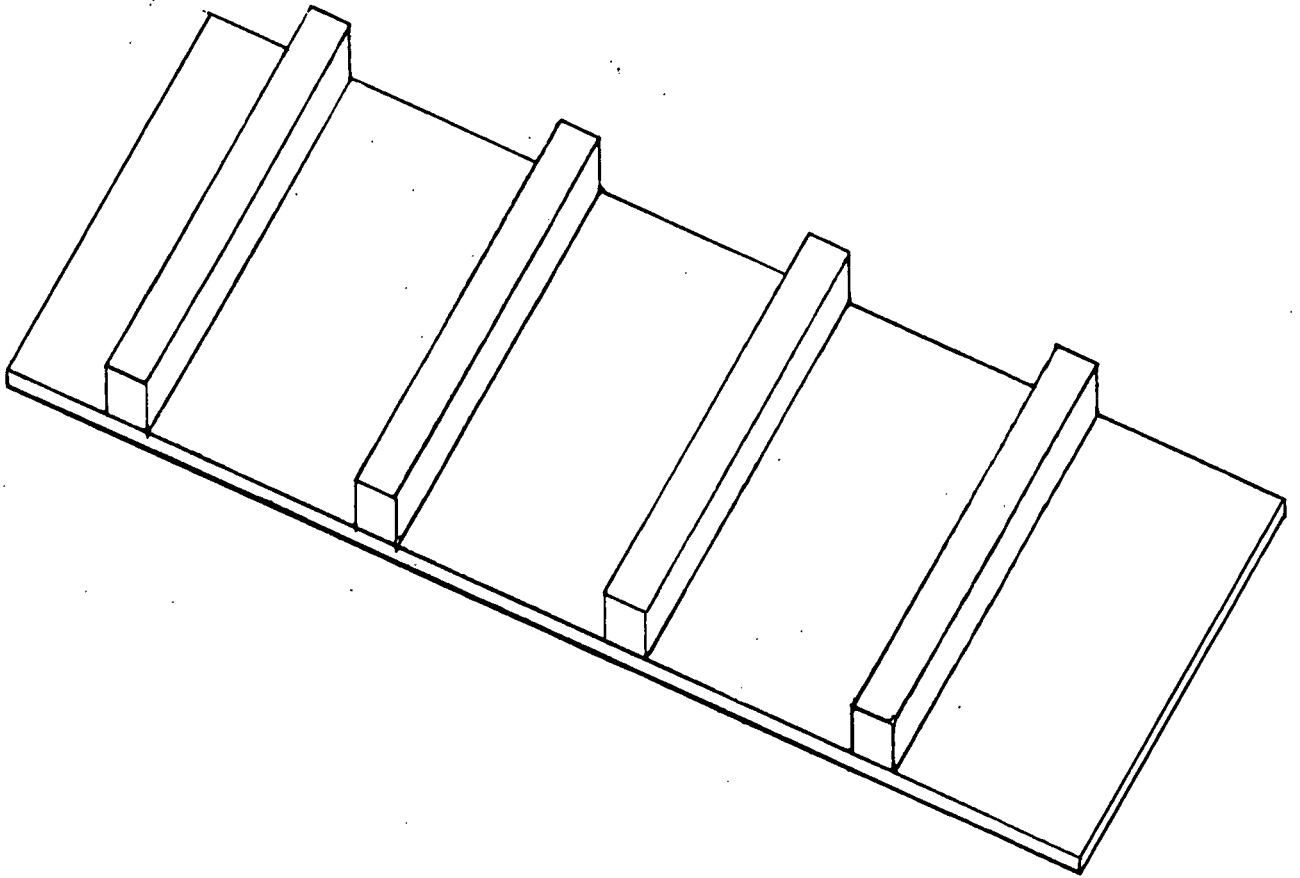
FIGURE 11: PLATE WITH TRANSVERSE BEAMS
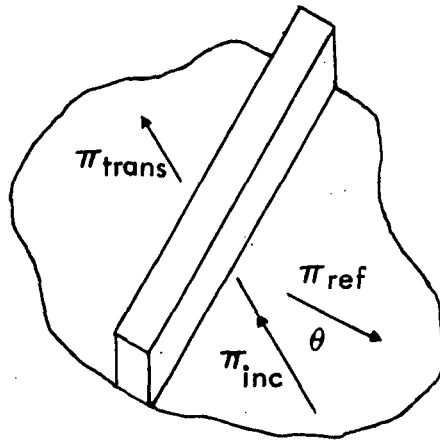
FIGURE 12a. INFINITE BEAM PLATE STRUCTURE
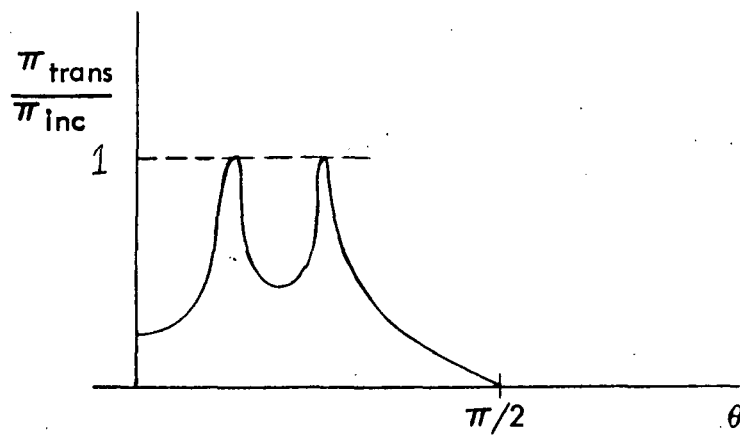
FIGURE 12b. TRANSMISSION AS A FUNCTION OF ANGLE OF INCIDENCE
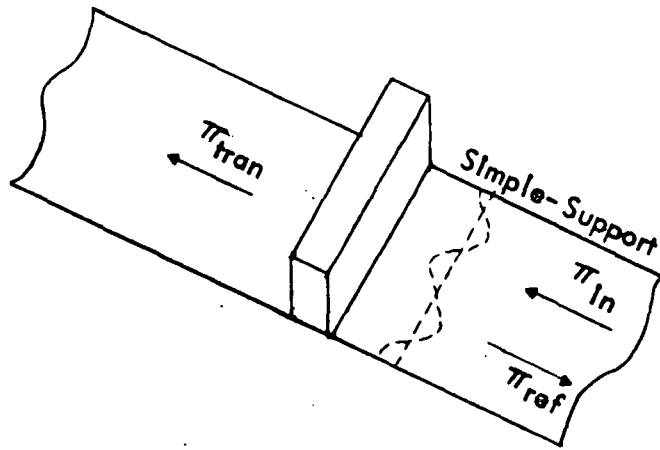
FIGURE 13a. BEAM PLATE STRUCTURE INFINITE IN ONE DIRECTION
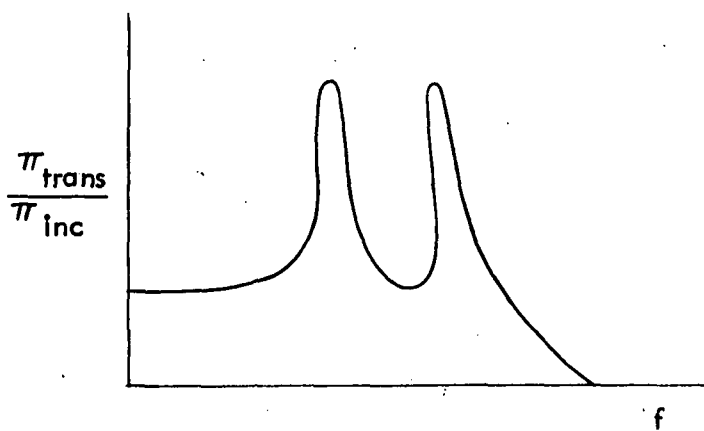
FIGURE 13b. TRANSMISSION AS A FUNCTION OF FREQUENCY
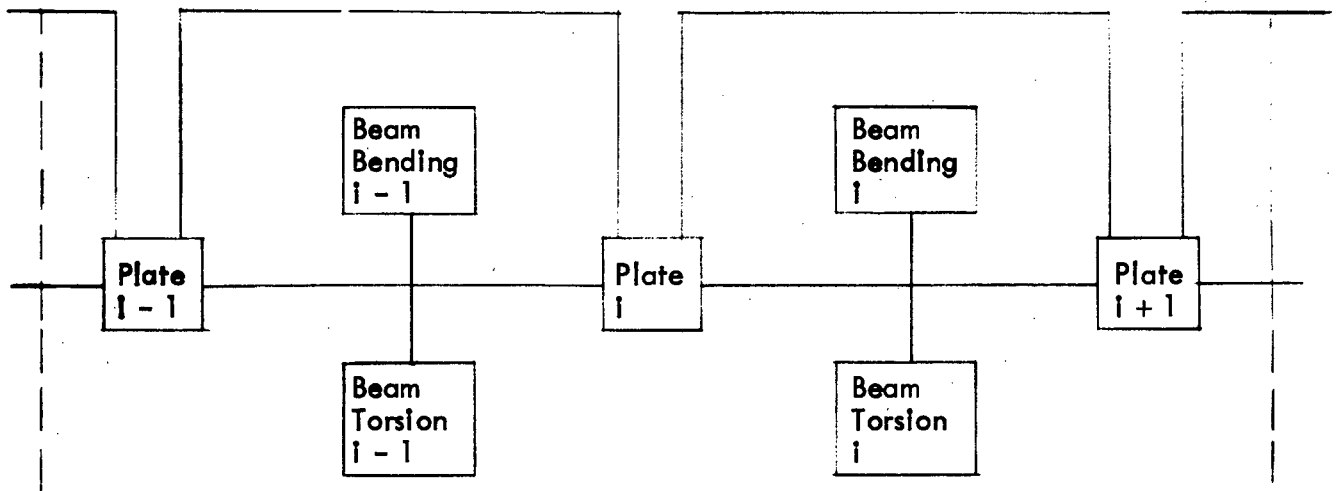
FIGURE 14. MODE GROUP ASSUMING EQUIPARTITION OF MODAL ENERGY IN EACH SUBPANEL AND BETWEEN BENDING AND TORSIONAL MODES IN THE BEAMS
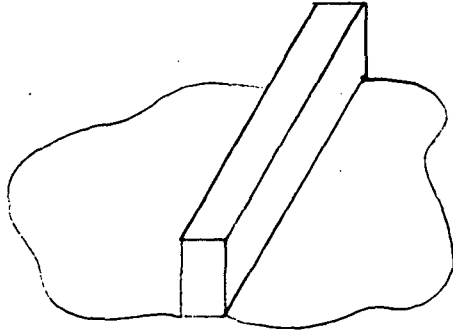
FIGURE 15. INFINITE BEAM-PLATE STRUCTURE
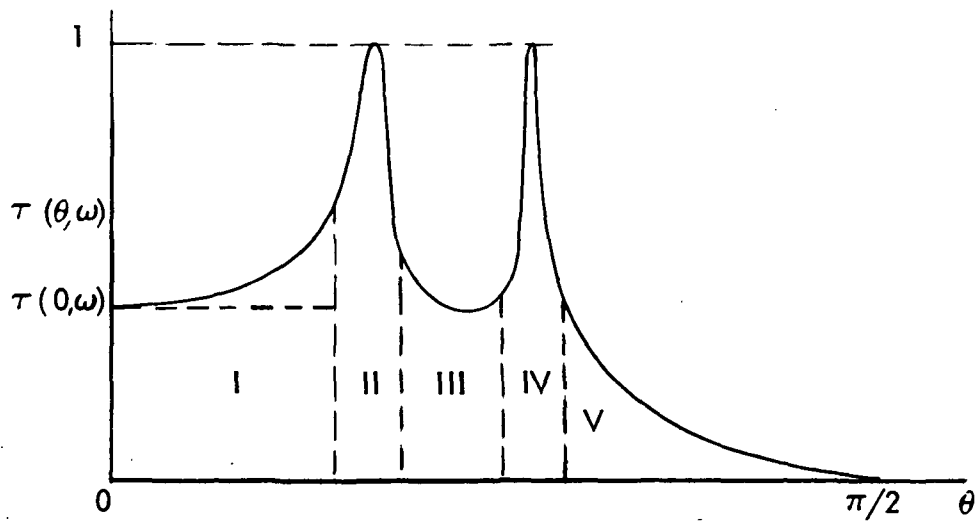
FIGURE 16. THE TRANSMISSION COEFFICIENT

3 Ft.

1/8"
5/8"
1/8"
5/8"

STIFFENERS

EQUALLY SPACED
STRINGERS

6 Ft.

6-1 5-1   Panel 4-1   Panel 3-1   2-1

Panel 4-2

6-2 5-2   Point   Panel 3-2   2-2
           x
           Impulsive
           Force

6-3 5-3   Panel 4-3   Panel 3-3   2-3

RINGS
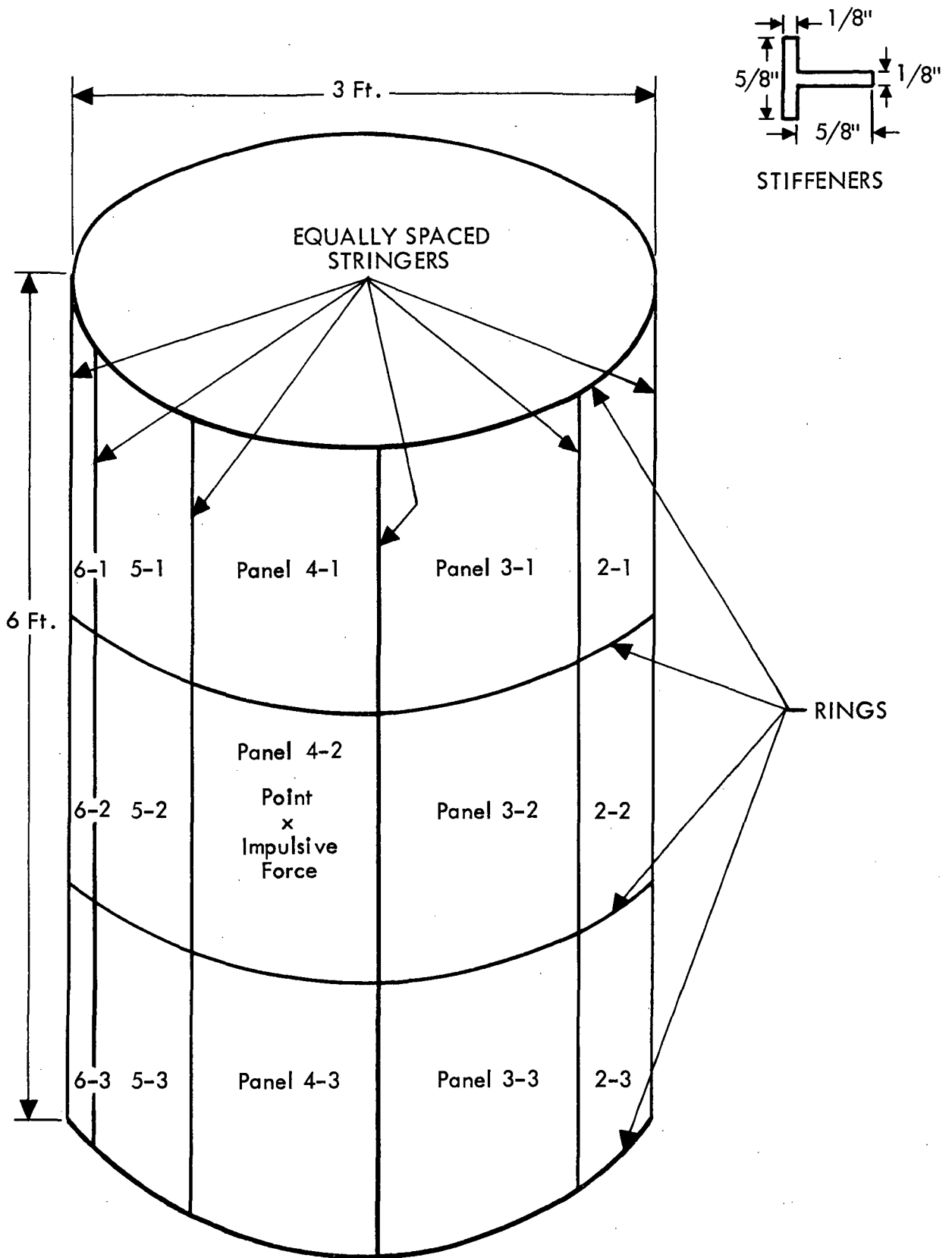
FIGURE 17. PANEL IDENTIFICATION OF THE CYLINDRICAL SHELL
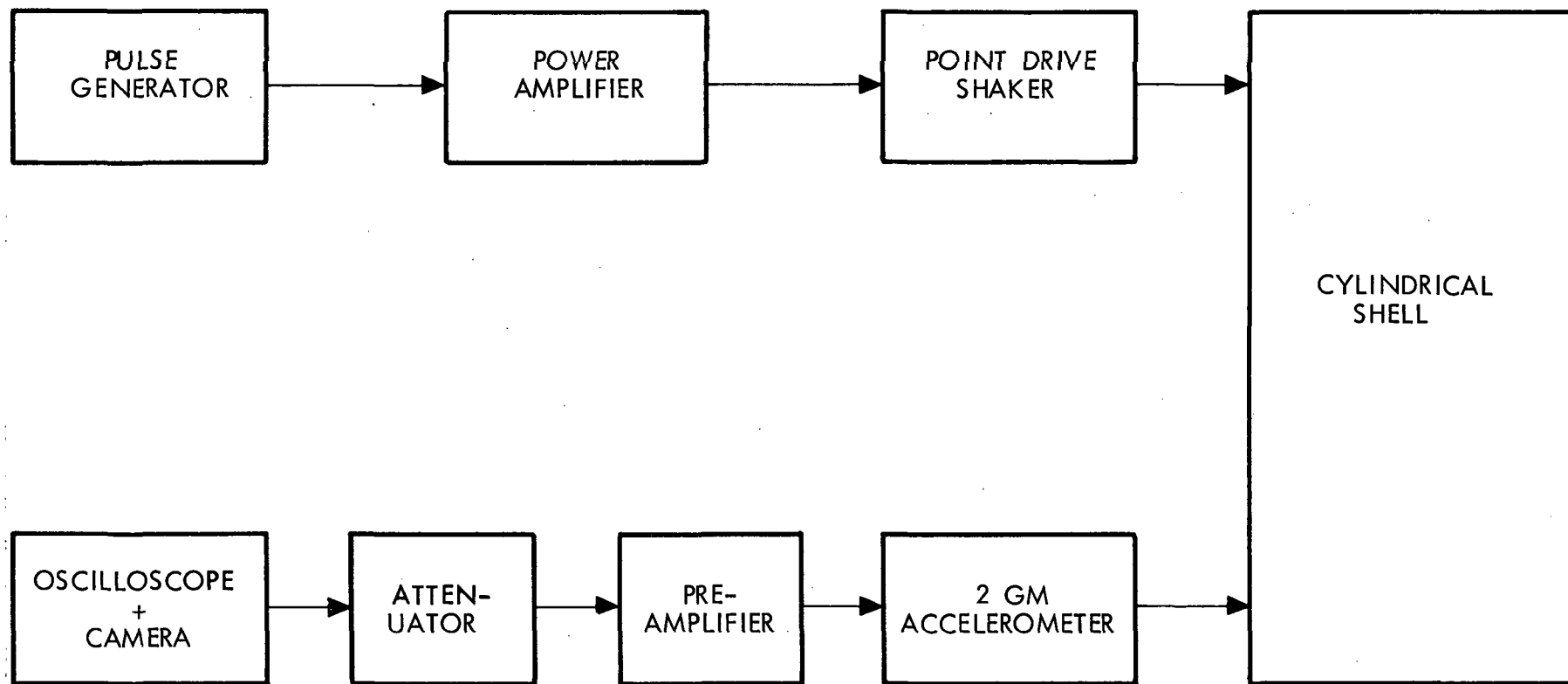
FIGURE 18.   BENDING-WAVE SHOCK TRANSMISSION TEST SET-UP
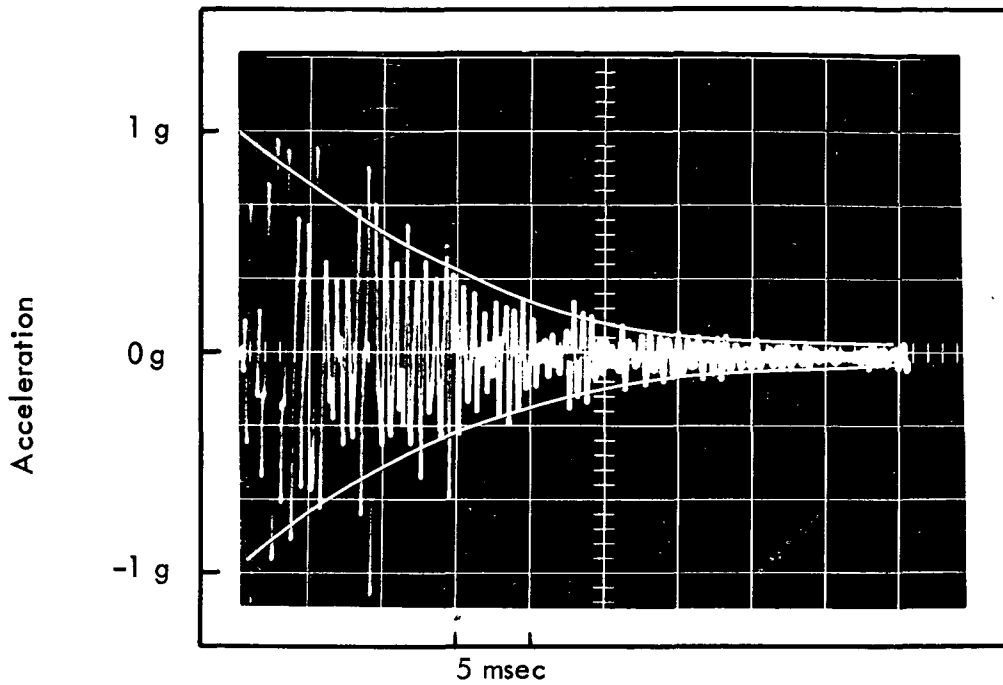
PANEL 4-2
DRIVEN PANEL
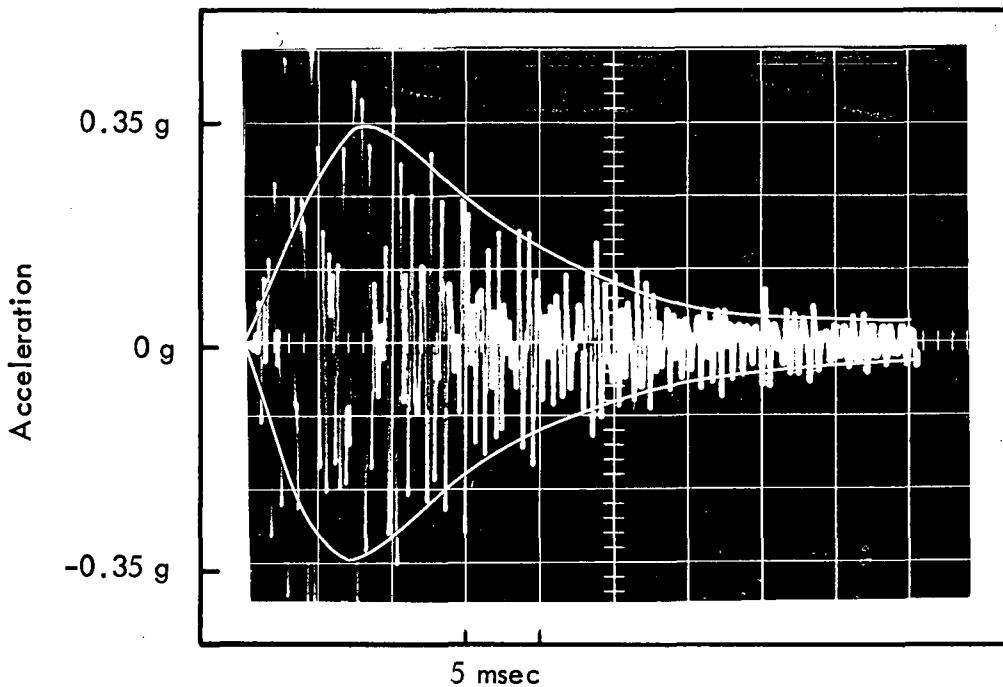
PANEL 5-2 ONE
PANEL AWAY
FROM DRIVEN
PANEL

FIGURE 19. BENDING-WAVE SHOCK TRANSMISSION IN THE MIDDLE
CIRCUMFERENTIAL ROW OF PANELS OF THE CYLINDRICAL
SHELL - FILTERED RESPONSE IN THE 2000 HZ OCTAVE
BAND
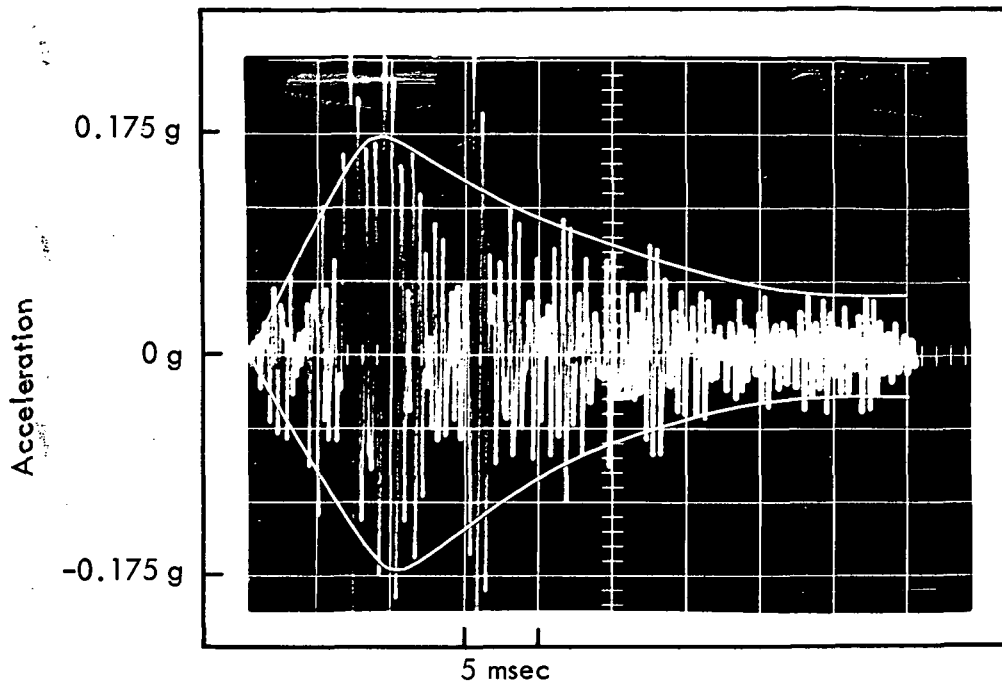
PANEL 6-2
TWO PANELS
AWAY FROM
DRIVEN PANEL
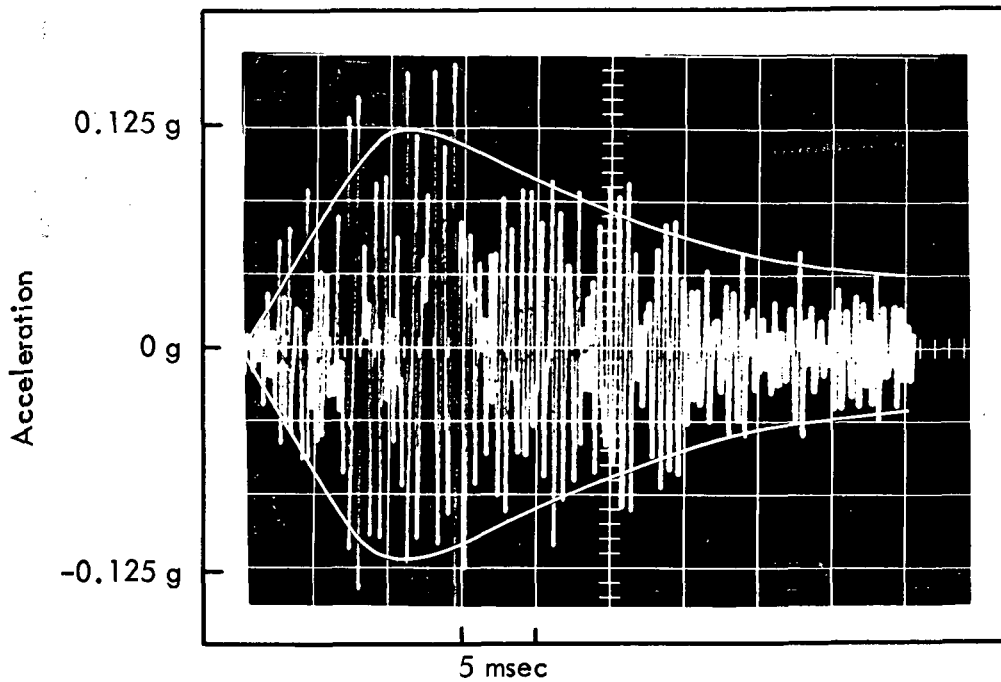
PANEL 7-2
THREE PANELS
AWAY FROM
DRIVEN PANEL

FIGURE 20. BENDING-WAVE SHOCK TRANSMISSION IN THE MIDDLE CIRCUMFERENTIAL ROW OF PANELS OF THE CYLINDRICAL SHELL - FILTERED RESPONSE IN THE 2000 HZ OCTAVE BAND
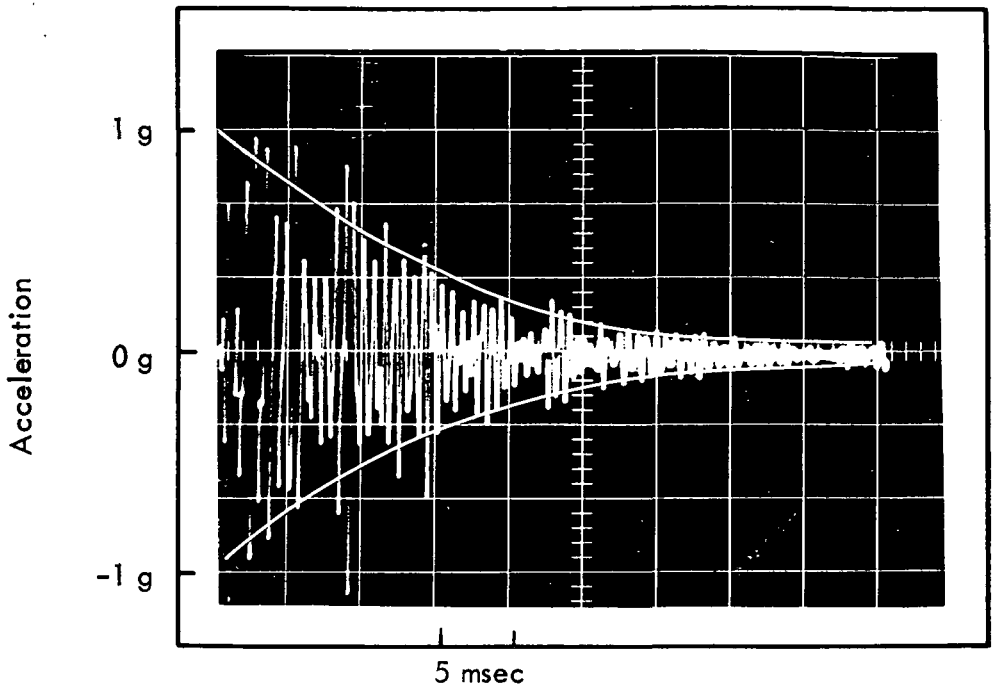
PANEL 4-2
DRIVEN PANEL
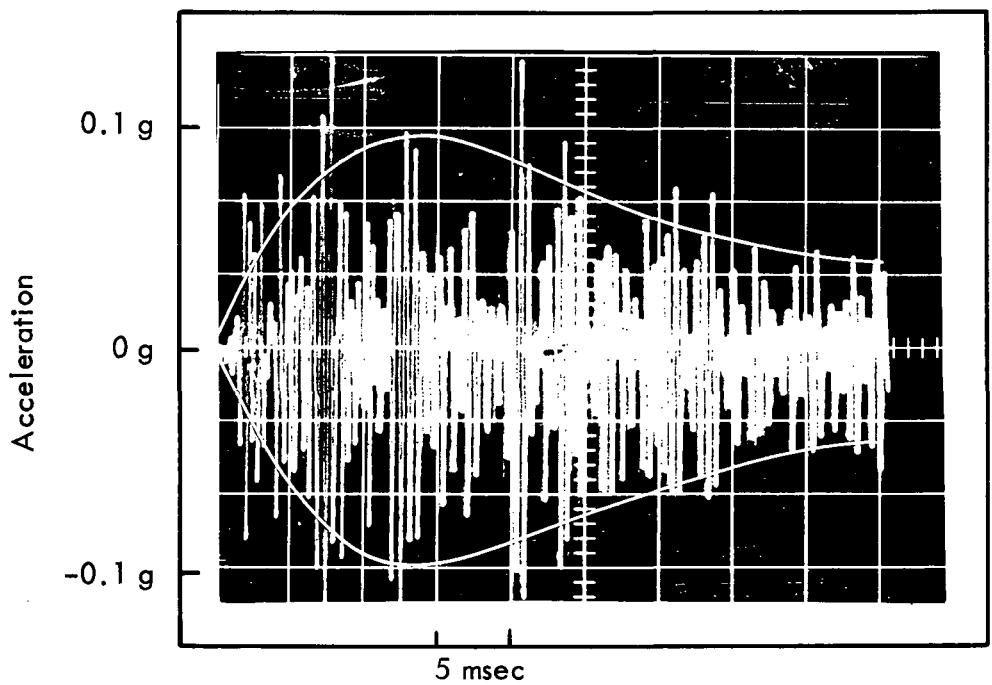
PANEL 4-1
ONE PANEL
ABOVE DRIVEN
PANEL

FIGURE 21. BENDING-WAVE SHOCK TRANSMISSION ACROSS A RING
OF THE CYLINDRICAL SHELL - FILTERED RESPONSE IN THE
2000 HZ OCTAVE BAND
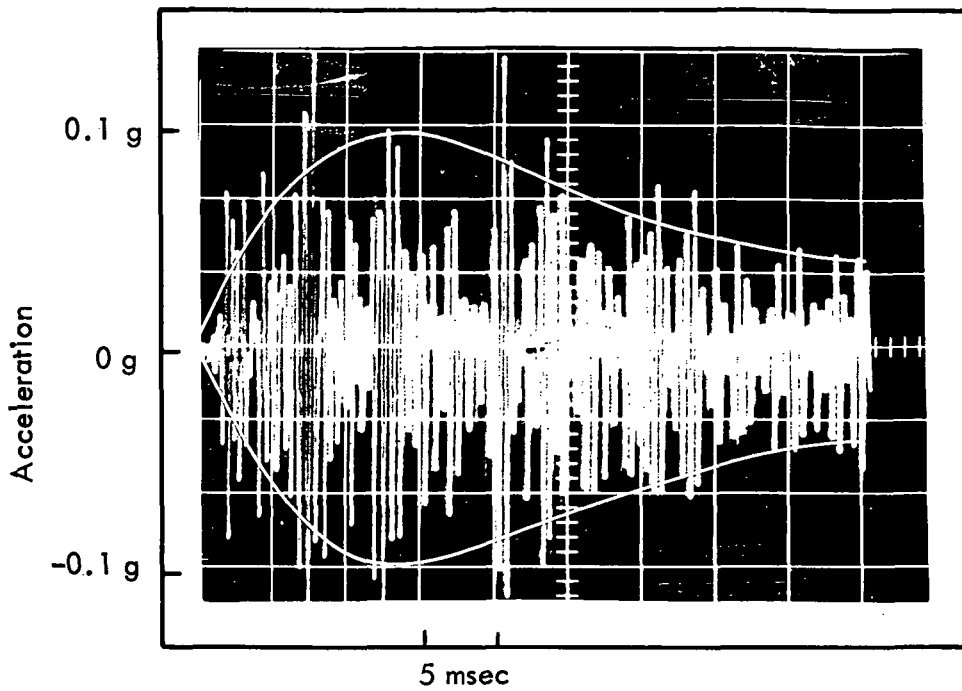
PANEL 4-1
ONE PANEL
ABOVE DRIVEN
PANEL
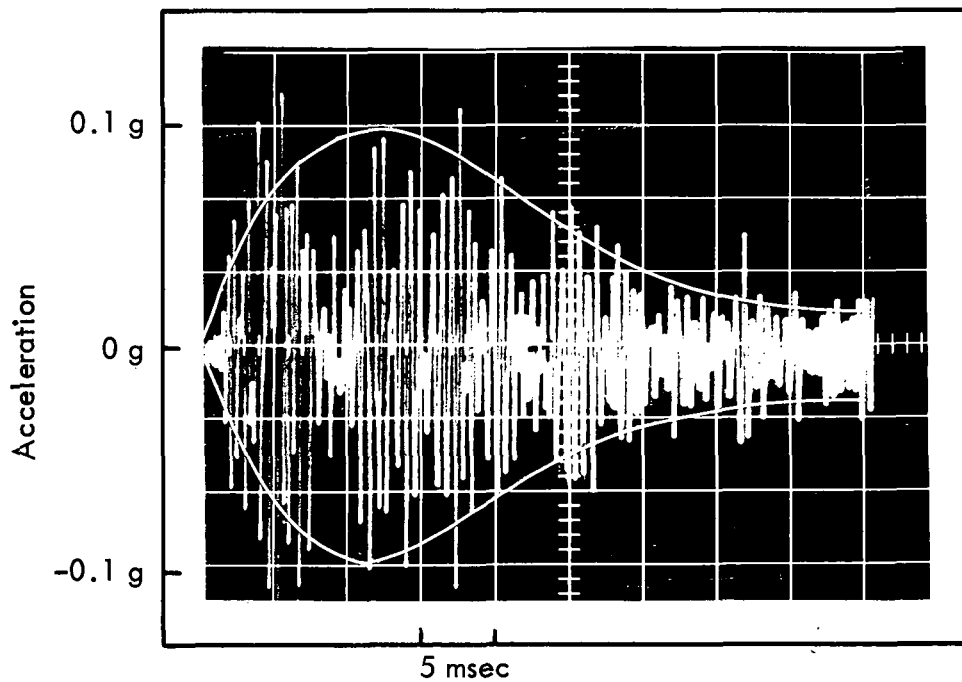
PANEL 5-1
ONE PANEL
AWAY FROM
PANEL 4-1

FIGURE 22. BENDING-WAVE SHOCK TRANSMISSION IN THE TOP CIRCUMFERENTIAL ROW OF PANELS OF THE CYLINDRICAL SHELL - FILTERED RESPONSE IN THE 2000 HZ OCTAVE BAND
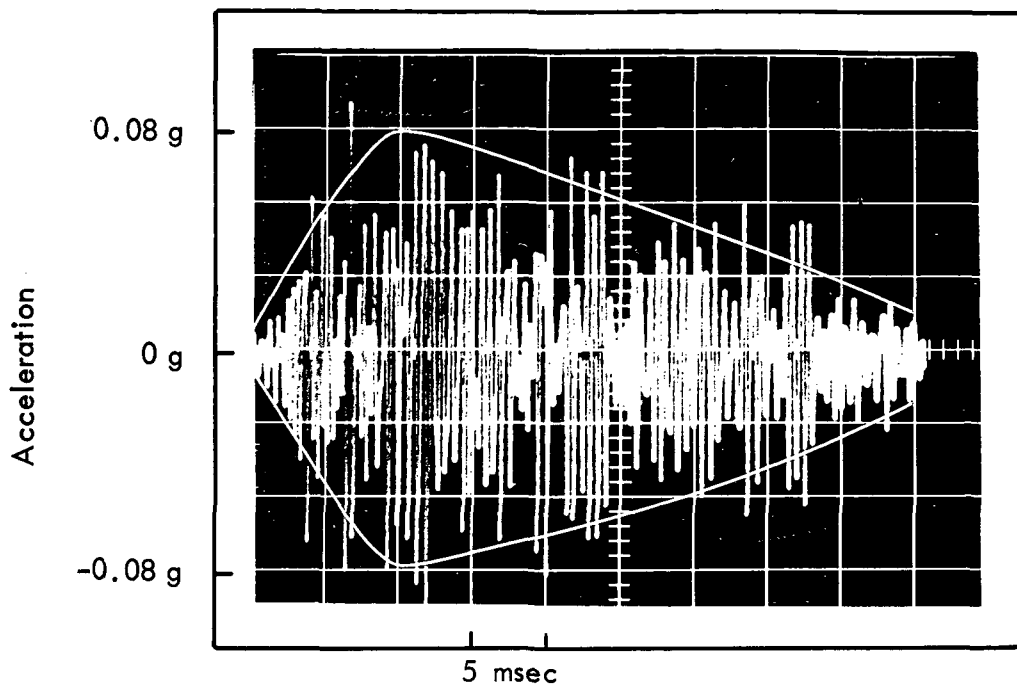
PANEL 6-1
TWO PANELS
AWAY FROM
PANEL 4-1
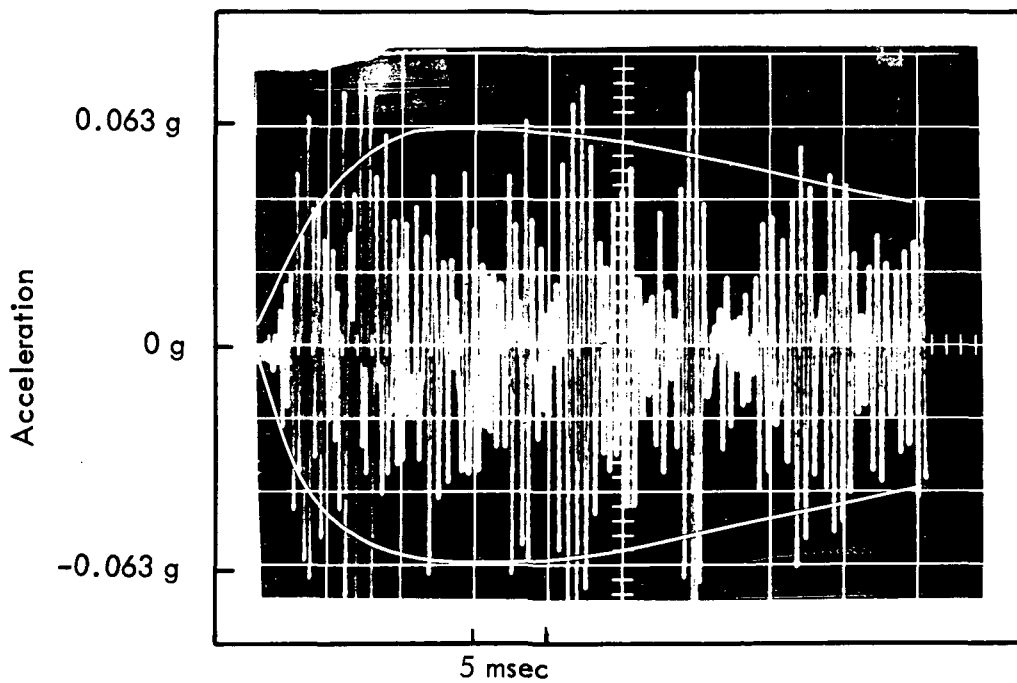
PANEL 7-1
THREE PANELS
AWAY FROM
PANEL 4-1

FIGURE 23. BENDING-WAVE SHOCK TRANSMISSION IN THE TOP
CIRCUMFERENTIAL ROW OF PANELS OF THE CYLINDRICAL
SHELL - FILTERED RESPONSE IN THE 2000 HZ OCTAVE
BAND
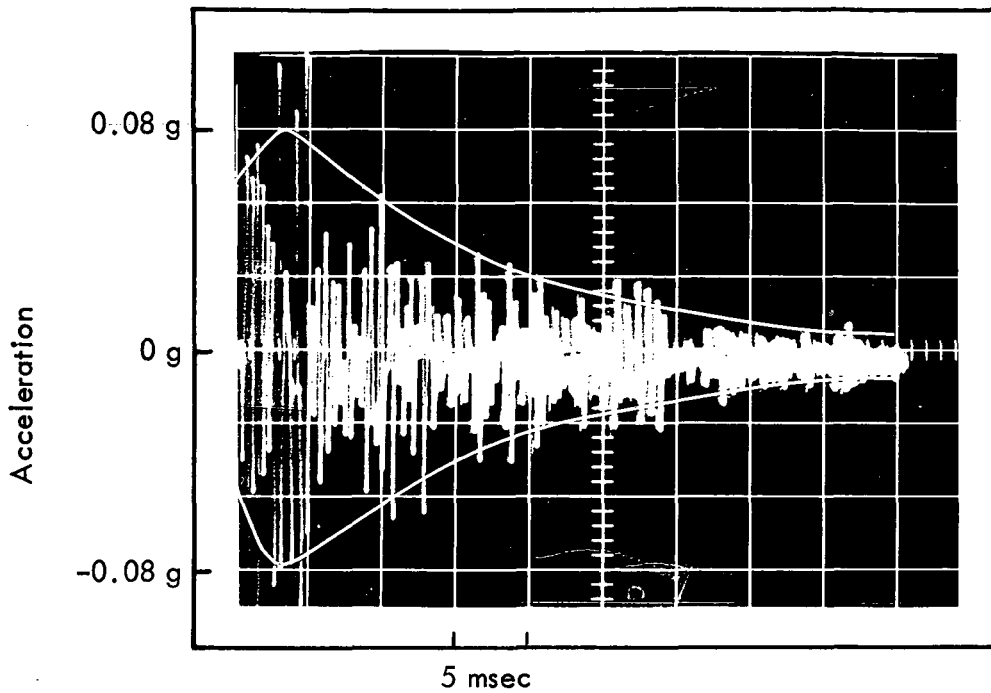
STRINGER
BETWEEN
PANELS 4-2
AND 5-2
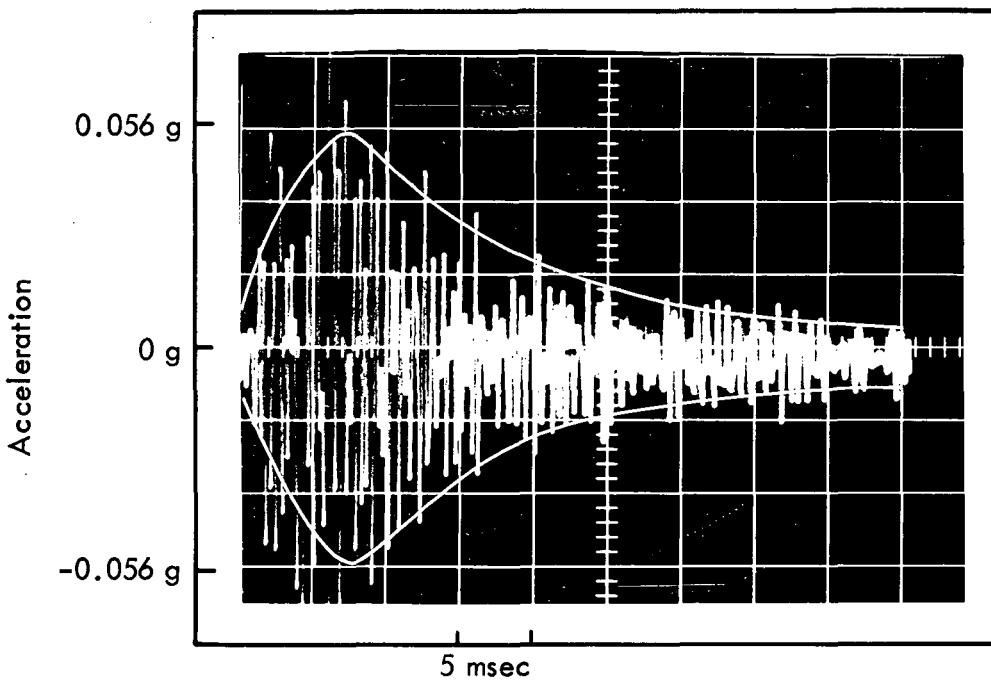
STRINGER
BETWEEN
PANELS 5-2
AND 6-2

FIGURE 24.   BENDING-WAVE SHOCK TRANSMISSION TO THE STRINGER
BEAM SEGMENTS - FILTERED RESPONSE IN THE 2000 HZ
OCTAVE BAND

Acceleration

0.0315 g

0 g

0.0315 g

5 msec

STRINGER
BETWEEN
PANELS 6-2
AND 7-2

Acceleration

0.0315 g

0 g

-0.0315 g

5 msec
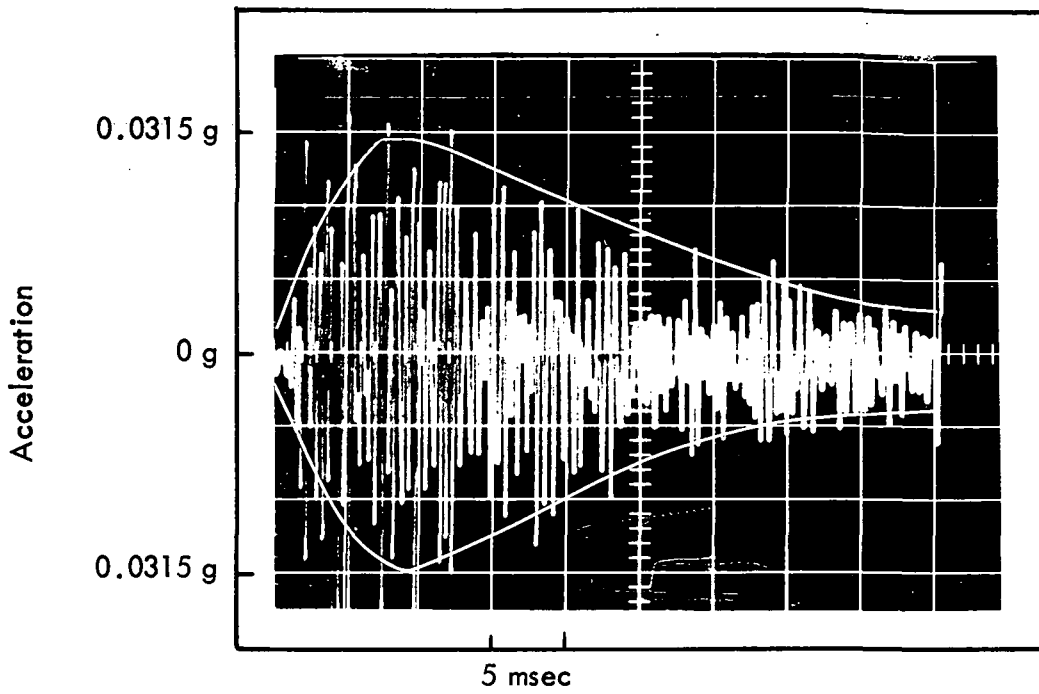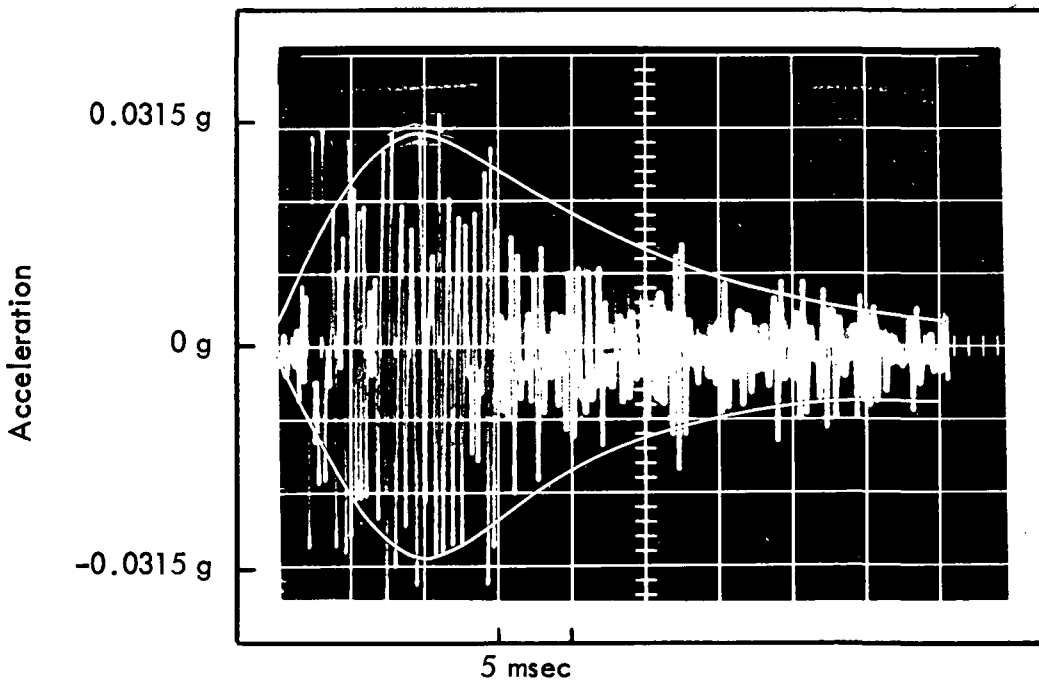
STRINGER
BETWEEN
PANELS 7-2
AND 8-2

FIGURE 25. BENDING-WAVE SHOCK TRANSMISSION TO THE STRINGER BEAM SEGMENTS - FILTERED RESPONSE IN THE 2000 HZ OCTAVE BAND
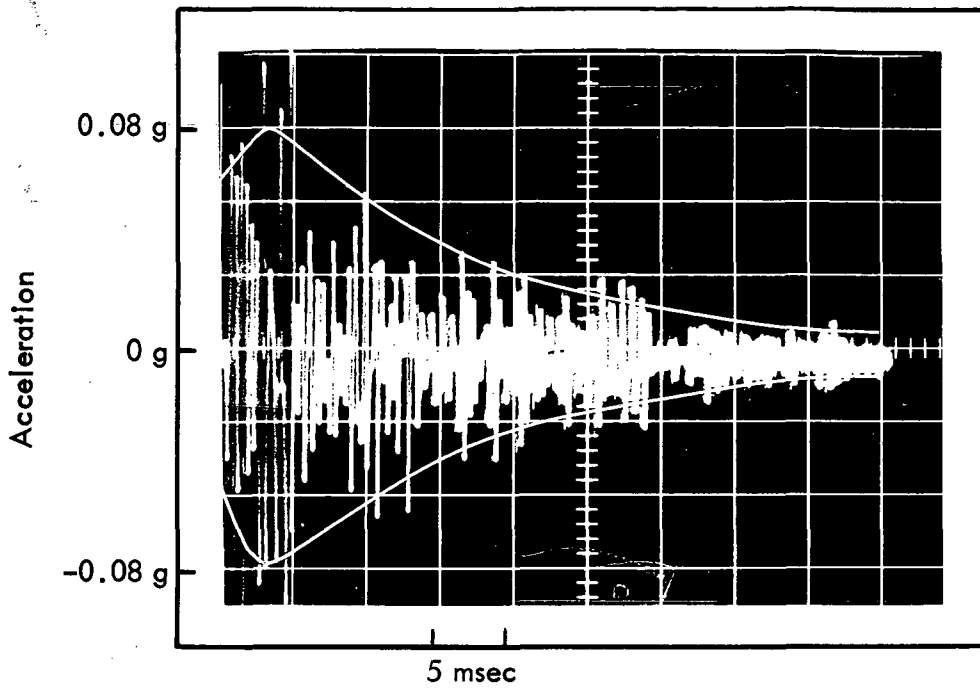
STRINGER
BETWEEN
PANELS 4-2
AND 5-2
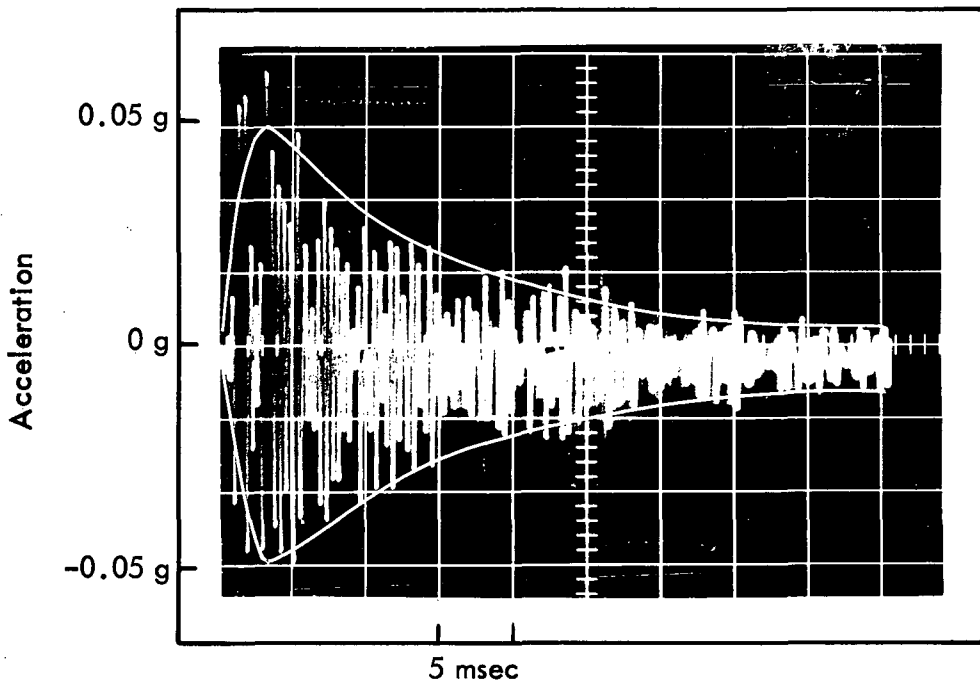
STRINGER
BETWEEN
PANELS 4-1
AND 5-1

FIGURE 26. BENDING-WAVE SHOCK TRANSMISSION TO THE STRINGER
BEAM SEGMENTS - FILTERED RESPONSE IN THE 2000 HZ
OCTAVE BAND
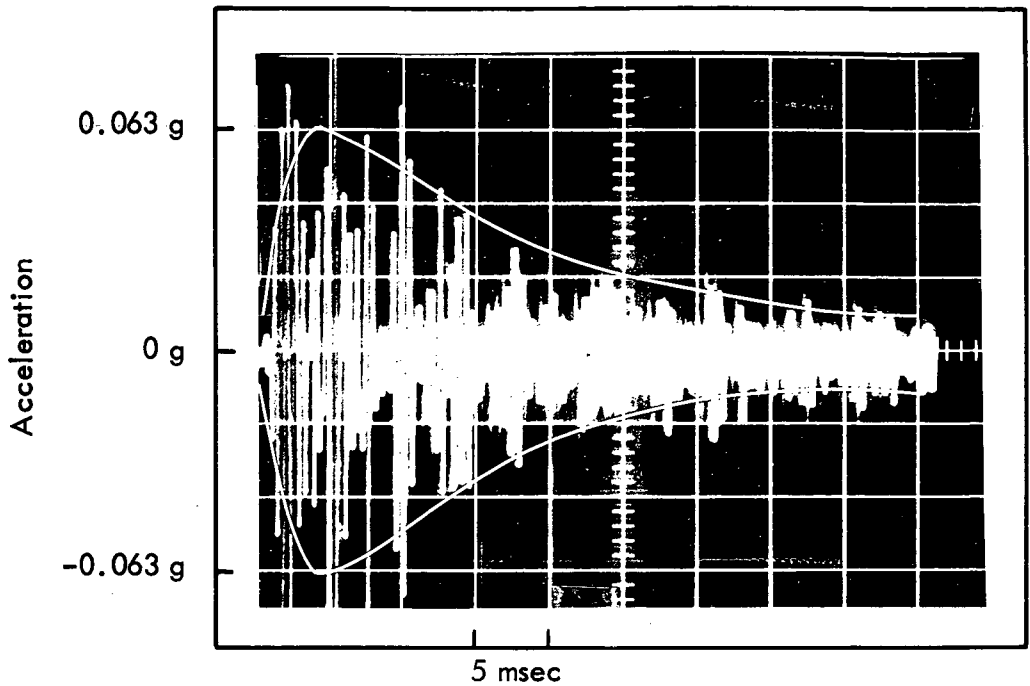
RING BETWEEN
PANELS 4-2
AND 4-1
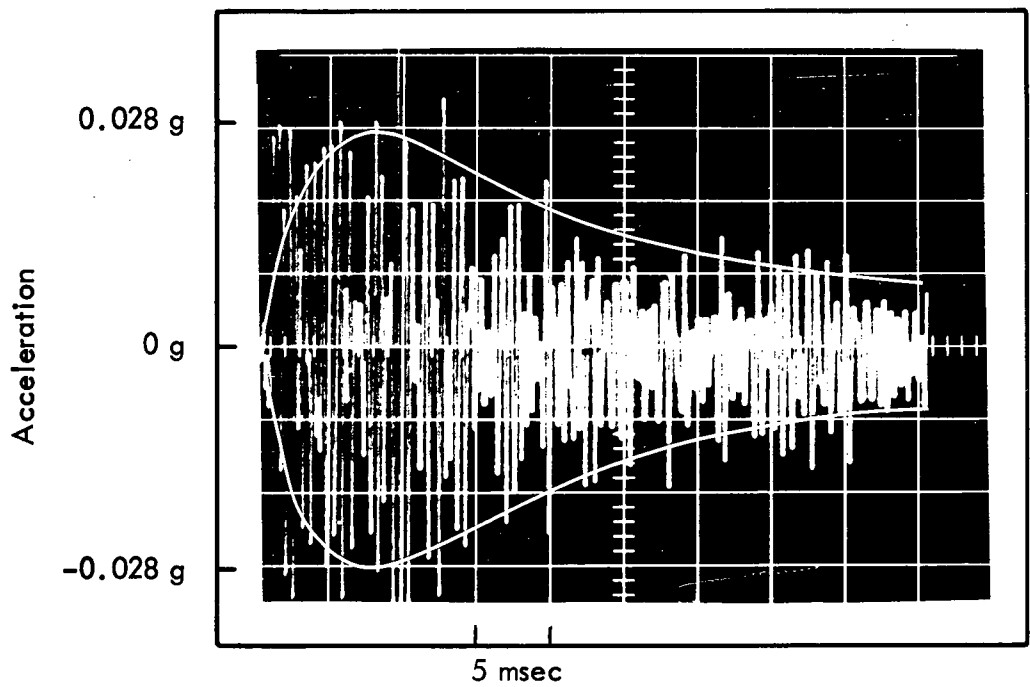
RING BETWEEN
PANELS 5-2
AND 5-1

FIGURE 27. BENDING-WAVE SHOCK TRANSMISSION TO THE RING
SEGMENTS - FILTERED RESPONSE IN THE 2000 HZ
OCTAVE BAND

Acceleration

0.028 g

0 g

-0.028 g

5 msec

RING BETWEEN
PANELS 6-2
AND 6-1

Acceleration

0.025 g

0 g

-0.025 g

5 msec
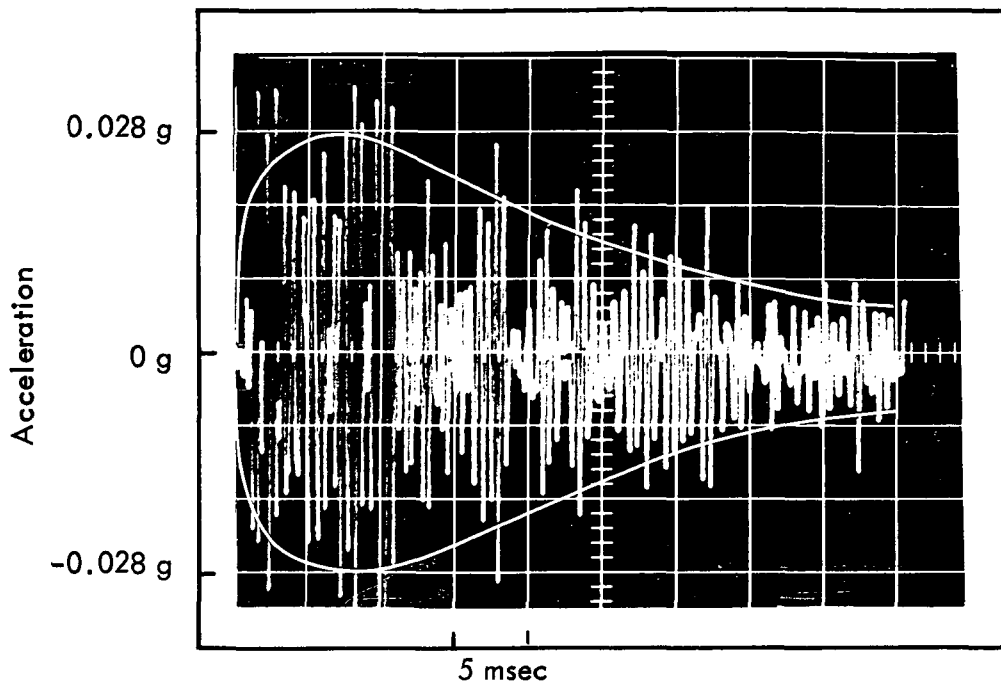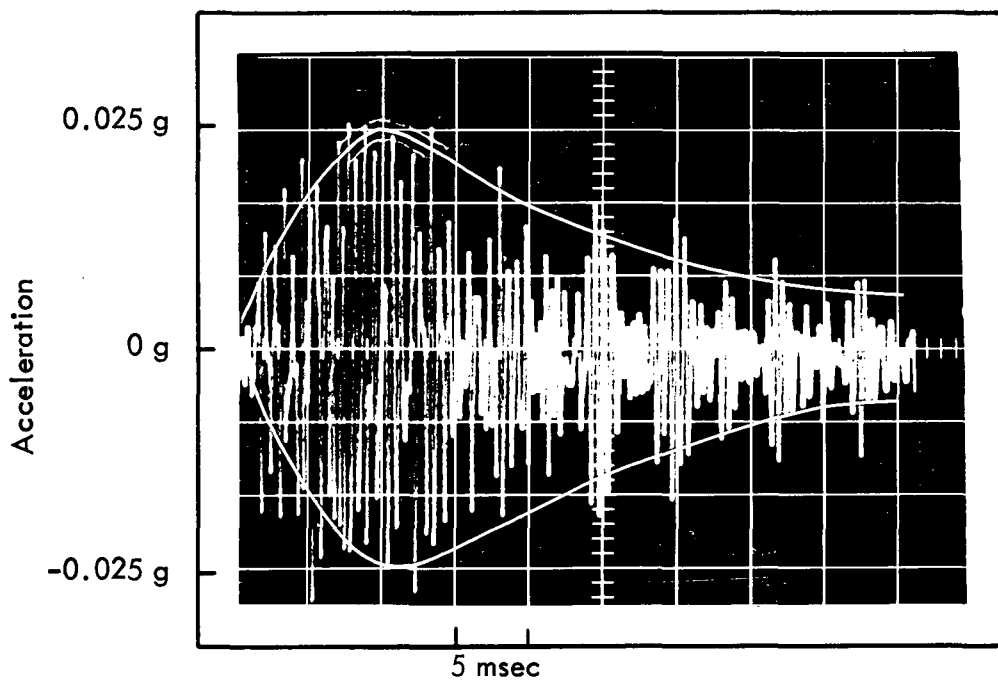
RING BETWEEN
PANELS 7-2
AND 7-1

FIGURE 28. BENDING-WAVE SHOCK TRANSMISSION TO THE RING SEGMENTS – FILTERED RESPONSE IN THE 2000 HZ OCTAVE BAND
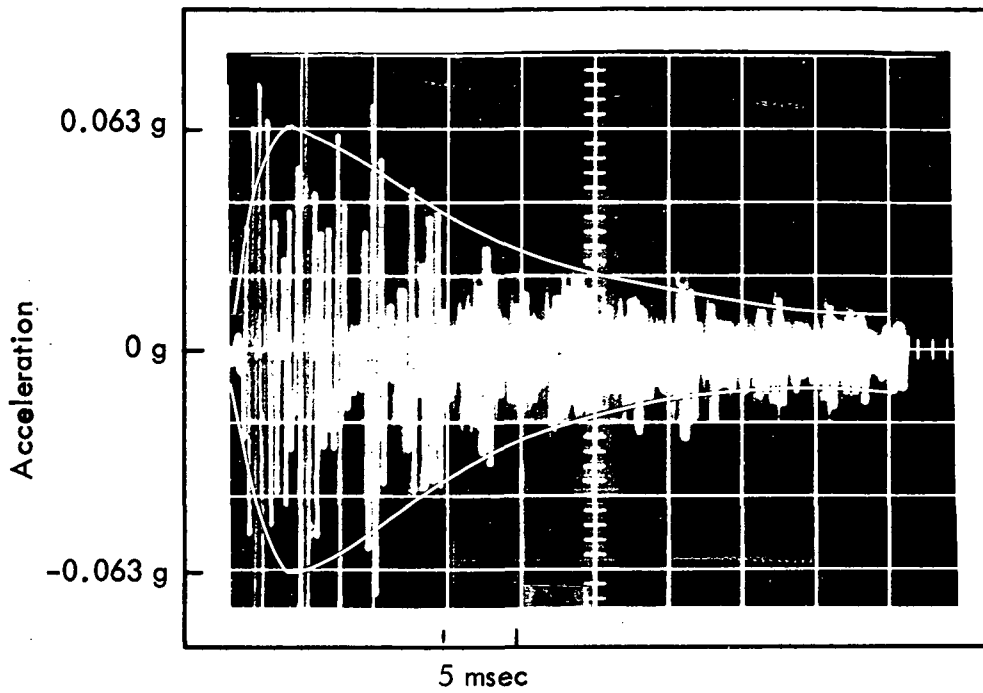
RING BETWEEN
PANELS 4-2
AND 4-1
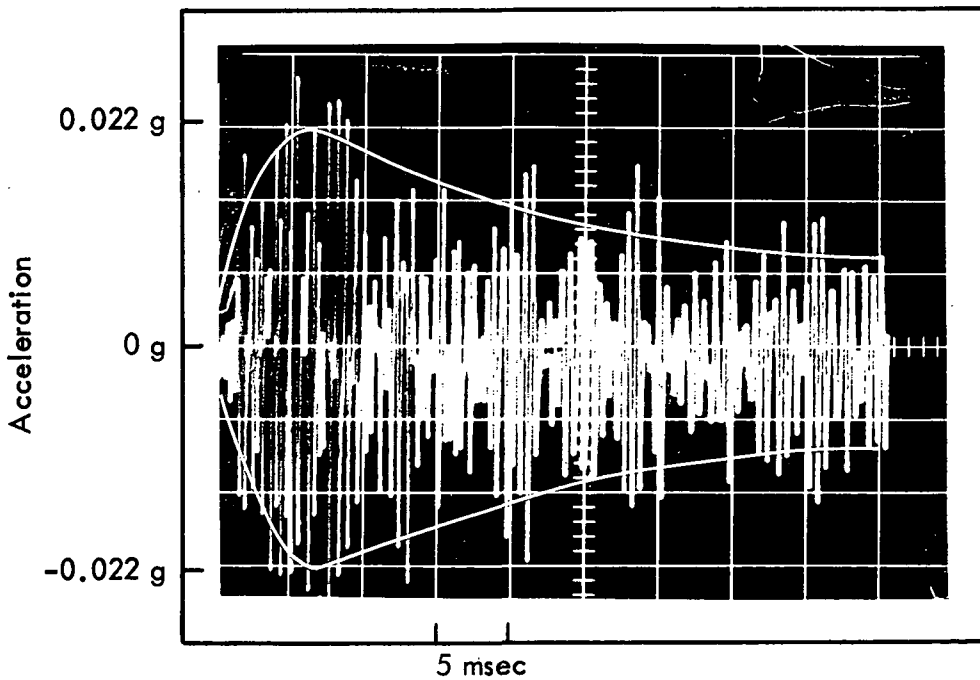
RING ABOVE
PANEL 4-1

FIGURE 29. BENDING-WAVE SHOCK TRANSMISSION TO THE RING
SEGMENTS - FILTERED RESPONSE IN THE 2000 HZ
OCTAVE BAND
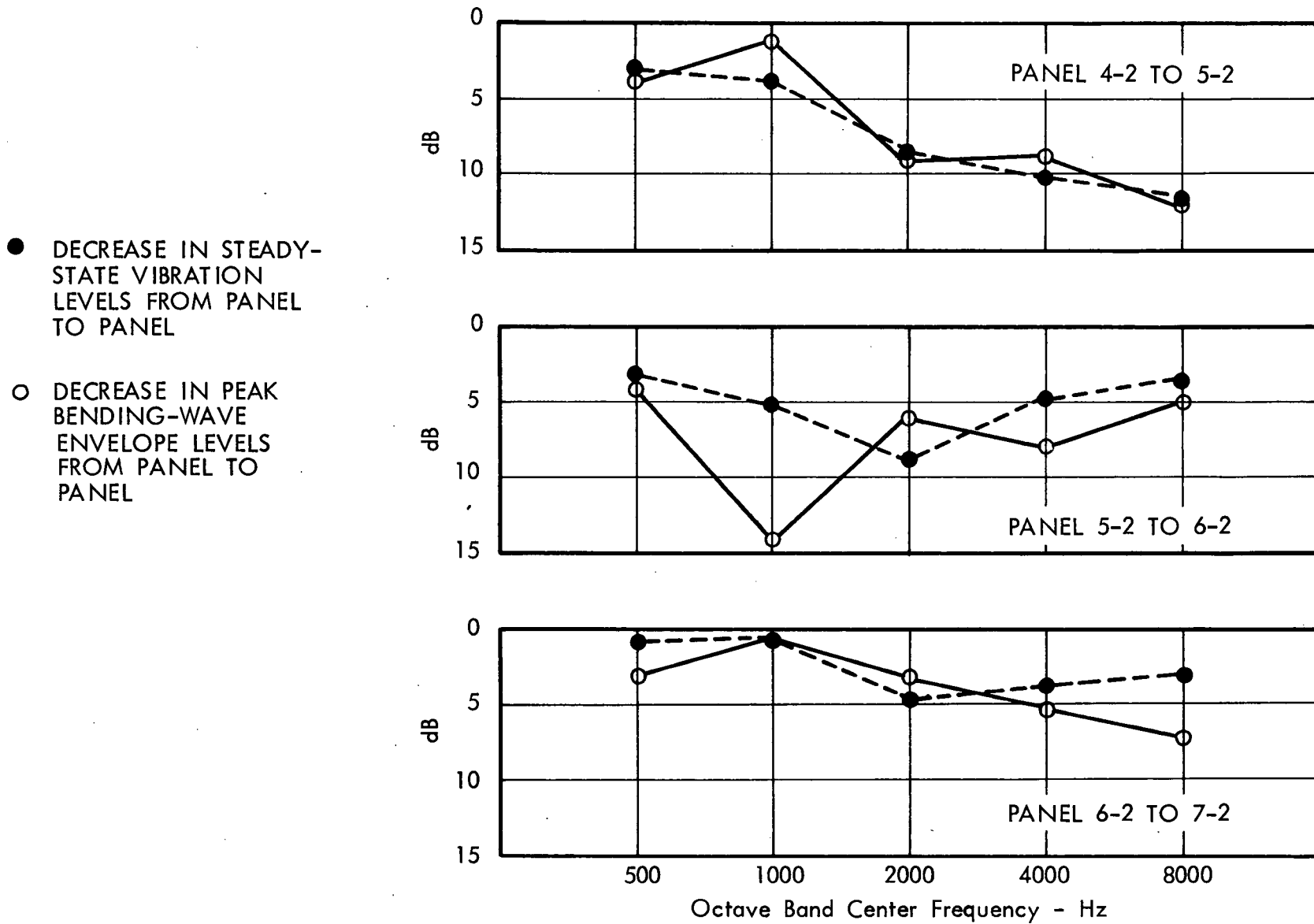
FIGURE 30. COMPARISON OF STEADY-STATE VIBRATION LEVEL REDUCTION FROM PANEL TO PANEL WITH REDUCTION OF PEAK BENDING-WAVE SHOCK ENVELOPES

DECREASE IN STEADY-STATE VIBRATION LEVELS FROM PANEL TO PANEL

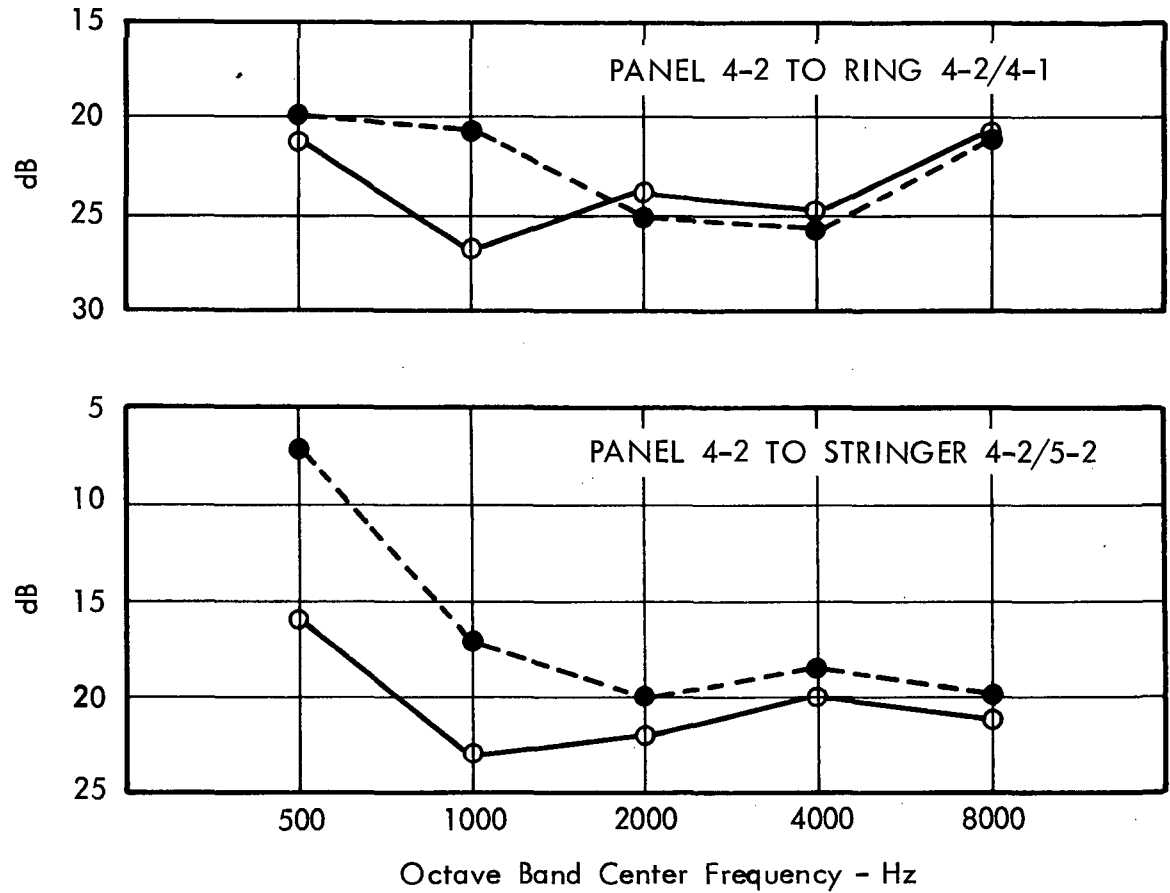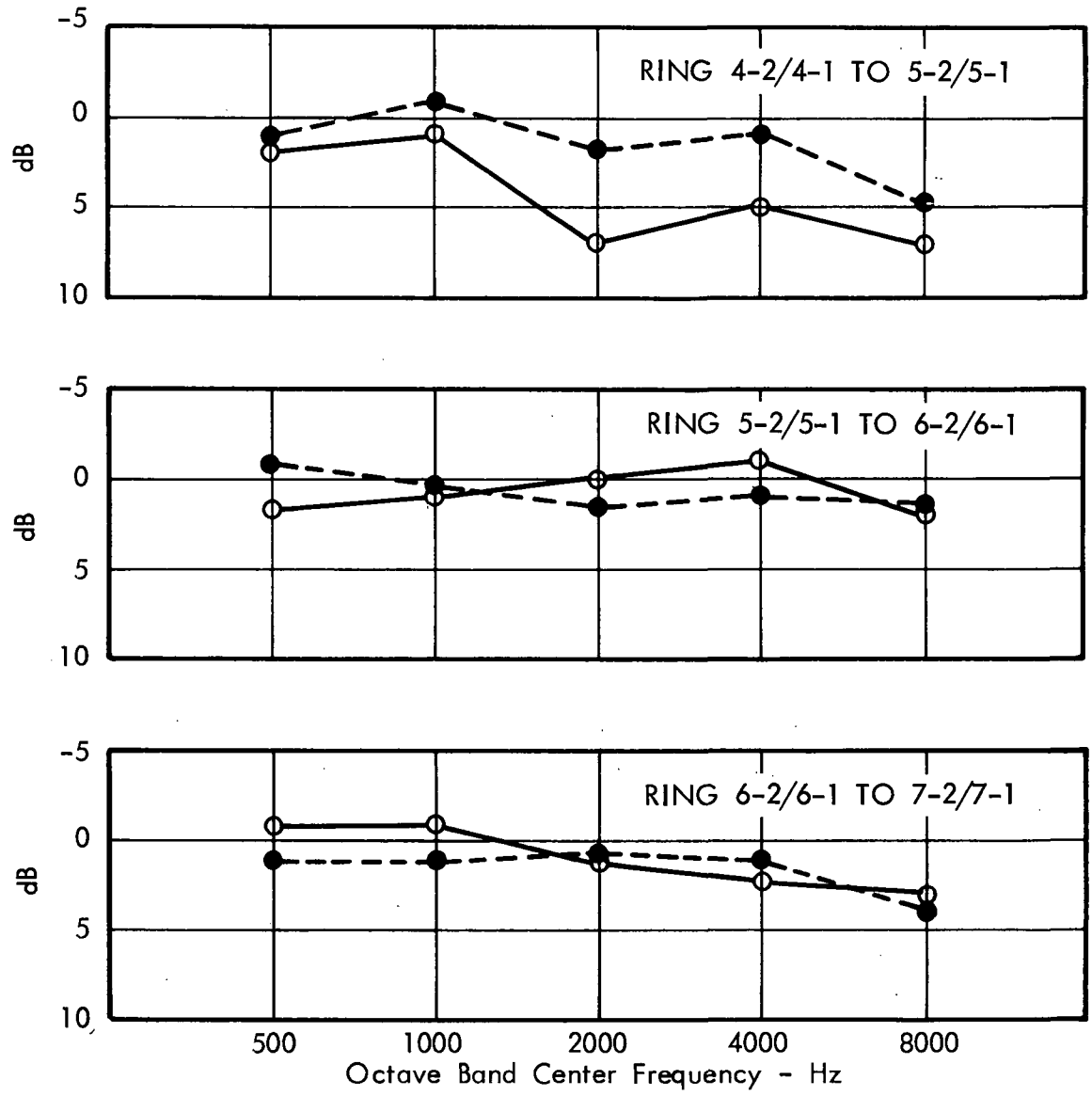DECREASE IN PEAK BENDING-WAVE ENVELOPE LEVELS FROM PANEL TO PANEL
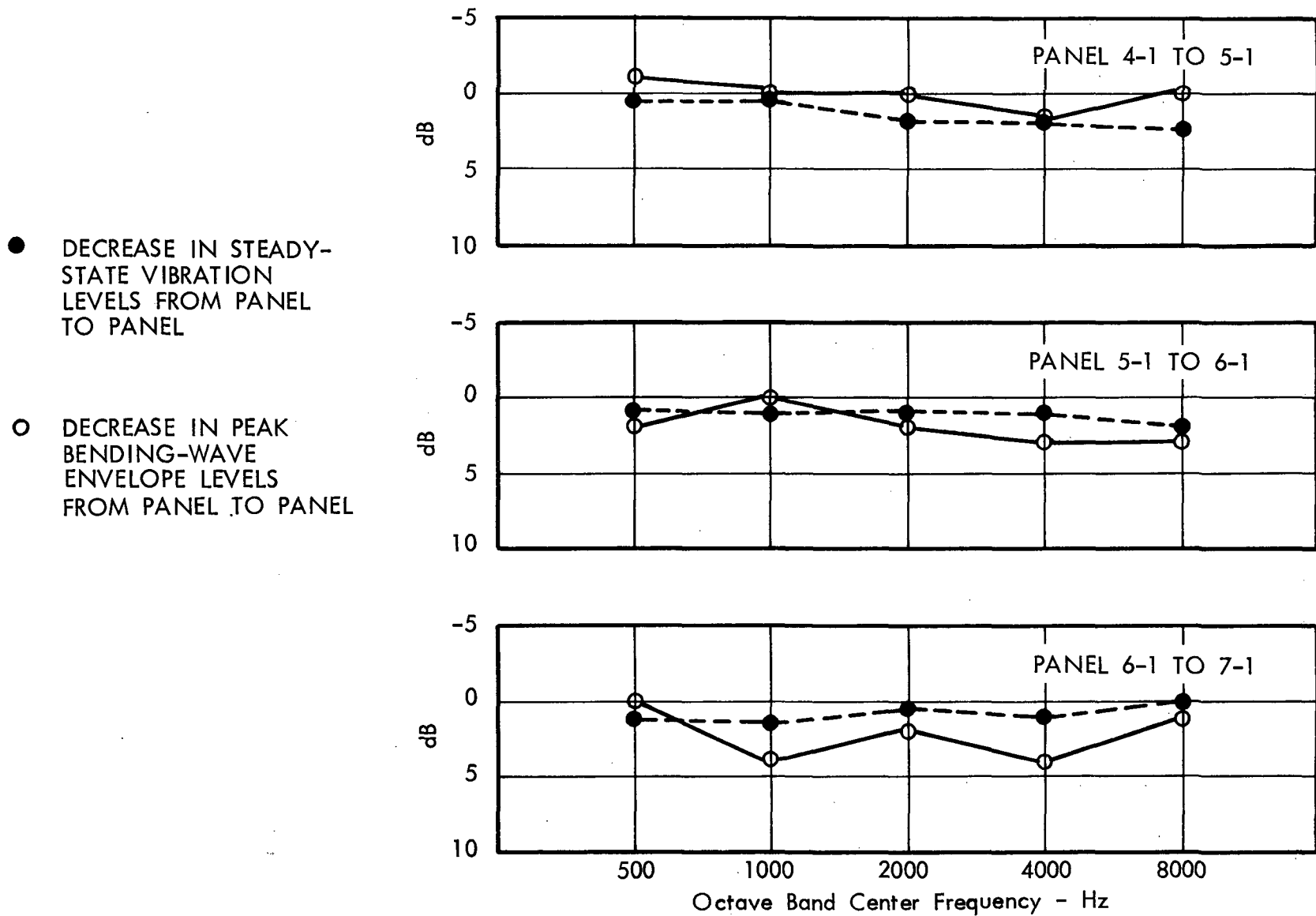
FIGURE 31. COMPARISON OF STEADY-STATE VIBRATION LEVEL REDUCTION FROM PANEL TO PANEL WITH REDUCTION OF PEAK BENDING-WAVE SHOCK ENVELOPES
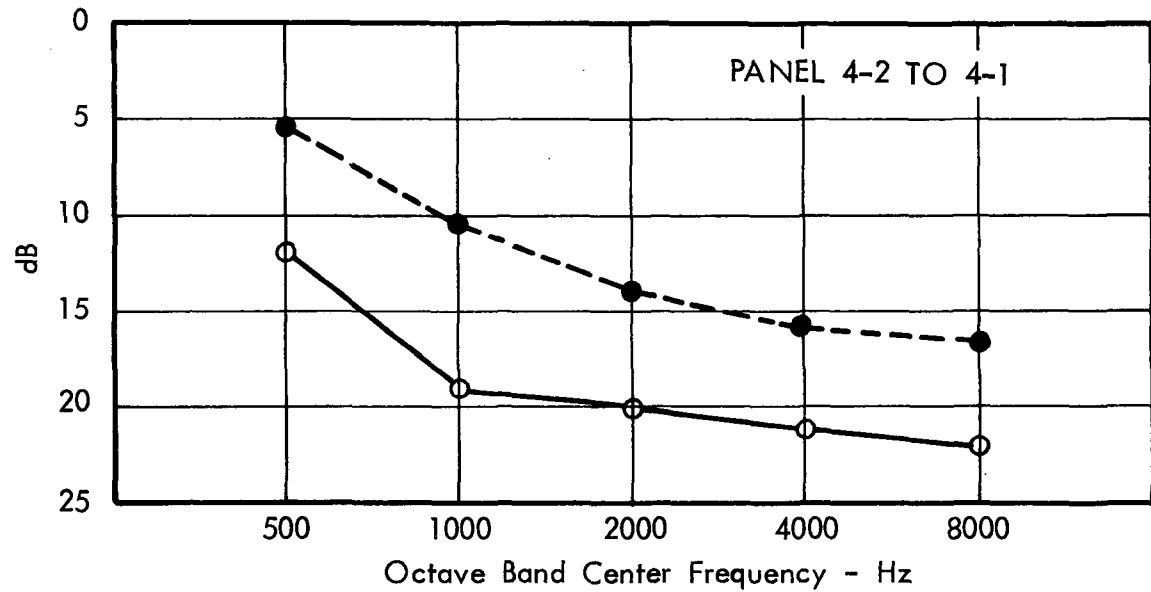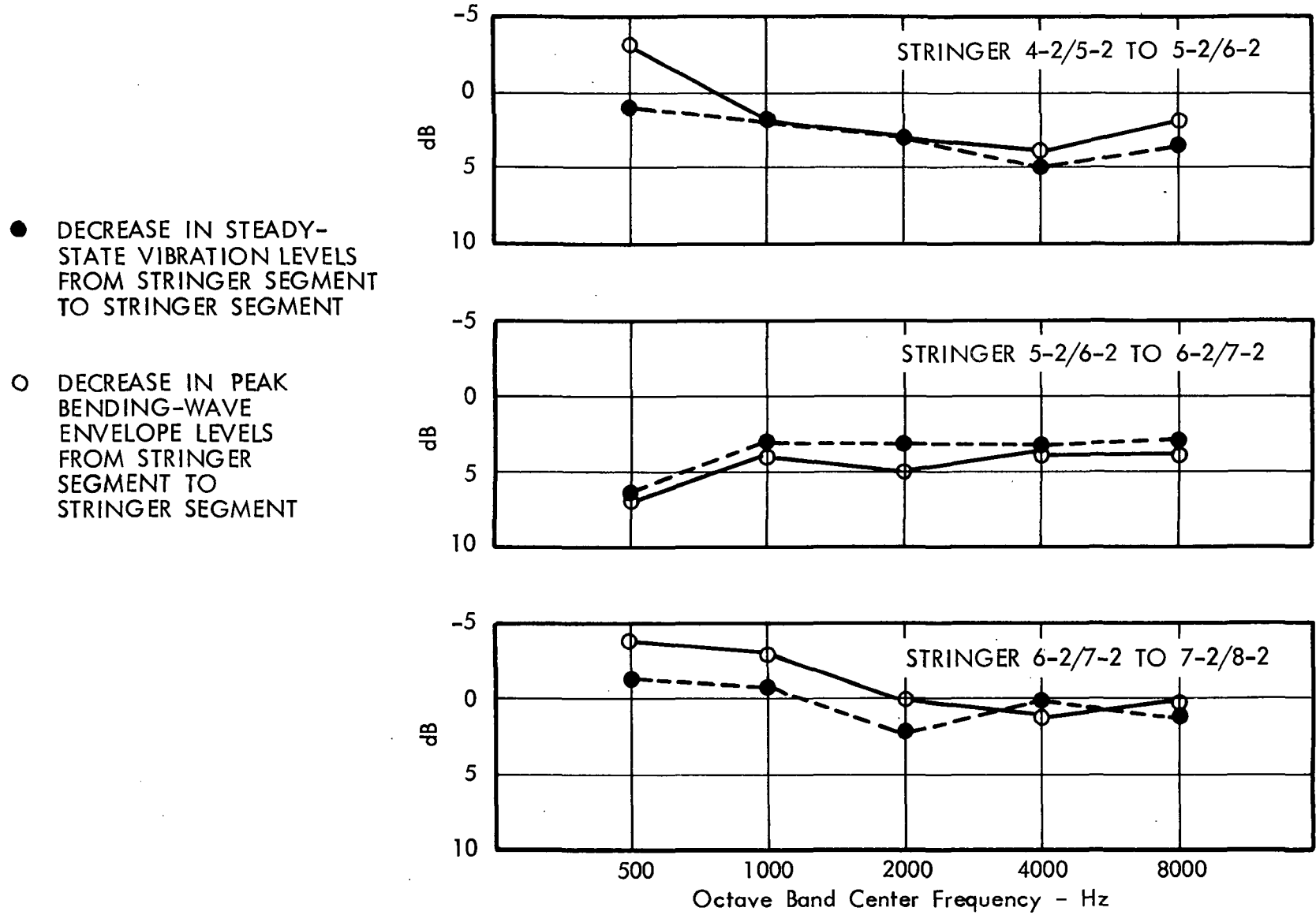
FIGURE 32.   COMPARISON OF STEADY-STATE VIBRATION LEVEL REDUCTION FROM PANEL TO PANEL WITH REDUCTION OF PEAK BENDING-WAVE SHOCK ENVELOPES

DECREASE IN STEADY-STATE VIBRATION LEVELS FROM PANEL TO BEAM

DECREASE IN PEAK BENDING-WAVE ENVELOPE LEVELS FROM PANEL TO PANEL

PANEL 4-2 TO RING 4-2/4-1

PANEL 4-2 TO STRINGER 4-2/5-2

Octave Band Center Frequency - Hz

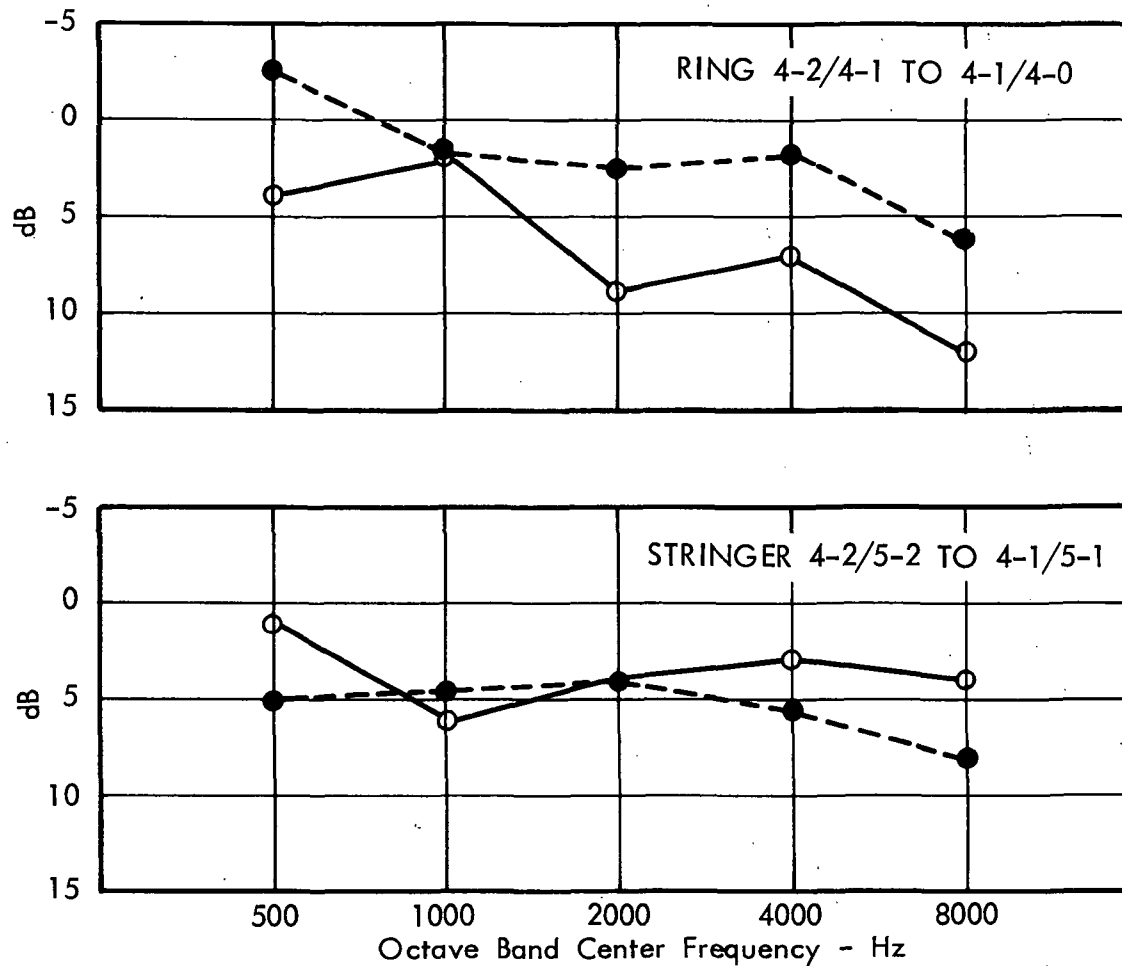FIGURE 33. COMPARISON OF STEADY-STATE VIBRATION LEVEL REDUCTION FROM EXCITED PANEL TO ADJACENT BEAMS WITH REDUCTION OF PEAK BENDING-WAVE SHOCK ENVELOPES

FIGURE 34. COMPARISON OF STEADY-STATE VIBRATION LEVEL REDUCTION ALONG A RING WITH REDUCTION OF PEAK BENDING-WAVE SHOCK ENVELOPES

● DECREASE IN STEADY-
STATE VIBRATION LEVELS
FROM STRINGER SEGMENT
TO STRINGER SEGMENT

O DECREASE IN PEAK
BENDING-WAVE
ENVELOPE LEVELS
FROM STRINGER
SEGMENT TO
STRINGER SEGMENT

FIGURE 35. COMPARISON OF STEADY-STATE VIBRATION LEVEL REDUCTION FROM STRINGER TO STRINGER WITH REDUCTION OF PEAK BENDING-WAVE SHOCK ENVELOPES

- ● DECREASE IN STEADY-STATE VIBRATION LEVELS FROM BEAM SEGMENT TO BEAM SEGMENT

- ○ DECREASE IN PEAK BENDING-WAVE ENVELOPE LEVELS BEAM SEGMENT TO BEAM SEGMENT

RING 4-2/4-1 TO 4-1/4-0

STRINGER 4-2/5-2 TO 4-1/5-1

Octave Band Center Frequency - Hz

FIGURE 36.   COMPARISON OF STEADY-STATE-VIBRATION LEVEL REDUCTION FROM RING TO RING AND ALONG A STRINGER WITH REDUCTION OF PEAK BENDING-WAVE SHOCK ENVELOPES
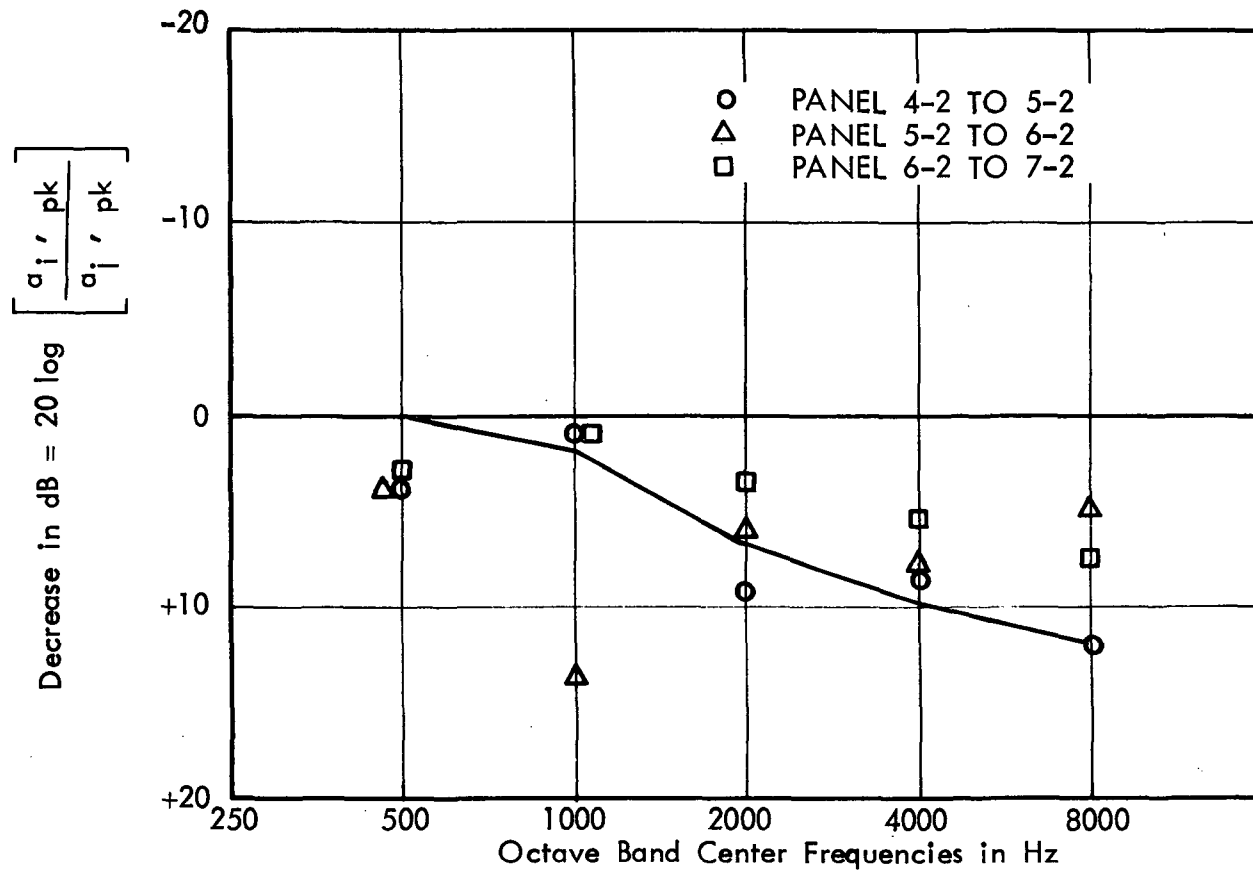
FIGURE 37.   COMPARISON OF PREDICTED AND MEASURED PEAK SHOCK BENDING ENERGY DECAY FROM SUBPANEL TO SUBPANEL
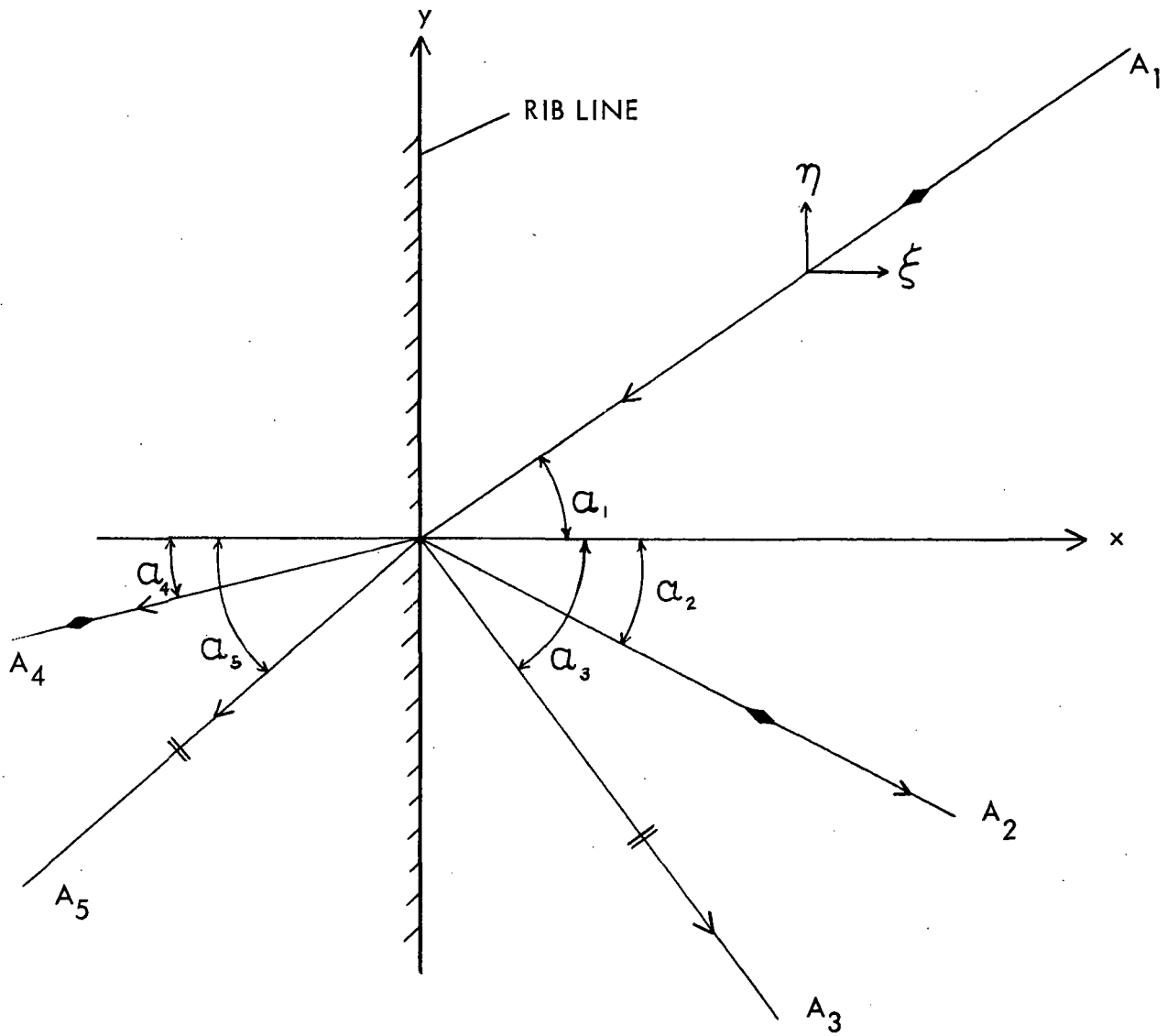
PANEL: thickness, h

radius of gyration, κ

mass density, ρ

longitudinal wavespread, c_ℓ

shear wavespread, c_T

RIB: cross sectional area, A_r

mass density, ρ_r

radius of gyration about axis z, κ_r

elastic modulus, Y_o

longitudinal wave speed, c_ℓ
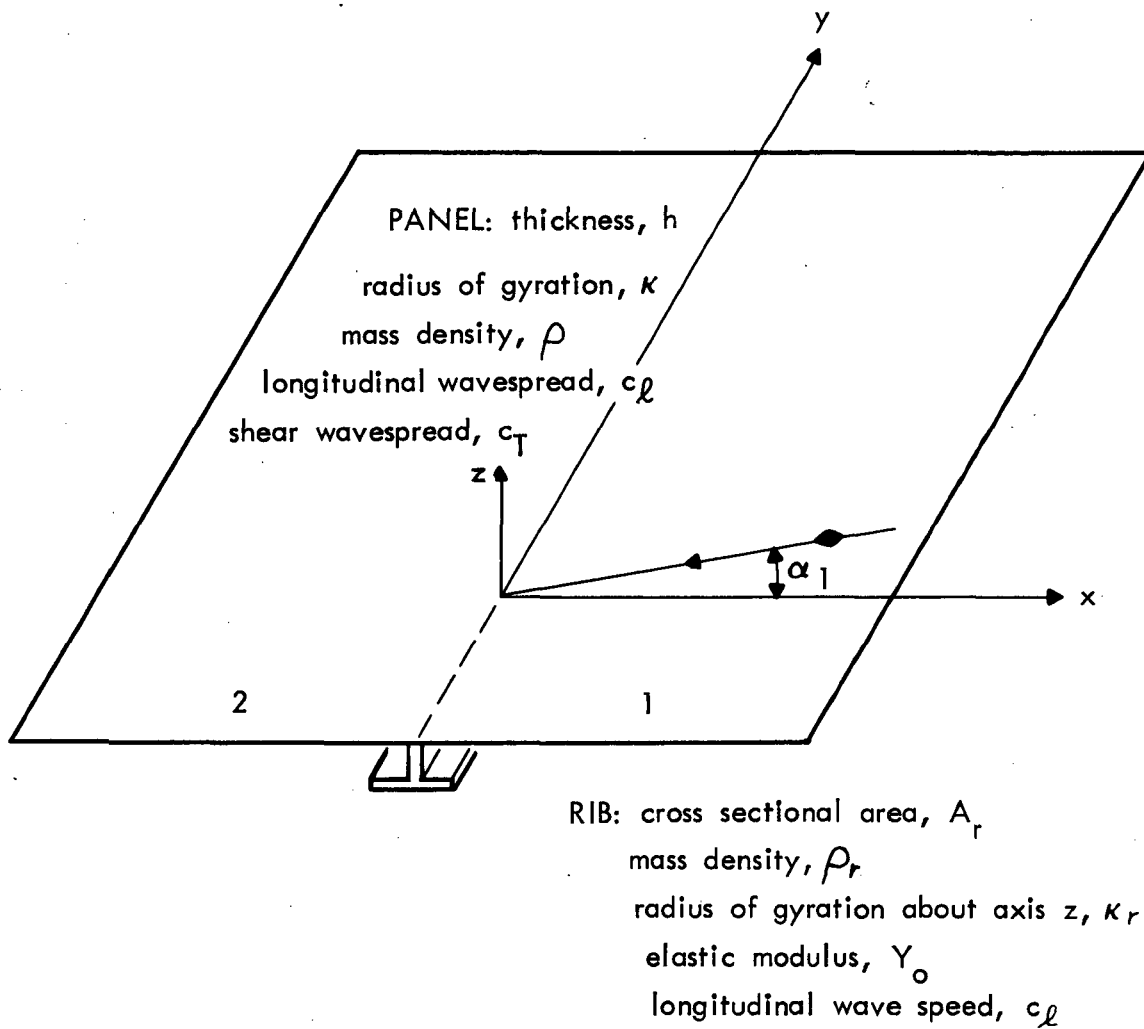
FIGURE 38.   PANEL REINFORCING BEAM CONFIGURATION

FIGURE 39. POSTULATED DISTORTIONAL AND DILATATIONAL WAVES
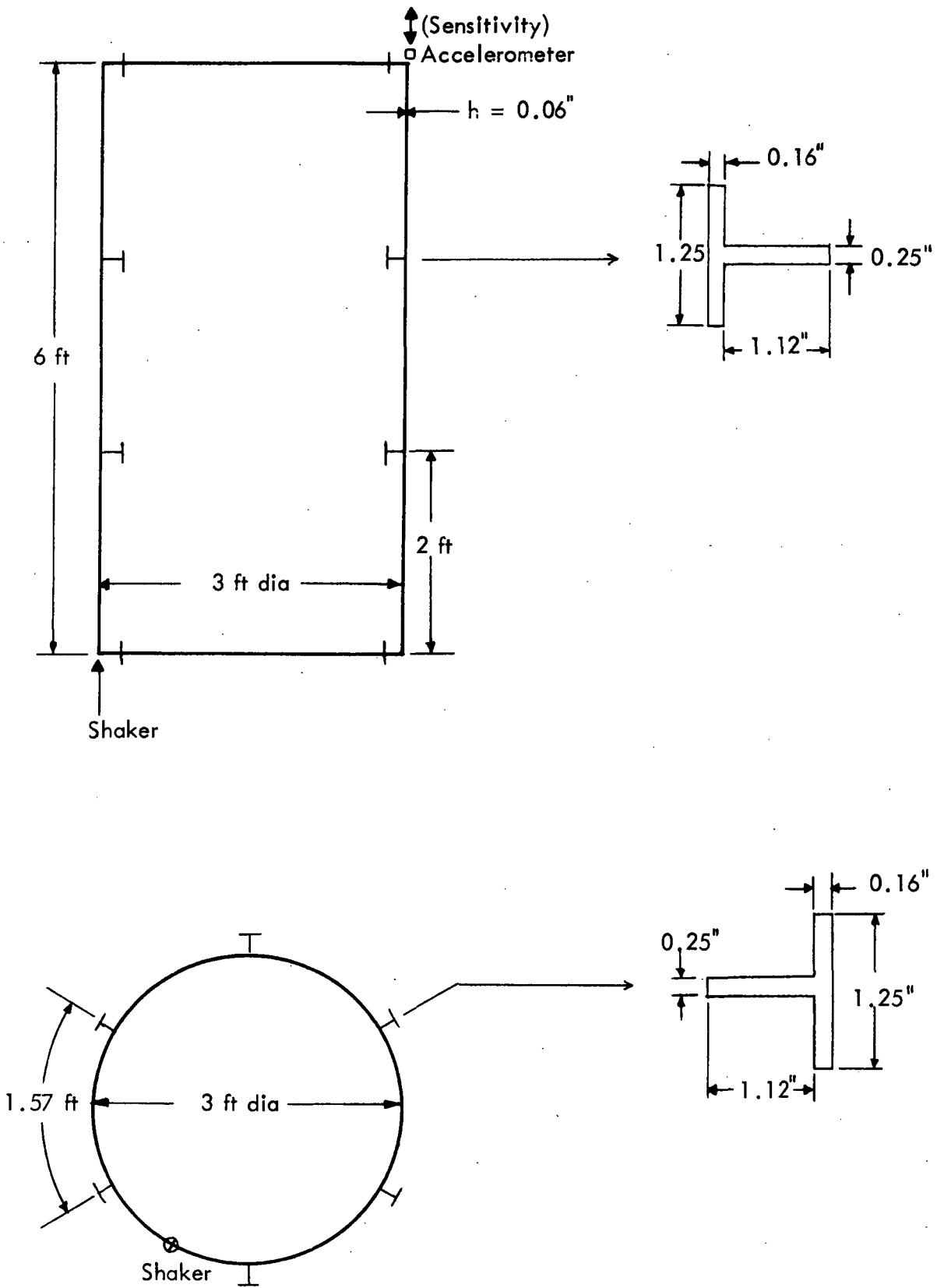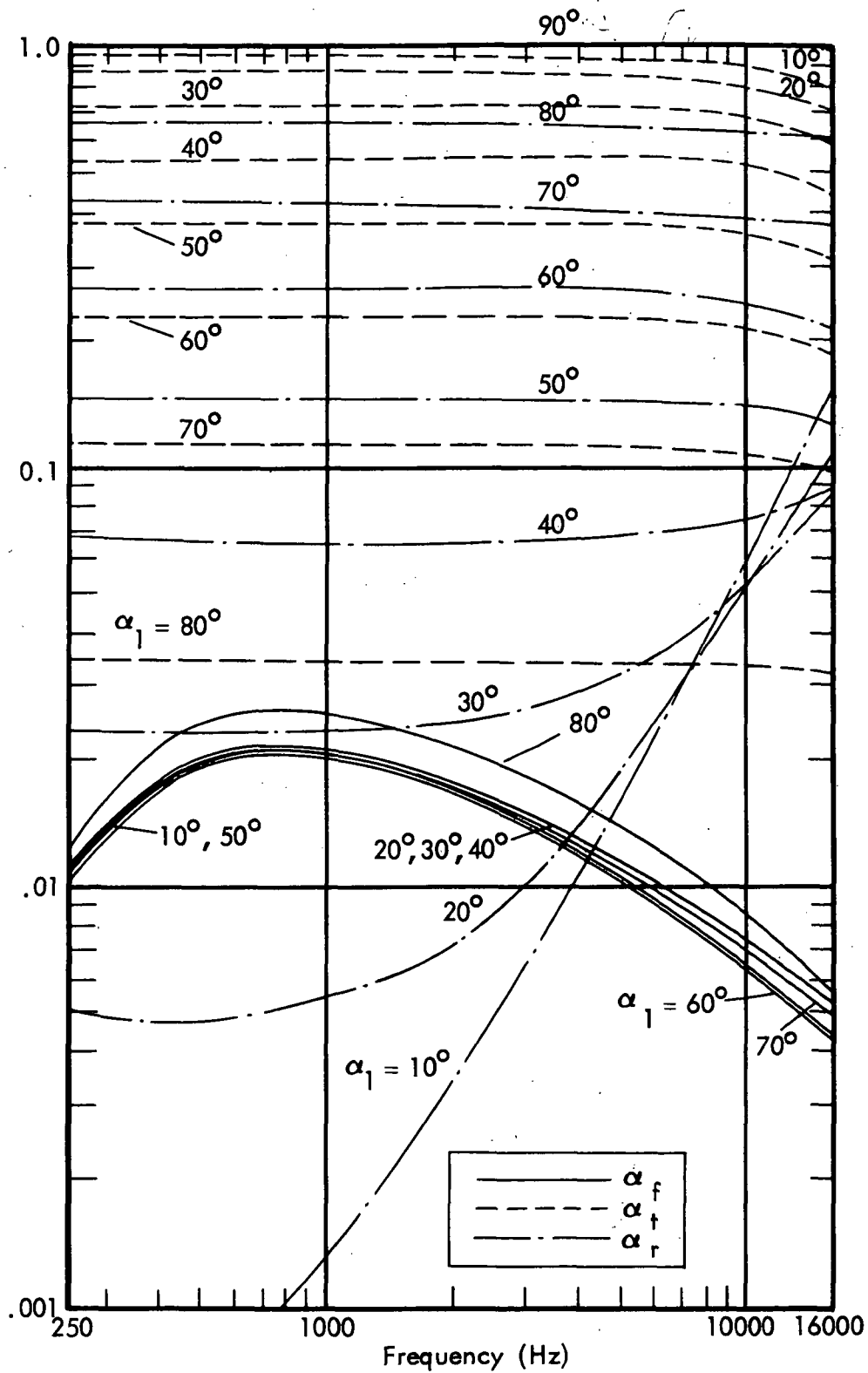
FIGURE 40. RIBBED CYLINDER MODEL

FIGURE 41.   TRANSMISSION, REFLECTION, AND FLEXURAL
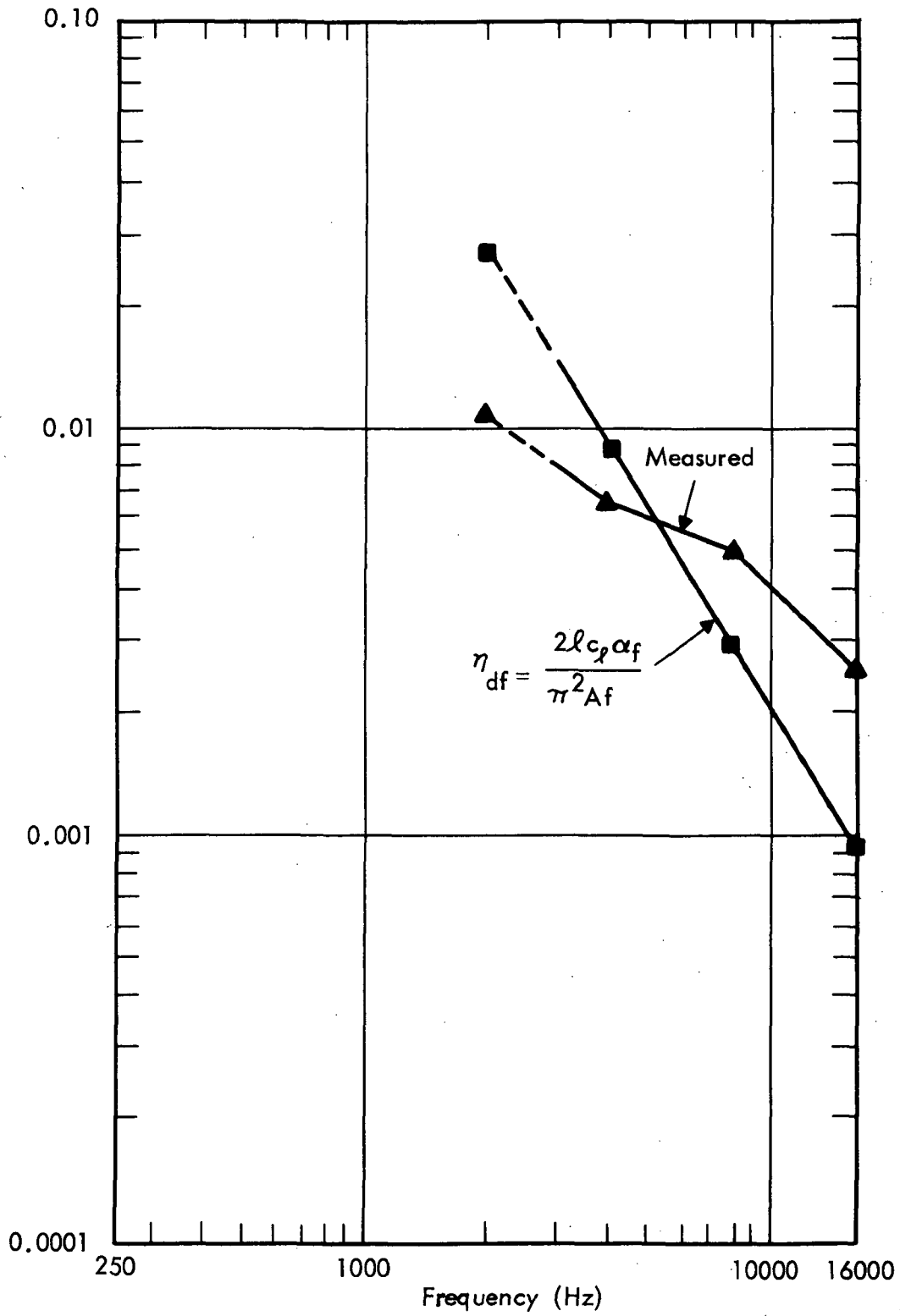   LOSS COEFFICIENTS

FIGURE 42. COUPLING LOSS FACTOR, η_{df}
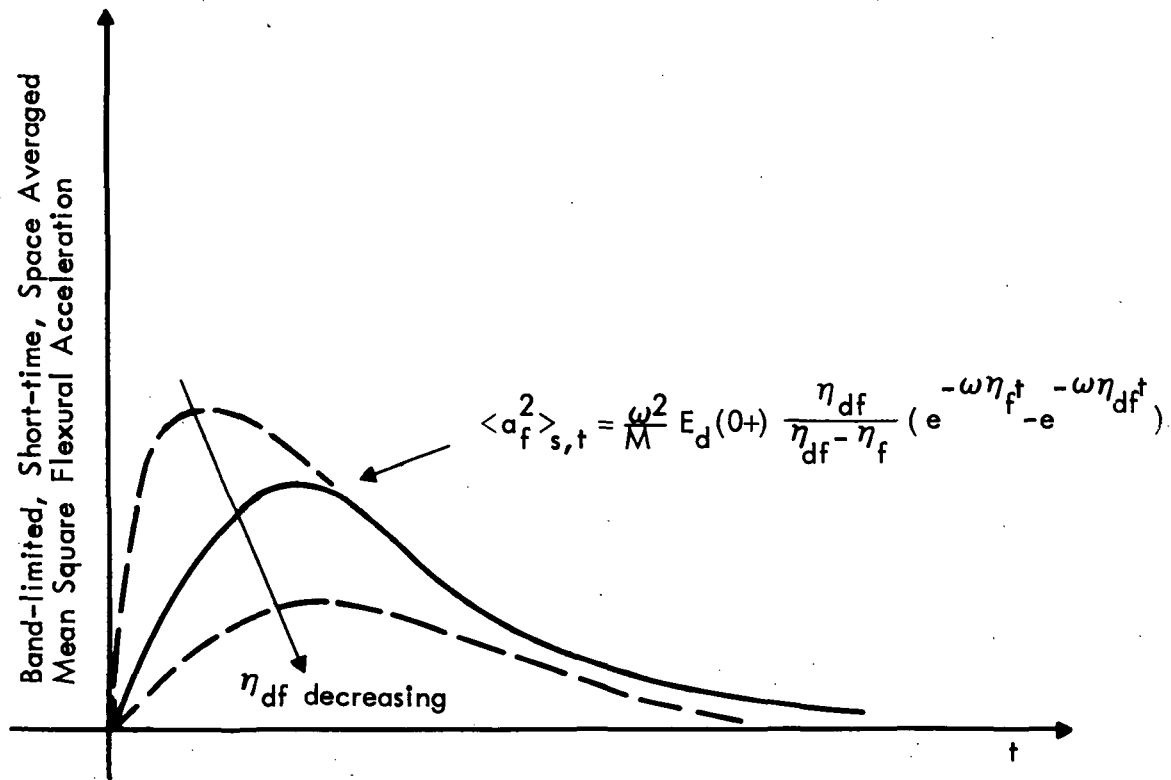(Dilatation to Flexure)

FIGURE 43. PREDICTED FLEXURAL RESPONSE DUE TO A TRANSIENT (IMPULSIVE) SOURCE SHOCK DIRECTLY INTO THE PLANE OF THE SKIN